Stability and Computation of Dynamic Patterns in PDEs

Wolf-Jürgen Beyn and Denny Otten and Jens Rottmann-Matthes

Abstract Nonlinear waves are a common feature in many applications such as the spread of epidemics, electric signaling in nerve cells, and excitable chemical reactions. Mathematical models of such systems lead to time-dependent PDEs of parabolic, hyperbolic or mixed type. Common types of such waves are fronts and pulses in one, rotating and spiral waves in two, and scroll waves in three space dimensions. These patterns may be viewed as relative equilibria of an equivariant evolution equation where equivariance is caused by the action of a Lie group. Typical examples of such actions are rotations, translations or gauge transformations. The aim of the lectures is to give an overview of problems related to the theoretical and numerical analysis of such dynamic patterns. One major theoretical topic is to prove nonlinear stability and relate it to linearized stability determined by the spectral behavior of linearized operators. The numerical part focusses on the freezing method which uses equivariance to transform the given PDE into a partial differential algebraic equation (PDAE). Solving these PDAEs generates moving coordinate systems in which the above-mentioned patterns become stationary.

Wolf-Jürgen Beyn
Department of Mathematics, Bielefeld University, e-mail: beyn@math.uni-bielefeld.de

Denny Otten
Department of Mathematics, Bielefeld University e-mail: dotten@math.uni-bielefeld.de

Jens Rottmann-Matthes
Department of Mathematics, Bielefeld University e-mail: jrottman@math.uni-bielefeld.de

Supported by CRC 701 'Spectral Structures and Topological Methods in Mathematics', Bielefeld University

1 Dynamics of patterns and equivariance: traveling waves in one space dimension

The first lecture is of introductory character and serves to introduce basic notions and properties. We use the well known topic of traveling wave solutions in order to illustrate the topics of this course such as equivariance, stability with asymptotic phase, spectral properties, and the associated computational problems. There are by now quite a few monographs and survey articles that treat this topic and we refer to [29],[39],[69],[60].

1.1 Traveling fronts and pulses

Consider a parabolic system in one space variable

$$u_t(x,t) = u_{xx}(x,t) + f(u(x,t)), \quad x \in \mathbb{R},\, t \geqslant 0, \tag{1}$$

where $f : \mathbb{R}^m \to \mathbb{R}^m$ is assumed to be sufficiently smooth and we look for smooth solutions $u(x,t) \in \mathbb{R}^m$, $x \in \mathbb{R}$, $t \geqslant 0$. In the following we omit arguments in (1) and simply write

$$u_t = u_{xx} + f(u), \quad x \in \mathbb{R}, \quad t \geq 0. \tag{2}$$

Definition 1. A special solution of (2), which is of the form

$$u(x,t) = \overline{v}(x - \overline{\mu}t), \quad x \in \mathbb{R}, \quad t \in \mathbb{R} \tag{3}$$

for some $\overline{\mu} \in \mathbb{R}$ and some $\overline{v} : \mathbb{R} \to \mathbb{R}^m$, is called a **traveling wave** if the limits

$$\lim_{\xi \to \infty} \overline{v}(\xi) = u_+, \; \lim_{\xi \to -\infty} \overline{v}(\xi) = u_- \tag{4}$$

exist and satisfy $f(u_\pm) = 0$. The function $\overline{v} : \mathbb{R} \to \mathbb{R}^m$ is called the **profile** of the wave and the value $\overline{\mu} \in \mathbb{R}$ is called its velocity. In case $u_+ \neq u_-$ one speaks of a **front solution** and in case $u_+ = u_-$ of a **pulse solution**.

Note that the wave moves to the right if $\overline{\mu} > 0$ and to the left if $\overline{\mu} < 0$. In case $\overline{\mu} = 0$ we have a standing wave.

Example 1 (Nagumo equation). This well known example with $m = 1$ is given by the equation

$$u_t = u_{xx} + u(1-u)(u-\alpha), \tag{5}$$

where $0 < \alpha < 1$ is a parameter. For this equation there is a simple explicit formula of a traveling front due to Huxley

$$\bar{v}(\xi) = \frac{1}{1+\exp\left(-\frac{\xi}{\sqrt{2}}\right)},\ \xi \in \mathbb{R}, \quad \bar{\mu} = \sqrt{2}\left(\alpha - \frac{1}{2}\right), \tag{6}$$

with $u_+ = 1$ and $u_- = 0$. The wave travels to the right if $\alpha > \frac{1}{2}$ and to the left if $\alpha < \frac{1}{2}$. The following Figure 1 shows the profile and the time-dependent solution (3) for the special case $\alpha = \frac{1}{4}$:

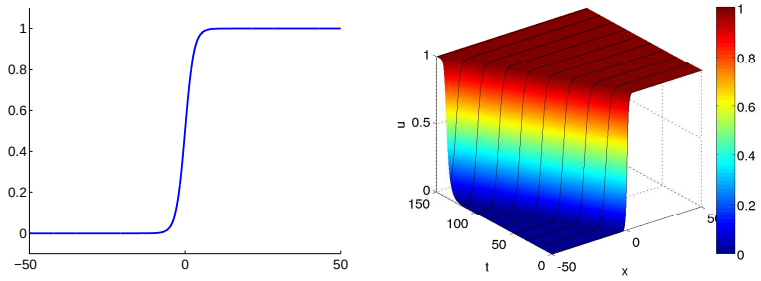

Fig. 1 Profile of the Nagumo front (left) and space-time diagram (right) for $\alpha = \frac{1}{4}$

1.2 Traveling waves and ODEs

Usually, both the profile and the velocity of a traveling wave are unknown. Hence the task is to find a function v and a parameter μ such that $u(x,t) = v(x-\mu t)$ solves (2). This leads to solving a second order ordinary differential equation for v with boundary conditions given at infinity

$$0 = v_{xx} + \mu v_x + f(v), \quad \lim_{x\to\pm\infty} v(x) = u_\pm, \quad f(u_\pm) = 0. \tag{7}$$

Introducing $V = \begin{pmatrix} v_1 \\ v_2 \end{pmatrix} = \begin{pmatrix} v \\ v_x \end{pmatrix}$, this can be rewritten as a first order system of dimension $2m$

$$\begin{pmatrix} v_1 \\ v_2 \end{pmatrix}_x = V_x = F(V,\mu) = \begin{pmatrix} v_2 \\ -\mu v_2 - f(v_1) \end{pmatrix}, \quad \lim_{x\to\pm\infty} V(x) = V_\pm = \begin{pmatrix} u_\pm \\ 0 \end{pmatrix}. \tag{8}$$

Traveling pulses and fronts therefore correspond to **homoclinic** and **heteroclinic orbits** that connect two steady states V_- to V_+ of the dynamical system (8) for a specific value of the parameter μ.

Example 2 (Nagumo equation). For an illustration we return to the Nagumo equation (6), where the first order system (8) reads

$$\begin{pmatrix} v_1 \\ v_2 \end{pmatrix}_x = \begin{pmatrix} v_2 \\ -\mu v_2 - v_1(1-v_1)(v_1-\alpha) \end{pmatrix}, \tag{9}$$

$$\lim_{x\to-\infty} \begin{pmatrix} v_1(x) \\ v_2(x) \end{pmatrix} = \begin{pmatrix} 0 \\ 0 \end{pmatrix}, \quad \lim_{x\to\infty} \begin{pmatrix} v_1(x) \\ v_2(x) \end{pmatrix} = \begin{pmatrix} 1 \\ 0 \end{pmatrix}. \tag{10}$$

Figure 2 shows the phase diagrams of the two-dimensional system (9) for values $\mu < \bar{\mu}$, $\mu = \bar{\mu}$, and $\mu > \bar{\mu}$, where $\bar{\mu} = -\frac{\sqrt{2}}{4}, \alpha = \frac{1}{4}$. At the value $\mu = \bar{\mu}$ we have a heteroclinic orbit connecting the two saddles $(0,0)$ and $(1,0)$.

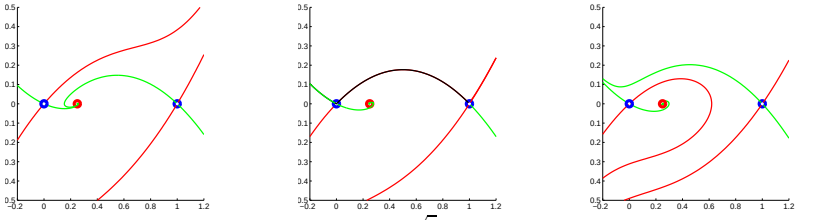

(a) $-\frac{2}{4} = \mu < \bar{\mu}$ (b) $-\frac{\sqrt{2}}{4} = \mu = \bar{\mu}$ (c) $-\frac{1}{4} = \mu > \bar{\mu}$

Fig. 2 Phase diagrams of (9) for $\alpha = \frac{1}{4}$ and μ-values close to $\bar{\mu} = -\frac{\sqrt{2}}{4}$

We briefly discuss how to compute the profile $v(x) \in \mathbb{R}^m$ and $\mu \in \mathbb{R}$ from

$$V_x = F(V,\mu), \lim_{x\to\pm\infty} V(x) = V_\pm, F(V_\pm,\mu) = 0. \tag{11}$$

Note that such connecting orbits always come in families. If (V,μ) solves (11) then so does $(V(\cdot-\gamma),\mu)$ for any $\gamma \in \mathbb{R}$. In order to eliminate this ambiguity one introduces a **phase condition** and solves the following boundary value problem for (V,μ)

$$V_x = F(V,\mu), x \in \mathbb{R}, \quad \Psi(V) := (\hat{V}_x, V - \hat{V})_{L^2} = 0. \tag{12}$$

Here the phase condition uses an initial approximation or template function $\hat{V}$ which we require to have the correct limits $\lim_{x\to\pm\infty} \hat{V}(x) = V_\pm$ and such that the inner product in (12) exists. In Section 2 we will motivate this condition and discuss alternatives.

For numerical computations one chooses a bounded interval $J = [x_-, x_+]$ and then solves the following boundary value problem for $V \in C^1(J,\mathbb{R}^m)$, $\mu \in \mathbb{R}$,

$$V_x = F(V,\mu), x \in J, \quad (\hat{V}_x\big|_J,\, V - \hat{V}\big|_J)_{L^2(J)} = 0 \tag{13}$$

$$P_+(\mu)(V(x_+) - V_+) = 0, \quad P_-(\mu)(V(x_-) - V_-) = 0. \tag{14}$$

The most common choice for the boundary operators $P_\pm$ are **projection boundary conditions** which require the endpoint $V(x_-)$ to lie in the linear approximation of the unstable manifold at V_- and $V(x_+)$ to lie in the linear approximation of the stable manifold at V_+, see Figure 3. Concretely, one chooses $P_+ = P_+(\mu) \in \mathbb{R}^{m_u \times m}$ of maximal rank such that $P_+(\mu)DF(V_+,\mu) = \Lambda_+ P_+(\mu)$ and such that the spectrum of $\Lambda_+ \in \mathbb{R}^{m_u \times m_u}$ coincides with the spectrum of $DF(V_+,\mu)$ with positive real part. The rows of P_+ then span the left unstable eigenvectors of $DF(V_+,\mu)$ which are orthogonal to the right stable eigenvectors. Similarly, one chooses $P_-(\mu) \in \mathbb{R}^{m_s \times m}$ such that the rows of P_- span the left stable eigenvectors of $DF(V_-,\mu)$. Note that in general the projection matrices depend on μ so that the boundary value problem (13) becomes nonlinear both in V and μ. We refer to [8],[23],[30] for various methods that allow to compute such projection matrices depending smoothly on a parameter. Finally, note that the boundary value problem (13) has the same number of equations and boundary conditions provided $m_s + m_u = m$, which is obviously satisfied in the homoclinic case but an assumption in the heteroclinic case. There is also a well established theory that studies the errors when passing from the infinite problem (12) to the finite problem (13), (14), see [8].

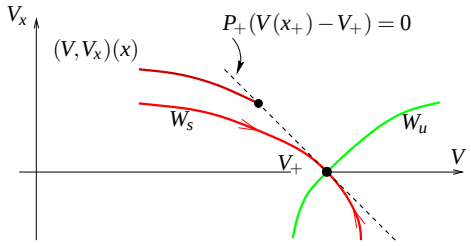

Fig. 3 Linear approximation of the stable manifold by projection boundary conditions.

1.3 Dynamics of PDE and shift equivariance

Let us return to the time-dependent equation (2) in a slightly more general form

$$u_t = Au_{xx} + f(u,u_x),\ x \in \mathbb{R},\ t \geqslant 0,\ u(x,t) \in \mathbb{R}^m, \tag{15}$$

where $A \in \mathbb{R}^{m \times m}$ is assumed to be positive definite and $f : \mathbb{R}^{2m} \to \mathbb{R}^m$ is smooth. For a fixed $\mu \in \mathbb{R}$ we transform into a moving coordinate frame via $u(x,t) = v(x - \mu t, t)$. This leads to

$$v_t = Av_{xx} + \mu v_x + f(v, v_x). \tag{16}$$

This is a parabolic system for which a traveling wave $u(x,t) = \bar{v}(x - \bar{\mu}t)$ now appears as a steady state $(\bar{v}, \bar{\mu})$. In fact, we have a family of steady states $(\bar{v}(\cdot - \gamma), \bar{\mu}), \gamma \in \mathbb{R}$.

In Section 3 we will deal with the classical Hodgkin-Huxley system for which $m = 4$. Then the matrix A is only positive semidefinite since there is no diffusion in 3 of 4 variables. The system (15) is then of mixed hyperbolic-parabolic type and this creates extra difficulties, both theoretically as well as numerically, see section 3.

In the following it will be useful to phrase (15) in a more abstract way as

$$u_t = F(u), \quad F(u) = Au_{xx} + f(u, u_x), \tag{17}$$

where we consider F as an operator

$$F : Y = w + H^2(\mathbb{R}, \mathbb{R}^m) \to L^2(\mathbb{R}, \mathbb{R}^m) = X. \tag{18}$$

Here L^2, H^2 are standard Lebesgue and Sobolev spaces, the function $w \in C^2(\mathbb{R}, \mathbb{R}^m)$ satisfies for some $\varepsilon > 0$

$$|w(x) - u_\pm| + |w_x(x)| + |w_{xx}(x)| \leqslant Ce^{-\varepsilon|x|}, x \in \mathbb{R},$$

and we assume $f(u_\pm, 0) = 0$. We have carefully chosen Y as an affine space in order to incorporate traveling fronts with different limits at $\pm\infty$. Under these assumptions, using Sobolev embedding one can show that F maps Y into X.

Now consider the shift operator as an action of the group $G = \mathbb{R}$ on Y

$$a : G \times Y \to Y \,, (\gamma, u) \mapsto a(\gamma, u), \quad [a(\gamma, u)](x) = u(x - \gamma), x \in \mathbb{R}. \tag{19}$$

Obviously, $a(\gamma, u)$ has the following properties for $u, v \in Y$, $\gamma, \gamma_1, \gamma_2 \in G$, $\lambda \in \mathbb{R}$,

$$\begin{aligned} a(\gamma_1 + \gamma_2, u) &= a(\gamma_1, a(\gamma_2, u)), && \text{homomorphism,} \\ a(\gamma, \lambda u + (1-\lambda)v) &= \lambda a(\gamma, u) + (1-\lambda)a(\gamma, v) && \text{affine linearity w.r.t. u.} \end{aligned}$$

Moreover, the action immediately extends to $X = L^2(\mathbb{R}, \mathbb{R}^m)$ with the same properties. We often write $a(\gamma)u$ instead of $a(\gamma, u)$, in particular when $a(\gamma)$ is a linear operator on X.

The most important property of the operator F is **equivariance under the action of the group**, i.e.

$$a(\gamma)F(u) = F(a(\gamma)u), \; u \in Y, \; \gamma \in G. \tag{20}$$

This follows from

$$(Fu)(\cdot - \gamma) = Au_{xx}(\cdot - \gamma) + f(u(\cdot - \gamma), u_x(\cdot - \gamma)) = F(u(\cdot - \gamma)), \gamma \in \mathbb{R}.$$

Thus, we have recast (15) as an abstract **equivariant evolution equation** (17), (20).

Some further notations are useful. For a given element $v \in Y$ the set

$$\mathcal{O}_G(v) = \{a(\gamma)v : \gamma \in G\}$$

is called its **group orbit**. For the shift action (19) the group orbit of a function consists of all its translates. A **relative equilibrium** of (17) is a solution $\bar{u}(t), t \in \mathbb{R}$ that lies in a single group orbit, i.e.

$$\bar{u}(t) = a(\gamma(t))\bar{v}, \quad \text{for some } \bar{v} \in Y,\ \gamma(\cdot) \in C^1(\mathbb{R}, G). \tag{21}$$

In this sense, traveling waves $\bar{u}(x,t) = \bar{v}(x - \bar{\mu}t)$ are relative equilibria w.r.t. shift equivariance where in this special case $\gamma(t) = \bar{\mu}t$.

1.4 Stability with asymptotic phase

In the previous section we saw that traveling waves, and relative equilibria in general, always appear in families. In order to take this into account the classical notion of Lyapunov stability is modified as follows.

Definition 2. A traveling wave solution $u(x,t) = \bar{v}(x - \bar{\mu}t)$ of the system (15) is called **asymptotically stable with asymptotic phase** with respect to given norms $\|\cdot\|_1$ and $\|\cdot\|_2$ on Y, if for any $\varepsilon > 0$ there exists a $\delta > 0$ such that for any initial data $u_0 \in Y$ with $\|u_0 - \bar{v}\|_1 \leqslant \delta$ there exists some $\gamma_\infty \in \mathbb{R}$ with the following property. The Cauchy problem $u_t = Au_{xx} + f(u, u_x), u(\cdot, 0) = u_0$ has a unique solution $u(\cdot, t) \in Y$, $t \geqslant 0$ and

$$\|u(\cdot,t) - \bar{v}(\cdot - \bar{\mu}t - \gamma_\infty)\|_2 \begin{cases} \leqslant \varepsilon & \text{for all } t \geqslant 0, \\ \to 0 & \text{as } t \to \infty. \end{cases} \tag{22}$$

In general, the value γ_∞ depends on the initial function u_0 and is called the **asymptotic phase**. The definition is not completely rigorous since it leaves open the precise notion of solution and of the associated function spaces. These depend on the particular type of application. Note that our formulation allows an affine space for Y as in (18). For PDEs with hyperbolic parts it is important to use two different norms in the definition, see Section 3. Then initial perturbations often must be measured in stronger norms than perturbations of solutions. On the other hand, for parabolic systems it is often possible to use the same Sobolev norm $\|\cdot\|_{H^1}$ for both norms. For various stability theorems we refer to the monographs [39], [69] and to the survey article [60].

An essential feature of all stability results are the spectral properties of the linearized differential operator

$$\Lambda = A\partial_{xx} + (\bar{\mu}I + D_2 f(\bar{v}, \bar{v}_x))\,\partial_x + D_1 f(\bar{v}, \bar{v}_x). \tag{23}$$

We introduce coefficient matrices in (23) by writing

$$\Lambda = A\partial_{xx} + B(x)\partial_x + C(x) \tag{24}$$

and note that, due to our assumption, the following limits exist

$$B_\pm = \lim_{x\to\pm\infty} B(x) = \bar{\mu} I + D_2 f(u_\pm, 0), \quad C_\pm = \lim_{x\to\pm\infty} C(x) = D_1 f(u_\pm, 0). \tag{25}$$

1.5 Spectral properties of second order operators

In this section we recall basic facts about spectra of second order linear differential operators as they arise from linearizations at traveling waves. Since these operators are defined on the whole line they typically have essential as well as isolated spectrum. The essential spectrum is determined by the limit operators

$$\Lambda_\pm = A\partial_{xx} + B_\pm\partial_x + C_\pm \tag{26}$$

obtained from the coefficients in (25). The spectrum of $\Lambda_\pm$ can be computed by evaluating the so-called **dispersion relation**, see (30) below. On the contrary, it is not so easy to determine the remaining isolated eigenvalues, except for the fact that zero is always an eigenvalue due to shift equivariance.

Let us first look at the real scalar case of (26), i.e.

$$\Lambda_0 v = a v_{xx} + b v_x + c v, \quad a,b,c \in \mathbb{R}. \tag{27}$$

We look for eigenvalues $s \in \mathbb{C}$ with eigenfunctions of the form

$$v(x) = e^{i\omega x},\ x \in \mathbb{R},\ \omega \in \mathbb{R}. \tag{28}$$

This leads us to the dispersion relation

$$s = -a\omega^2 + ib\omega + c, \quad \omega \in \mathbb{R}. \tag{29}$$

Any value $s \in S = \{s = -a\omega^2 + ib\omega + c \mid \omega \in \mathbb{R}\}$ is an eigenvalue of Λ_0 with a bounded eigenfunction $e^{i\omega x}$. Standard function spaces such as L^2 or H^1 will not contain these eigenfunctions, but their presence leads to unbounded resolvents. For the scalar case with $a > 0, b \neq 0$ the algebraic set S is a left open parabola with the vertex at c, see Figure 4.

For the general operator (26) one has to consider two algebraic sets

$$S_\pm = \{s \in \mathbb{C} : \det(-\omega^2 A + i\omega B_\pm + C_\pm - sI) = 0 \text{ for some } \omega \in \mathbb{R}\}. \tag{30}$$

If, for instance, A is positive definite and $B_\pm$ is the identity then the curves in $S_\pm$ asymptotically attain a parabolic shape $s \sim i\omega - \omega^2\lambda_j$, where λ_j, $j = 1,\dots,m$ are the eigenvalues of A. Let us first recall some standard definitions from spectral theory.

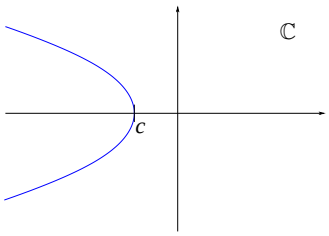

Fig. 4 Spectrum of $\Lambda_0 = a\partial_x^2 + b\partial_x + c$

Definition 3. Let X be a Banach space and let $\Lambda : \mathscr{D}(\Lambda) \subset X \to X$ be a densely defined closed operator. If $sI - \Lambda$ is one-to-one for $\lambda \in \mathbb{C}$ then the operator $R_s(\Lambda) = (sI - \Lambda)^{-1}$ is defined on $\mathscr{D}(R_s(\Lambda)) = \text{Range}(sI - \Lambda)$ and called the **resolvent of** Λ. Then one defines the **resolvent set**

$$\rho(\Lambda) = \{s \in \mathbb{C} : R_s(\Lambda) \text{ exists, } \mathscr{D}(R_s(\Lambda)) \text{ is dense, } R_s(\Lambda) \text{ bounded}\}, \tag{31}$$

the **spectrum** $\sigma(\Lambda) = \mathbb{C} \setminus \rho(\Lambda)$, the **point spectrum**

$$\sigma_{point}(\Lambda) = \{s \in \mathbb{C} \text{ is an isolated eigenvalue of finite multiplicity}\}, \tag{32}$$

and the **essential spectrum** $\sigma_{\text{ess}}(\Lambda) = \sigma(\Lambda) \setminus \sigma_{\text{point}}(\Lambda)$.

In the following we introduce the crucial
Spectral Condition (SC):
There exist $\beta, \lambda_{min} > 0$ such that $|\text{Re}\,\lambda| \geq \lambda_{\min}$ for all $\lambda \in \mathbb{C}$ which satisfy

$$\det(\lambda^2 A + \lambda B_\pm + C - sI) = 0, \text{ for some } \text{Re}\, s \geqslant -\beta. \tag{33}$$

If A is positive definite then a continuation argument shows that the algebraic sets $S_\pm$ lie in the half plane $\{z : \text{Re}\,(z) < -\beta\}$ and hence are bounded away from the imaginary axis. More generally, the following theorem from [39] shows that the spectral condition is also sufficient to guarantee that the essential spectrum of the variable coefficient operator Λ from (24) lies in this half plane.

Theorem 1. *(Essential spectrum of Λ, [39]) Let the variable coefficient operator Λ from* (24) *have continuous coefficients such that $B_\pm = \lim_{x\to\pm\infty} B(x)$ and $C_\pm = \lim_{x\to\pm\infty} C(x)$ exist and A is positive definite.*

Then the spectrum of the operator Λ considered in $L^2(\mathbb{R}, \mathbb{R}^m)$ satisfies

$$S_- \cup S_+ \subset \sigma_{ess}(\Lambda) \subset M^c, \tag{34}$$

where the algebraic sets $S_\pm$ are defined in (30) *and M is the unique connected component of $\mathbb{C} \setminus (S_- \cup S_+)$ that contains a right half plane $\{z : \text{Re}\, z \geqslant \zeta\}$ for some $\zeta \in \mathbb{R}$. Moreover, if the spectral condition **SC** holds then $\text{Re}\,\sigma_{ess}(\Lambda) \leqslant -\beta$.*

Since the proof is quite involved, we only describe the main idea, see [39]. Decompose $\Lambda = L + K$, where L has constant coefficients on both $\mathbb{R}_- = (-\infty, 0]$ and

$R_+^* = (0,\infty)$ and K is of lower order and has decaying coefficients

$$L = \begin{cases} \Lambda_- & \text{on } \mathbb{R}_-, \\ \Lambda_+ & \text{on } \mathbb{R}_+^*, \end{cases} \quad K = \begin{cases} (B(x)-B_-)\partial_x + (C(x)-C_-), & x \in \mathbb{R}_-, \\ (B(x)-B_+)\partial_x + (C(x)-C_+), & x \in \mathbb{R}_+^*. \end{cases} \tag{35}$$

Then, one applies the following theorem on invariance of the essential spectrum [36].

Theorem 2. *Let X be a Banach space, $L : \mathscr{D}(L) \subset X \to X$ be a closed linear operator and $K : \mathscr{D}(K) \supset \mathscr{D}(L) \to X$ be a linear operator such that $K(\lambda_0 I - L)^{-1}$ is compact for some $\lambda_0 \in \rho(L)$. Let $U \subset \mathbb{C}$ be open and connected such that $U \subset \rho(L) \cup \sigma_{\text{point}}(L)$. Then either $U \subset \rho(L+K) \cup \sigma_{\text{point}}(L+K)$ or U contains only eigenvalues of $L+K$.*

A perturbation K of an operator L for which $K(\lambda_0 I - L)^{-1}$ is compact, is called **relatively compact**. In the special case (35) one shows that $(\lambda_0 I - L)^{-1}$ is bounded from $L^2(\mathbb{R},\mathbb{R}^m)$ into $H^1(\mathbb{R},\mathbb{R}^m)$. Then, using the fact that the coefficients of K vanish as $x \to \pm\infty$ one shows compactness of the operator $K(\lambda_0 I - L)^{-1}$ as an operator in $L^2(\mathbb{R},\mathbb{R}^m)$ by invoking the Riesz-Fréchet compactness criterion in $L^2(\mathbb{R},\mathbb{R}^{m\times m})$, see [3].

We close this subsection with some remarks on the point spectrum $\sigma_{point}(\Lambda)$. Differentiating the equation $0 = \bar{v}_{xx} + \mu\bar{v}_x + f(\bar{v},\bar{v}_x)$ with respect to x leads to

$$0 = (\bar{v}_x)_{xx} + \mu\,(\bar{v}_x)_x + D_2 f(\bar{v},\bar{v}_x)\bar{v}_{xx} + D_1 f(\bar{v},\bar{v}_x)\bar{v}_x = \Lambda\bar{v}_x. \tag{36}$$

Hence, we always have $0 \in \sigma_{point}(\Lambda)$ with eigenfunction $\bar{v}_x = -\frac{d}{d\gamma} v(\cdot-\gamma)\Big|_{\gamma=0}$ provided this function is in the appropriate function space. The problem of detecting further eigenvalues in the domain M (see Theorem 2) can be reduced to studying zeros of the so-called **Evans function**, see [2],[52]. Several approaches have been developed for this purpose. However, if the analysis cannot be done explicitly one has to resort to numerical computations for detecting the point spectrum, compare [60],[17], [18],[43],[42],[48],[47],[59]. In Figure 5 we sketch the typical appearance of the spectrum, where we used that the operator Λ is sectorial in $L^2(\mathbb{R},\mathbb{R}^m)$.

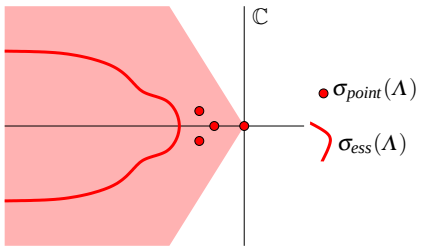

Fig. 5 Schematic picture of spectrum for a second order linear operator Λ.

For the stability results in the next subsection we will need the following
Eigenvalue condition (EC):
There are no isolated eigenvalues of finite multiplicity for Λ in $\mathrm{Re}\, s \geqslant -\beta$ except 0, and the eigenvalue 0 is algebraically simple.

1.6 Nonlinear stability of traveling waves and applications

With the preparation about the spectra of linear operators we may now formulate the main nonlinear stability theorem.

Theorem 3. *(Stability of traveling waves in H^1)*
Consider a parabolic system (15) *with a smooth nonlinearity f that satisfies*

$$f(v,v_x) = f_1(v)v_x + f_2(v), \tag{37}$$

$$f_1, f_2, f_1', f_2' \in C^1 \text{ globally Lipschitz}. \tag{38}$$

Let $u(x,t) = \bar{v}(x-\bar{\mu}t)$ be a traveling wave of (15) *such that the spectral condition (SC) and the eigenvalue condition (EC) are satisfied for the linearized operator Λ in* (23)*. Then the traveling wave $(\bar{v},\bar{\mu})$ is stable with asymptotic phase in the space $H^1(\mathbb{R},\mathbb{R}^m)$.*

Remark 1. Stability in $H^1(\mathbb{R},\mathbb{R}^m)$ means that the statement of Definition 2 holds with both norms taken to be $\|\cdot\|_{H^1}$. We refer to [39] for a proof of this result in case f depends only on u, but satisfies weaker assumptions than Lipschitz boundedness. For the version above see [66]. Note that (37) includes the important example of the viscous Burgers equation where $f(v) = vv_x$.

Proof (general idea from [39]): Nonlinear change of coordinates

$$v \to (\gamma,\tilde{v}) \quad \text{where} \quad v = \bar{v}(\cdot-\gamma)+\tilde{v}, \quad (\psi,\tilde{v})_{L^2} = 0, \tag{39}$$

where $\Lambda^*\psi = 0$ (left eigenfunction), $(\psi,\bar{v}_x)_{L^2} = 1$.
The transformed system is

$$\tilde{v}_t = QF(\tilde{v}+\bar{v}(\cdot-\gamma)), \qquad v(\cdot,0) = u_0 \tag{PDE1}$$

$$\gamma_t = R(\gamma,\tilde{v}), \qquad \gamma(0) = 0, \tag{ODE2}$$

where $Qu = u - \bar{v}_x(\psi,u)_{L^2}$ is the projector onto the orthogonal complement $\psi^\top$. The next steps are:

1. Show that the linearization $Q\Lambda$ of (PDE1) has spectrum $\mathrm{Re} \leqslant -\beta < 0$,
2. prove asymptotic stability of (PDE1) in H^1 uniformly in γ,
3. show $|\gamma_t| \leqslant Ce^{-\frac{\beta t}{2}}$ using (ODE2),
4. determine the asymptotic phase from $\gamma_\infty(\tilde{v}) = \gamma(0,\tilde{v}) + \int_0^\infty \gamma_\tau(\tau,\tilde{v})d\tau$. □

Example 3. **Nagumo equation**
As a first application we study the Nagumo wave from (5),(6). For this equation we have $u_- = 0$, $u_+ = 1$, $f(u_\pm) = 0$, $f'(u_-) = -\alpha$, $f'(u_+) = \alpha - 1$. The dispersion relation (29) leads to the two parabolas

$$S_\pm = \left\{ s = -\omega^2 + \bar{\mu}\omega + f'(u_\pm) : \omega \in \mathbb{R} \right\}, \tag{40}$$

which have their vertices at $-\alpha$ and $\alpha - 1$. Both lie in the negative half plane since $0 < \alpha < 1$, see the following Figure 6.

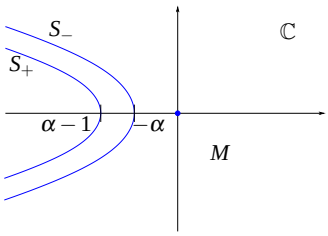

Fig. 6 Essential spectrum for the Nagumo front

Thus the spectral condition **(SC)** is satisfied. Moreover, one can show that 0 is indeed a simple eigenvalue and there are no further eigenvalues λ with $\mathrm{Re}\,\lambda > 0$ (see [39]).

Example 4 (FitzHugh-Nagumo system). As another example we mention the well studied FitzHugh-Nagumo system ([32])

$$u_t = \begin{pmatrix} u_1 \\ u_2 \end{pmatrix}_t = \begin{pmatrix} 1 & 0 \\ 0 & \varepsilon \end{pmatrix} u_{xx} + f(u) \tag{41}$$

$$f\begin{pmatrix} u_1 \\ u_2 \end{pmatrix} = \begin{pmatrix} u_1 - \frac{1}{3}u_1^3 - u_2 \\ \phi\,(u_1 + a - b u_2) \end{pmatrix}, \quad \phi, a, b > 0, \varepsilon \geqslant 0. \tag{42}$$

For an extensive study of the stability of traveling waves for this system we refer to Evans 1972–1975. We first choose parameter values $\varepsilon = 0.1$, $\phi = 0.08$, $a = 0.7$, $b = 3$ for which f has three zeros so that a traveling front occurs. For a parameter setting which leads to the classical FitzHugh Nagumo pulses, we refer to Example 7 below. Figure 7 shows the profile of both components for the traveling front (left) and a space-time plot of the first component of a solution for (41),(42) (right). In this case, we have

$$u_- = \begin{pmatrix} 1.1877 \\ 0.6292 \end{pmatrix}, \quad u_+ = \begin{pmatrix} -1.5644 \\ -0.2881 \end{pmatrix},$$

$$B_- = Df(u_-) = \begin{pmatrix} -0.4106 & -1 \\ 0.08 & -0.24 \end{pmatrix}, \quad B_+ = Df(u_+) = \begin{pmatrix} -1.4474 & -1 \\ 0.08 & -0.24 \end{pmatrix}$$

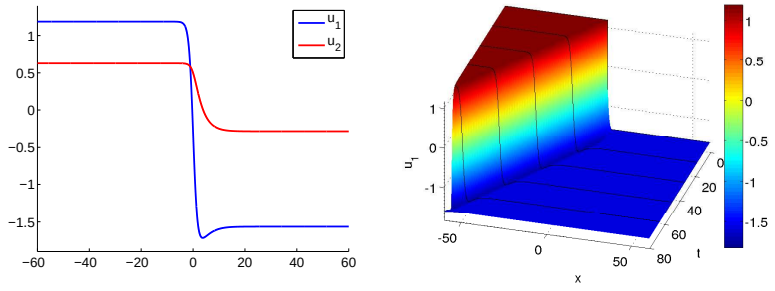

Fig. 7 Profile of the traveling wave for the FitzHugh-Nagumo system (left) and space-time diagram of u_1 (right) for $\varepsilon = 0.1$, $\phi = 0.08$, $a = 0.7$, $b = 3$.

and the dispersion relation (30) yields the two algebraic sets (cf. [10] for a drawing)

$$S_{\pm} = \left\{ s \in \mathbb{C} : \det\left(-\omega^2 \begin{pmatrix} 1 & 0 \\ 0 & \varepsilon \end{pmatrix} + i\omega B_{\pm} - sI \right) = 0 \text{ for some } \omega \in \mathbb{R} \right\}, \quad \varepsilon > 0.$$

1.7 Equivariant evolution equations

In Section 1.3 we already mentioned that traveling waves may be viewed as relative equilibria of an abstract evolution equation that has an equivariance property. In this section we will extend this abstract point of view and discuss an application to a wave which is traveling and rotating simultaneously. For some general theory of equivariant evolution equations we refer to [20],[31],[37].

As in (17) we consider the Cauchy problem for a general evolution equation

$$u_t = F(u), u(0) = u_0, \tag{43}$$

where we assume $F : Y \subset X \to X$ with X a Banach space and Y a dense subspace. The whole approach can be written in terms of Banach manifolds rather than Banach spaces. But, for the sake of simplicity, we avoid such a generalization. Note, however, that the treatment of traveling fronts already requires to use affine spaces for Y and X, compare Section 1.3.

Let G be a **Lie group**, i.e. a finite dimensional manifold with a smooth invertible group operation. By $\mathbb{1}$ we denote the unit element in G. The group operation $\circ$ induces the operators of left and right multiplication via

$$\circ : \begin{cases} G \times G \to G, \\ (\gamma, g) \to \gamma \circ g = L_{\gamma} g = R_g \gamma. \end{cases} \tag{44}$$

The Lie algebra $\mathscr{A}$ is the tangent space of G at $\mathbb{1}$, i.e. $T_{\mathbb{1}} G = \mathscr{A}$ and the derivative of the left multiplication $L_{\gamma} : G \to G$ is denoted by $dL_{\gamma}(g) : T_g G \to T_{\gamma \circ g} G$.

We further assume that the group G acts on X via

$$a: \begin{array}{ll} G \to GL[X], & a(\mathbb{1}) = I, \\ \gamma \to a(\gamma), & a(\gamma_1 \circ \gamma_2) = a(\gamma_1)a(\gamma_2). \end{array} \tag{45}$$

The evolution equation (43) is called **equivariant under the action of the group** if for all $\gamma \in G$,

$$F(a(\gamma)u) = a(\gamma)F(u) \text{ for all } u \in Y, \tag{46}$$

$$a(\gamma)Y \subset Y. \tag{47}$$

It is important to be careful with smoothness assumptions on the action. As our examples will show, it is reasonable to assume that the map $a(\cdot)v : \gamma \to a(\gamma)v$ is continuous for every $v \in X$ and continuously differentiable for every $v \in Y$. We will denote the derivative with respect to $\gamma \in G$ at $\mathbb{1}$ by

$$d\,[a(\mathbb{1})v] = d\,[a(\gamma)v]_{\gamma=\mathbb{1}} : \mathscr{A} = T_{\mathbb{1}}G \to X. \tag{48}$$

Our second example is an equation that is equivariant with respect to a two-dimensional Lie group.

Example 5 (Quintic-cubic Ginzburg Landau equation (QCGL)).

$$\begin{aligned} &u_t = \alpha u_{xx} + f(|u|^2)u, \quad u(x,t) \in \mathbb{C}, \quad \alpha \in \mathbb{C}, \\ &f(|u|^2) = \gamma|u|^4 + \beta\,|u|^2 + \delta, \quad \beta, \gamma, \delta \in \mathbb{C}. \end{aligned} \tag{49}$$

Note that $u(x,t)$ is complex-valued in this case. But we can rewrite (49) as a real system of dimension 2 which turns out to be parabolic in case $\operatorname{Re}\alpha > 0$. Suitable function spaces for this case are $X = C_{\text{unif}}(\mathbb{R},\mathbb{C})$, $Y = C^2_{\text{unif}}(\mathbb{R},\mathbb{C})$. Now the Lie group is $G = \mathbb{R} \times S^1 \ni (\tau,\theta)$ with the action given by

$$\begin{aligned} a(\tau,\theta)v(x) &= e^{-i\theta}v(x-\tau), && v \in X, \\ d\,[a(0,0)v]\,(\mu_\tau,\mu_\theta) &= -\mu_\tau v_x - i\mu_\theta v, && (\mu_\tau,\mu_\theta) \in \mathscr{A} = \mathbb{R}^2. \end{aligned} \tag{50}$$

Relative equilibria are of the form $u(x,t) = e^{-i\mu_\theta t}\overline{v}(x-\mu_\tau t)$ where μ_τ and μ_θ denote translational and rotational velocities, respectively. If both velocities are different from zero then we have a wave that rotates and travels simultaneously. In fact, for the parameter setting

$$\alpha = \frac{1+i}{2}, \quad \delta = -\frac{1}{2}, \quad \beta = \frac{5}{2} + i, \quad \gamma = -1 - \frac{i}{10},$$

the QCGL exhibits a rotating pulse ($\mu_\theta \neq 0$, $\mu_\tau = 0$) as well as a rotating and traveling wave ($\mu_\theta \neq 0$, $\mu_\tau \neq 0$). The real and imaginary parts of both types of solutions are shown in Figure 8 and 9. When hitting the boundary with Neumann boundary conditions, the pulse stops traveling but keeps rotating. Finally, recall that a relative equilibrium $\overline{v}$, $\overline{\mu} = (\mu_\tau,\mu_\theta)$ of the QCGL satisfies

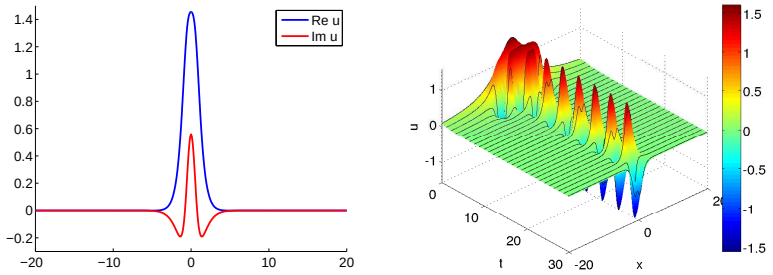

Fig. 8 Profile of the rotating wave of the QCGL (left) and space-time diagram of Reu (right) for $\alpha = \frac{1+i}{2}$, $\delta = -\frac{1}{2}$, $\beta = \frac{5}{2}+i$, $\gamma = -1-\frac{i}{10}$

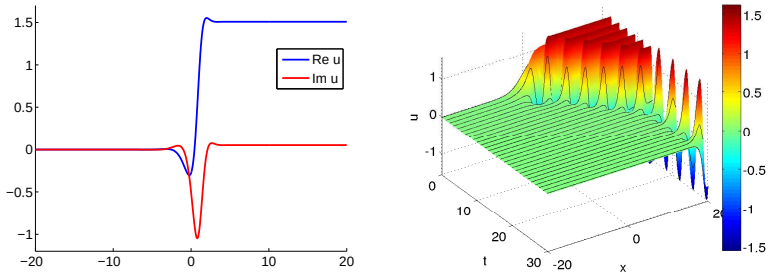

Fig. 9 Profile of the rotating and traveling wave of the QCGL (left) and space-time diagram of Reu (right) for $\alpha = \frac{1+i}{2}$, $\delta = -\frac{1}{2}$, $\beta = \frac{5}{2}+i$, $\gamma = -1-\frac{i}{10}$

$$0 = \alpha v_{xx} + f(|v|^2)v + \mu_\tau v_x + i\mu_\theta v. \tag{51}$$

We also point out that the stability theory outlined in Section 1.6 applies only to pulses for which $\lim_{x\to\pm\infty} \overline{v}(x) = 0$.

1.8 Summary

Let us summarize the results of this section:

- Traveling pulses and fronts can be computed from heteroclinic resp. homoclinic orbits of dynamical systems,
- Traveling fronts and pulses may be viewed as relative equilibria with respect to shift equivariance, this is a special case of abstract equivariant evolution equations,
- Nonlinear stability of traveling waves in Sobolev spaces can be derived from linear stability via a nonlinear change of coordinates,
- Linearized differential operators may have essential as well as point spectrum,

- The essential spectrum can be handled theoretically via the dispersion relation, while determining point spectrum often needs numerical computations,
- Nonlinear stability theory does not directly apply to waves that travel and rotate simultaneously.

2 Stability of traveling waves and the freezing method

In the previous lecture we already studied the stability of traveling waves with asymptotic phase. Our main assumptions are concerned with spectral properties of the differential operator that arises by linearizing about the profile of the wave. The basic idea is to transform into a coordinate system that moves with the velocity of the wave and then to perform a nonlinear transformation which allows to study the exponential decay towards the profile and the dynamics of the phase separately. All these transformations assume the knowledge of the exact wave and hence are not suitable for numerical calculations. In this section we study a numerical method that allows to circumvent this problem: the *freezing method*. The method was independently proposed in [58], [13]. Meanwhile, it has been extended to a variety of time-dependent partial differential equations, see [14], [15], and applied to control problems, for example [1]. There is also a parallel development by Cvitanović and co-workers (see [33] for a recent review and an application to a 5-dimensional Lorenz system), where the term 'method of sclices' is used for essentially the same approach.

The method introduces new time-dependent coordinates both in the underlying Lie group and in the function space. The extra degrees of freedom in the group is compensated by a corresponding number of phase conditions that try to keep the current profile as constant as possible. Altogether, one has to solve a partial differential algebraic equation (PDAE). For solutions of Cauchy problems that are close to relative equilibria this allows to adaptively compute moving coordinate systems within which the wave is *frozen*. Simultaneously, the flow on the group provides information about the speed and location of the original profile. The method can be formulated for equivariant evolution equations in general and thus has a wide range of applications. In this section we emphasize stability issues of the freezing method. In particular, we show that stability with asymptotic phase for a traveling wave turns into classical Lyapunov stability for the PDAE formulation.

2.1 Moving frames: the freezing method and phase conditions

Consider the Cauchy problem associated with (15),

$$u_t = Au_{xx} + f(u,u_x), \quad u(x,0) = u_0(x), \quad x \in \mathbb{R},\, t \geqslant 0. \tag{52}$$

The idea of the freezing method is to introduce new unknowns $v(x,t) \in \mathbb{R}^m$, $\gamma(t) \in \mathbb{R}$, such that the solution of (52) is of the form

$$u(x,t) = v(x-\gamma(t),t),\ x \in \mathbb{R},\ t \geqslant 0. \tag{53}$$

Inserting the ansatz into (52) and introducing $\mu(t) = \gamma_t(t)$ leads to a Cauchy problem for the position $\gamma(t)$ and the profile $v(\cdot,t)$,

$$\begin{aligned} v_t &= Av_{xx} + f(v,v_x) + \mu(t)v_x, \quad && v(\cdot,0) = u_0, \\ \gamma_t &= \mu(t), && \gamma(0) = 0. \end{aligned} \tag{54}$$

We note the similarity to equations (PDE1),(ODE2), but now we have not reduced the function space for v. Therefore, the system is not yet well posed. We compensate the extra variable $\mu(t)$ by an extra condition which is called a **phase condition** as in (12). There, the phase condition was used to remove the ambiguity in the traveling wave profile. Here, we use it to keep the time-dependent solution as constant as possible. We consider two possible choices for the phase condition, both based on a minimization principle.

1. **Fixed phase condition**
   Choose a template function $\hat{v} \in X$ where X is the underlying function space for solutions $u(\cdot,t), v(\cdot,t)$. As an example take the affine space $X = w + H^1(\mathbb{R},\mathbb{R}^m)$ where $w : \mathbb{R} \to \mathbb{R}^m$ is smooth and bounded and has the desired limit behavior $\lim_{x\to\pm\infty} w(x) = u_\pm$, cf. (7). In this case one may choose $\hat{v} = w$ or $\hat{v} = u_0 \in X$. The phase condition requires $\hat{v}$ to be the closest point to $v(\cdot,t)$ on the group orbit $\{\hat{v}(\cdot - g) : g \in \mathbb{R}\}$, i.e.

$$\min_{g\in\mathbb{R}} \|v(\cdot,t) - \hat{v}(\cdot - g)\|_{L^2} = \|v(\cdot,t) - \hat{v}(\cdot)\|_{L^2}. \tag{55}$$

   The necessary condition is (cf. (12))

$$0 = \frac{d}{dg}\|v(\cdot,t) - \hat{v}(\cdot - g)\|^2_{L^2}|_{g=0} = 2(v(\cdot,t) - \hat{v}, \hat{v}_x)_{L^2}. \tag{56}$$

   Thus, instead of (52) the freezing method solved the following partial differential algebraic equation (PDAE)

$$\begin{aligned} v_t &= Av_{xx} + f(v,v_x) + \mu(t)v_x, \quad && v(\cdot,0) = u_0, \\ 0 &= (v - \hat{v}, \hat{v}_x)_{L^2} && \\ \gamma_t &= \mu(t), && \gamma(0) = 0. \end{aligned} \tag{57}$$

   This is a PDAE of index 2. Differentiating the constraint with respect to t and inserting the PDE leads to

$$\begin{aligned} v_t &= Av_{xx} + f(v,v_x) + \mu v_x, && v(\cdot,0) = u_0, \\ 0 &= \mu(v_x,\hat{v}_x)_{L^2} + (Av_{xx} + f(v,v_x),\hat{v}_x)_{L^2} = \psi_{\text{fix}}(v,\mu) \\ \gamma_t &= \mu(t), && \gamma(0) = 0. \end{aligned} \tag{58}$$

If $(v_x,\hat{v}_x)_{L^2} \neq 0$ the constraint can be solved for μ and hence (58) is a PDAE of index 1.

2. **Orthogonality phase condition**
Here we select the phase shift such that $\|v_t(\cdot,t)\|_{L^2}$ is minimal at each time instance t, i.e.

$$\begin{aligned} 0 = \frac{d}{d\mu}\|v_t(\cdot,t)\|_{L^2}^2|_{\mu=\mu(t)} &= \frac{d}{d\mu}\|Av_{xx} + f(v,v_x) + \mu v_x\|_{L^2}^2|_{\mu=\mu(t)} \\ &= 2\left[\mu(t)(v_x,v_x)_{L^2} + (Av_{xx} + f(v,v_x),v_x)_{L^2}\right]. \end{aligned} \tag{59}$$

Therefore, instead of (52) we solve the PDAE

$$\begin{aligned} v_t &= Av_{xx} + f(v,v_x) + \mu v_x, && v(\cdot,0) = u_0, \\ 0 &= \mu(v_x,v_x)_{L^2} + (Av_{xx} + f(v,v_x),v_x)_{L^2} = \psi_{\text{orth}}(v,\mu), \\ \gamma_t &= \mu(t), && \gamma(0) = 0. \end{aligned} \tag{60}$$

This PDAE is of index 1 provided $(v_x,v_x)_{L^2} \neq 0$, i.e. if v is nonconstant. Note that ψ_{orth} differs from ψ_{fix} only in replacing the template function $\hat{v}$ by v. Since (60) requires no previous knowledge of a template it is easier to apply far away from any traveling wave. However, close to a traveling wave, the system (58) turns out to be more robust, in particular when fixing $\hat{v} = v(\cdot,T)$ at some later time T and leaving it constant from then on.

To summarize, we replace (52) by a PDAE of the general form

$$\begin{aligned} v_t &= Av_{xx} + f(v,v_x) + \mu v_x, \quad v(\cdot,0) = u_0, \\ 0 &= \psi(v,\mu) \\ \gamma_t &= \mu(t), \qquad\qquad \gamma(0) = 0, \end{aligned} \tag{61}$$

where $\psi : X \times \mathbb{R} \to \mathbb{R}$. Using a proper notion of solutions, one can show that any solution of (61) leads to a solution of (52) via (53), cf. [13],[53]. Conversely, if $u(\cdot,t)$ solves (52) then we obtain a solution of (61), provided the implicit ODE

$$\psi(u(\cdot+\gamma(t),t),\gamma_t(t)) = 0, \quad \gamma(0) = 0$$

has a unique solution $\gamma(t)$ on the interval under consideration.

2.2 Numerical experiments with traveling fronts and pulses

For numerical computations we solve the PDAE (61) on a large interval $J = [x_-, x_+]$, and we use two-point boundary conditions given by a map $\mathscr{B} : \mathbb{R}^{4m} \to \mathbb{R}^{2m}$,

$$\begin{aligned} v_t &= Av_{xx} + f(v, v_x) + \mu v_x \text{ in } J \times [0,\infty), & v(\cdot,0) &= u_0|_J, \\ 0 &= \psi_J(v,\mu), & \mathscr{B}((v,v_x)(x_-),(v,v_x)(x_+)) &= 0, \\ \gamma_t &= \mu(t), & \gamma(0) &= 0. \end{aligned} \tag{62}$$

Examples for $\mathscr{B}$ are Neumann boundary conditions $\mathscr{B}((v,v_x)(x_-),(v,v_x)(x_+)) = (v_x(x_-),v_x(x_+))$ and projection boundary conditions (cf. (14), note that $\mu(t)$ enters into the projection matrices).

Example 6 (Nagumo equation). Our first example is the Nagumo equation (5),

$$\begin{aligned} v_t &= v_{xx} + v(1-v)(v-\alpha) + \mu v_x, & v(\cdot,0) &= u_0|_J, \\ 0 &= \psi_J(v,\mu) \\ \gamma_t &= \mu(t), & \gamma(0) &= 0, \end{aligned} \tag{63}$$

with parameter $\alpha = \frac{1}{4}$, solved on $J = [-50,50]$, with $\triangle x = 0.1$, $\triangle t = 0.1$ For the nonfrozen system on $J = [x_-, x_+]$, the front forms and travels to the left as we expect, see Figure 10(a). When it reaches the boundary it dies out due to Neumann

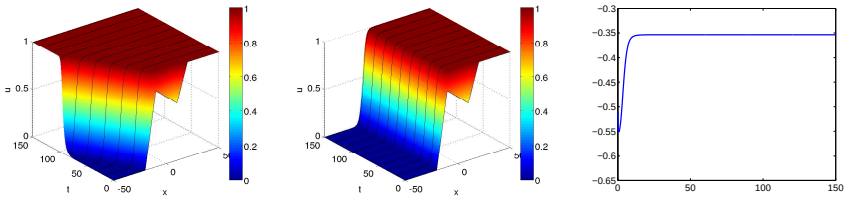

(a) (b) (c)

Fig. 10 Traveling front $u(x,t)$ of the original Nagumo equation (a), solution $v(x,t)$ of the frozen Nagumo equation (b), time dependence of velocity $\mu(t)$ (c). Piecewise linear initial function, Neumann boundary conditions, fixed phase condition with reference function $\hat{v} = u_0$ and parameter value $\alpha = \frac{1}{4}$.

boundary conditions. On the contrary, the front stabilizes for the frozen system, see Figure 10(b), the variable $\mu(t)$ approaches the final speed $\bar{\mu} = -\frac{\sqrt{2}}{4}$ of the front, see Figure 10(c), while the value of $\gamma(t)$ still indicates the position of the front on the real line.

Our conclusion is that the longtime behavior of the initial boundary value problem on the finite interval (62) can be completely different from the behavior of the original system (52) when truncated to the same interval, although on the infinite

line both systems are equivalent. The freezing method aims at a moving coordinate system in which a pattern close to the initial data becomes stationary, and this behavior is stable under truncation to a bounded domain. In the following subsections we will provide theorems which make this observation rigorous.

Example 7 (FitzHugh-Nagumo system). Our second example is the FitzHugh-Nagumo system, which in the frozen form reads

$$\begin{aligned} v_t &= Av_{xx} + f(v) + \mu v_x, & v(\cdot,0) &= v_0, \\ 0 &= \psi_J(v,\mu), & \mathscr{B}((v,v_x)(x_-),(v,v_x)(x_+)) &= 0, \\ \gamma_t &= \mu(t), & \gamma(0) &= 0. \end{aligned} \tag{64}$$

with $v = (v_1, v_2)^T$,

$$A = \begin{pmatrix} 1 & 0 \\ 0 & \varepsilon \end{pmatrix}, \quad f(v) = \begin{pmatrix} v_1 - \frac{1}{3}v_1^3 - v_2 \\ \phi\,(v_1 + a - bv_2) \end{pmatrix},$$

parameters $\varepsilon = 0.1$, $a = 0.7$, $b = 0.8$, $\phi = 0.08$, solved on $J = [-60, 60]$, with $\triangle x = 0.1$, $\triangle t = 0.1$. For these parameter values, the function f admits only one zero at $(v_1, v_2)^T = (-1.1994, -0.6243)^T$ and pulses occur. Note that (64) is a parabolic system due to $\varepsilon > 0$. The case $\varepsilon = 0$ leads to a coupled hyperbolic-parabolic system with principal term being $\mu v_{2,x}$ in the second equation. We consider such mixed systems later in Section 3. Starting with a ramp-like function for the voltage v_1,

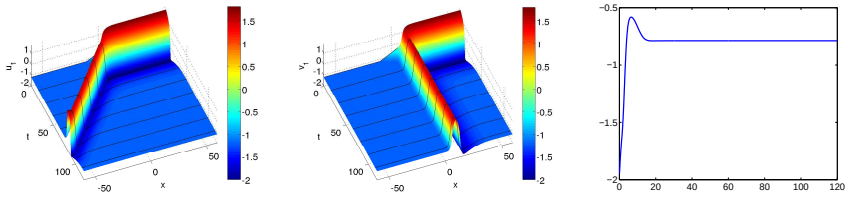

(a) (b) (c)

Fig. 11 u_1 component of traveling pulse (a) of the nonfrozen and v_1 component of frozen pulse (b) with velocity $\mu(t)$ (c) of the frozen FitzHugh-Nagumo system with piecewise linear initial function, Neumann boundary conditions, fixed phase condition with reference function $\hat{v} = u_0$ and parameter values $\varepsilon = 0.1$, $a = 0.7$, $b = 0.8$, $\phi = 0.08$.

the pulse forms as expected and travels to the left until it dies out at the boundary, see Figure 11(a). On the contrary, as above the freezing method captures the shape of the pulse and makes it stationary, see Figure 11(b). Simultaneously, the correct speed of the pulse is attained by the variable $\mu(t)$, which tends to $\bar{\mu} = -0.7892$, see Figure 11(c).

An interesting phenomenon happens when the system is started with a pulse-like initial function. Then two pulses develop, one traveling to the left, the other traveling

to the right, see Figure 12(a). Which of these two traveling pulses is captured by the freezing system, is unpredictable and can be affected, for instance, by the solver tolerances. In this example, the fixed phase condition happens to freeze the left going pulse while the right going one dies out at the boundary, see Figure 12(b). The velocity $\mu(t)$ of the left frozen pulse nears $\bar{\mu} = -0.7892$, see Figure 12(d). On the contrary, the orthogonal phase condition freezes the right going pulse and the left going one dies out, see Figure 12(c). The velocity $\mu(t)$ of the right frozen pulse tends to $\bar{\mu} = 0.7892$, see Figure 12(e) as expected.

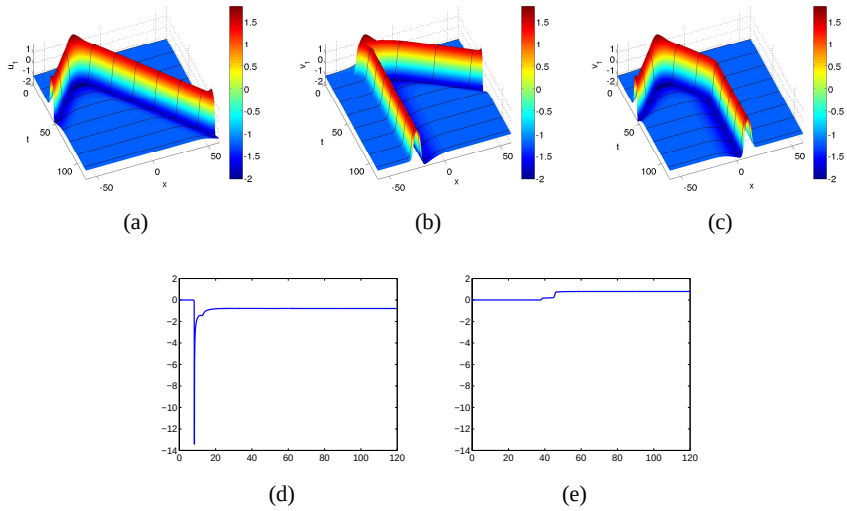

Fig. 12 u_1-component of traveling wave of the nonfrozen system (a) for a pulse-like initial function in the FitzHugh-Nagumo system. v_1-component of frozen pulse with fixed phase condition (b) and orthogonal phase condition (c). Figures (d) and (e) show the time dependence of the velocity $\mu(t)$ for cases (b) and (c), respectively. For all plots Neumann boundary conditions and the reference function $\hat{v} = u_0$ are used, parameter values are $\varepsilon = 0.1$, $a = 0.7$, $b = 0.8$, $\phi = 0.08$.

The experiments from Example 7 show two new problems that will be dealt with in the following lectures.

1. For parabolic systems coupled to ODEs, the freezing method leads to mixed hyperbolic-parabolic systems with the newly introduced convection term entering the principal part of the equation. The stability theory for such systems is much more subtle than for parabolic systems (cf. Section 1.6) and will be topic of Section 3.
2. When the solutions exhibit multiple fronts and pulses, there is no longer a common moving frame in which the patterns become stationary. The freezing method then tends to capture one of the patterns and let the others travel towards the boundary. In Section 5 we discuss an extension of the freezing method that al-

lows to handle multiple coordinate frames and to deal with weak and strong interactions of patterns.

2.3 Error analysis of numerical approximations

The experiments of the previous subsection suggest that the PDAE formulation (61) is robust with respect to numerical approximations such as truncation to a bounded interval with two-point boundary conditions and subsequent discretization of time and space. Such expectations have been made rigorous in the work of V. Thümmler [66],[68],[67]. It is shown in [68] in which sense relative equilibria of parabolic systems are inherited by numerical discretizations, and in [67] conditions are set up that guarantee asymptotic stability of these discretized equilibria. Moreover, the exponential rate of convergence is proved to be independent of the truncated interval and of the step-size used. Below we will only consider the case of traveling waves and indicate the main results. We also mention the paper [5] where the nonlocal equations obtained by eliminating μ from the phase condition in (61), have been treated directly by truncation to a finite interval.

We consider a finite difference approximation of the PDAE (57) on an equidistant grid $J_h = \{x_n = nh : n = n_-, \dots, n_+\}$ with step-size $h > 0$. For functions $v_n = v(x_n), x_n = nh$, defined on an extended grid $J_h^e = \{nh : n = n_- - 1, \dots, n_+ + 1\}$, we use standard difference quotients as follows,

$$\begin{aligned}
\delta_+ v_n &= \frac{1}{h}(v_{n+1} - v_n), \quad n = n_- - 1, \dots, n_+, \\
\delta_- v_n &= \frac{1}{h}(v_n - v_{n-1}), \quad n = n_-, \dots, n_+ + 1, \\
\delta_+ \delta_- v_n &= \frac{1}{h^2}(v_{n-1} - 2v_n + v_{n+1}), \quad n = n_-, \dots, n_+, \\
\delta_0 v_n &= \frac{1}{2}(\delta_+ v_n + \delta_- v_n), \quad n = n_-, \dots, n_+.
\end{aligned}$$

Leaving time continuous, a spatial discretizaton of (57) leads to the following DAE:

$$\begin{aligned}
v_{n,t} =& A\delta_+\delta_- v_n + f(v_n, \delta_0 v_n) + \mu \delta_0 v_n, \quad n = n_-, \dots, n_+, \\
0 =& (\delta_0 \hat{v}, v - \hat{v})_{L^2(J_h)} \\
\eta =& P_- v_{n_-} + Q_- \delta_0 v_{n_-} + P_+ v_{n_+} + Q_+ \delta_0 v_{n_+},
\end{aligned} \tag{65}$$

where $P_\pm, Q_\pm \in \mathbb{R}^{2m,m}$ are given boundary matrices and $\eta = P_- u_- + P_+ u_+$ (see Section 1.3 for $u_\pm$). Here and in the following we use discrete analogs $L^2(J_h)$, $H^1(J_h)$, $H^2(J_h)$ of the Sobolev spaces $L^2(J,\mathbb{R}^m), H^1(J,\mathbb{R}^m), H^2(J,\mathbb{R}^m)$. The following conditions are imposed on the continuous problem.

Cont1: The function $\overline{v} \in w + H^2(\mathbb{R},\mathbb{R}^m)$ (cf. (18)) is a traveling wave of speed $\overline{\mu} \in \mathbb{R}$ for equation (15) such that $u_\pm = \lim_{x\to\pm\infty} \overline{v}(x)$.

Cont2: The nonlinearity f satisfies the condition (37) from Theorem 3.
Cont3: 0 is a simple eigenvalue of the linearized operator Λ from (23), and 0 lies in the set M defined in Theorem 1.

Note that the condition $0 \in M$ is weaker than the spectral condition **SC** (cf. (33)) which requires $\{\mathrm{Re}\, z \geq -\beta\} \subset M$. It implies that the quadratic eigenvalue problems $(\lambda^2 A + \lambda B_\pm + C_\pm)y = 0$ have m eigenvalues with real part positive and m with real part negative. More precisely, there are matrices $Y^s_\pm, \Lambda^s_\pm \in \mathbb{R}^{m,m}$ which solve the quadratic invariant subspace equation,

$$AY^s_\pm(\Lambda^s_\pm)^2 + B_\pm Y^s_\pm \Lambda^s_\pm + C_\pm Y^s_\pm = 0, \quad \mathrm{Re}\,(\sigma(\Lambda^s_\pm)) < 0. \tag{66}$$

such that $\mathrm{rank}\begin{pmatrix} Y^s_\pm \\ Y^s_\pm \Lambda^s_\pm \end{pmatrix} = m$. Similarly, there exist $Y^u_\pm, \Lambda^u_\pm \in \mathbb{R}^{m,m}$ satisfying the same conditions except $\mathrm{Re}\,(\sigma(\Lambda^u_\pm)) > 0$. The next two conditions impose a coupling between boundary matrices and data of the continuous problem.
Discrete 1: $\eta = P_- u_- + P_+ u_+$ (consistency of boundary values)
Discrete 2: $\det\left(\begin{pmatrix} P_- & Q_- \end{pmatrix} \begin{pmatrix} Y^s_- \\ Y^s_- \Lambda^s_- \end{pmatrix} \middle| \begin{pmatrix} P_+ & Q_+ \end{pmatrix} \begin{pmatrix} Y^u_+ \\ Y^u_+ \Lambda^u_+ \end{pmatrix} \right) \neq 0$

Condition **Discrete 2** ensures that modes increasing at $\pm\infty$ can be controlled by the boundary conditions, see [10]. Note that the columns of $\begin{pmatrix} Y^s_- \\ Y^s_- \Lambda^s_- \end{pmatrix}$ determine growing solutions of (the first order version of) Λ at $-\infty$ while those of $\begin{pmatrix} Y^u_+ \\ Y^u_+ \Lambda^u_+ \end{pmatrix}$ determine growing solutions at $+\infty$.

Theorem 4. *([68]) Assume **Cont1-3**, let $\hat{v} \in w + H^2(\mathbb{R}, \mathbb{R}^m)$ be a template function such that $(\bar{v}_x, \hat{v}_x)_{L^2} \neq 0$ and let the boundary matrices satisfy **Discrete1,2**. Then there exist $C, \rho, T, h_0, \alpha > 0$ such that the DAE* (65) *has a steady state (v^h, μ^h) for all $0 < h \leq h_0$, $T \leq \min(n+, -n_-)h$ which is unique in the ball*

$$\left\| \bar{v}|_{J_h} - v^h \right\|_{H^2(J_h)} + |\bar{\mu} - \mu^h| \leq \rho.$$

Moreover the following error estimate holds

$$\left\| \bar{v}|_{J_h} - v^h \right\|_{H^2(J_h)} + |\bar{\mu} - \mu^h| \leq C\left[h^2 + \exp(-\alpha h \min(n_+, -n_-))\right]. \tag{67}$$

The estimate (67) shows, that the errors due to finite difference approximation and truncation to a bounded interval simply add up. Under the extra conditions that $\hat{v}$ decays exponentially as $x \to \pm\infty$, one can show (see [68, Th.2.6]) that the linearization of the right hand side of (65) at (v^h, μ^h) has an eigenvalue close to 0 and an eigenfunction close to $\bar{v}_x|_{J_h}$ with the same estimate as in (67).

For a stronger statement on the asymptotic stability of the 'discrete traveling wave' (v^h, μ^h), more conditions are needed (see [67]). In particular, the assumptions of the Stability theorem 3 are assumed to hold. Further, condition **Discrete 2** now is strengthened to

$$\det\left(\begin{pmatrix} P_- & Q_- \end{pmatrix} \begin{pmatrix} Y_-^s(s) \\ Y_-^s(s)\Lambda_-^s(s) \end{pmatrix} \middle| \begin{pmatrix} P_+ & Q_+ \end{pmatrix} \begin{pmatrix} Y_+^u(s) \\ Y_+^u(s)\Lambda_+^u(s) \end{pmatrix} \right) \neq 0, \quad \mathrm{Re}\,(s) \geq -\beta, \tag{68}$$

where $Y_\pm^s = Y_\pm^s(s)$, $\Lambda_\pm^s = \Lambda_\pm^s(s)$ solve the s-dependent equation

$$AY_\pm^s(\Lambda_\pm^s)^2 + B_\pm Y_\pm^s \Lambda_\pm^s + (C_\pm - sI)Y_\pm^s = 0, \quad \mathrm{Re}\,(\sigma(\Lambda_\pm^s)) < 0, \tag{69}$$

cf. (66). Under a final condition on the Dirichlet and Neumann parts of the boundary matrices (see [67, Hypothesis 2.6]), the following estimate holds for the solutions $v_n(t), \mu(t)$ of the time-dependent DAE (65),

$$\|v(t) - v^h\|_{H^1(J_h)} + |\mu(t) - \mu^h| \leq Ce^{-\alpha t}, \quad t \geq 0,\ h \leq h_0,\ \pm n_\pm h > T, \tag{70}$$

provided $\|v(0) - v^h\|_{H^1(J_h)} \leq \rho$ and v^0, μ^0 are consistent initial values (cf. [67, Sec.2.1]). It is worth noting that all constants C, ρ, α, T in this result do neither depend on the step-size h nor on the values of n_-, n_+. While the extra condition [67, Hypothesis 2.6] is satisfied for all standard choices such as Dirichlet, Neumann or periodic boundary conditons, condition (68) is essential for the stability of the discretized traveling wave. As shown in [67, Sec.5.2] by a counterexample, violating (68) at one value of s can destabilize the discrete wave by spurious oscillations while the continuous wave is perfectly stable.

2.4 The freezing method in an abstract setting

The freezing method of the previous section can be generalized to equivariant evolution systems on Banach manifolds, see [14],[68]. For simplicity, we consider here the setting of Banach spaces as in Section 1.7. Generalizing (53), the solution of (43) is written as

$$u(t) = a(\gamma(t))v(t), \quad \gamma(t) \in G, v(t) \in Y. \tag{71}$$

Then, $a(\gamma)F(v) = F(a(\gamma)v) = F(u) = u_t = a(\gamma)v_t + d[a(\gamma)v]\gamma_t$ holds and hence

$$v_t = F(v) - a(\gamma)^{-1} d[a(\gamma)v]\gamma_t. \tag{72}$$

It is convenient to introduce $\mu(t) \in \mathscr{A} = T_{\mathbb{1}}G$ via $\gamma_t(t) = dL_{\gamma(t)}\mu(t)$. Then differentiating $a(\gamma)a(g)v = a(L_\gamma g)v$ with respect to $g \in G$ at $g = \mathbb{1}$ leads to $a(\gamma)d[a(\mathbb{1})v]\mu = d[a(\gamma)v]dL_\gamma(\mathbb{1})\mu$. Therefore, (72) can be rewritten as $v_t = F(v) - d[a(\mathbb{1})v]\mu$. Finally, we add $\dim G$ phase conditions $\psi(v,\mu) = 0$ defined by a functional $\psi : Y \times \mathscr{A} \to \mathscr{A}^*$. This leads to the abstract formulation of the freezing method as differential algebraic evolution equation (DAEV)

$$\begin{aligned} v_t &= F(v) - d[a(\mathbb{1})]v]\mu, \quad v(0) = u_0, \\ 0 &= \psi(v,\mu), \\ \gamma_t &= dL_\gamma \mu, \qquad\qquad\qquad \gamma(0) = \mathbb{1}. \end{aligned} \tag{73}$$

The last equation of this system is called the **reconstruction equation** in [58]. It is decoupled from the first two equations and can be solved in a post-processing step in order to obtain the orbit within the group. If a continuous inner product $(\cdot,\cdot)_X$ on X is given, the two phase conditions discussed in Section 2.1, generalize to

$$(d[a(\mathbb{1})\hat{v}]\lambda, v - \hat{v})_X = 0 \quad \text{for all } \lambda \in \mathscr{A}, \tag{74}$$

$$(d[a(\mathbb{1})v]\lambda, v_t)_X = 0 \quad \text{for all } \lambda \in \mathscr{A}, \tag{75}$$

see Figure 13. Differentiating (74) with respect to t and inserting the differential

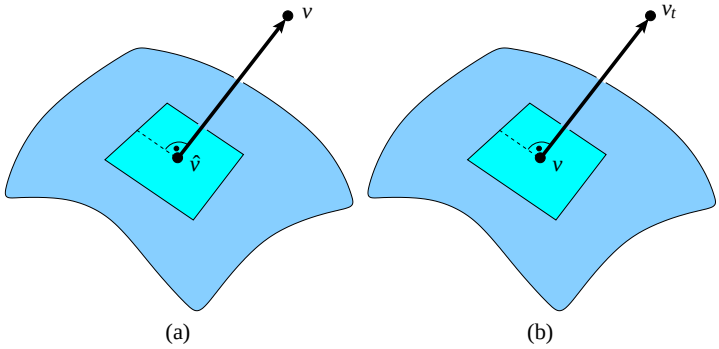

Fig. 13 Illustration of fixed phase condition $v - \hat{v} \perp T_{\hat{v}}\mathscr{O}(\hat{v}) = \mathscr{R}(d[a(\mathbb{1})\hat{v}])$ with group orbit $\mathscr{O}(\hat{v}) = \{a(\gamma)\hat{v} : \gamma \in G\}$ (a), illustration of orthogonal phase condition $v_t \perp T_v\mathscr{O}(v) = \mathscr{R}(d[a(\mathbb{1})v])$ with group orbit $\mathscr{O}(v)$ (b).

equation from (73) into both, leads to the phase fixing operators (cf. (58),(60))

$$\psi_{\text{fix}}(v,\mu)\lambda = (d[a(\mathbb{1})\hat{v}]\lambda, F(v))_X - (d[a(\mathbb{1})\hat{v}]\lambda, d[a(\mathbb{1})v]\mu)_X, \quad \lambda \in \mathscr{A}, \tag{76}$$

$$\psi_{\text{orth}}(v,\mu)\lambda = (d[a(\mathbb{1})v]\lambda, F(v))_X - (d[a(\mathbb{1})v]\lambda, d[a(\mathbb{1})v]\mu)_X, \quad \lambda \in \mathscr{A}. \tag{77}$$

If the map $d[a(\mathbb{1})v] : \mathscr{A} \to X$ is one to one, then the linear system $\psi_{\text{orth}}(v,\mu) = 0$ has a unique solution $\mu \in \mathscr{A}$ and hence (73) is a DAEV of index 1.

2.5 A numerical experiment with a two-dimensional group

Example 8 (Quintic-cubic Ginzburg Landau equation (QCGL)). As an example we treat the quintic-cubic Ginzburg Landau equation from example 2. With the group

operations from (50) the DAEV (73) with $\psi = \psi_{\text{fix}}$ yields the following PDAE to be solved

$$\begin{aligned} v_t &= \alpha v_{xx} + f(|v|^2)v + \mu_1 v_x + \mu_2 iv, && v(0) = u_0, \\ 0 &= (\hat{v}_x, v - \hat{v})_{L^2} = (iv, v - \hat{v})_{L^2} = 0, \\ \tau_t &= \mu_1, \ \theta_t = \mu_2, && \tau(0) = \theta(0) = 0. \end{aligned} \tag{78}$$

For the parameter values

$$\alpha = 1, \quad \beta = 3 + i, \quad \gamma = 3 + i, \quad \delta = -2.75 + i, \tag{79}$$

one finds a rotating pulse with translational velocity $\bar{\mu}_1 = 0$ and rotational velocity $\bar{\mu}_2 =$, see Figure 14(a)-(c), and a pulse that rotates and travels simultaneously with

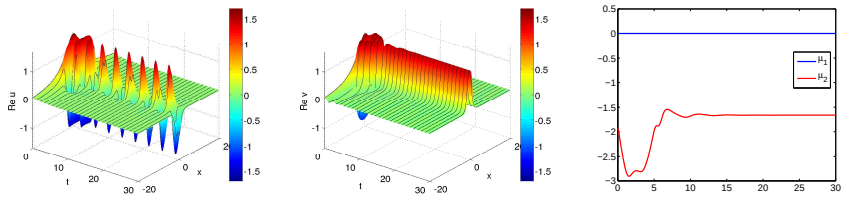

(a) (b) (c)

Fig. 14 Real part of the rotating pulse $u(x,t)$ of the nonfrozen system (a) and of the frozen pulse $v(x,t)$ (b), with velocities (μ_1, μ_2) (c) for the frozen QCGL. Solution by COMSOL Multiphysics with piecewise linear finite elements, Neumann boundary conditions, fixed phase condition with template function $\hat{v} = u_0$ and parameter values from (79).

translational velocity $\bar{\mu}_1 = 1.18$ and $\bar{\mu}_2 = -2.801$, see Figure 15(a)-(c). In both

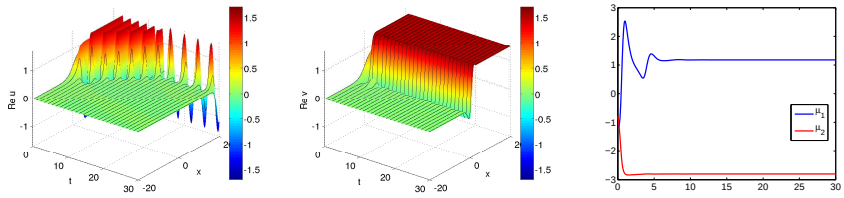

(a) Reu (b) Rev (c) μ_1, μ_2

Fig. 15 Real part of the traveling and rotating pulse $u(x,t)$ for the nonfrozen system (a) and $v(x,t)$ for the frozen system (b), time-dependence of velocities (μ_1, μ_2) (c). Further data are as in Figure 14.

cases, freezing of patterns is successful. Note, however, that the stability analysis of

[67] applies only to the first case, since the profile $v(x)$ keeps rotating as $x \to \infty$ and only its absolute value converges.

2.6 Summary

Let us summarize the main results of this section.

- The freezing method allows to automatically generate moving frames in which traveling waves become asymptotically constant.
- For the discretized PDAE formulation, one can prove existence of a 'discrete traveling wave' as well as their asymptotic stability with rates independent of the discretization parameters. For such a result one needs the original wave to satisfy the standard stability conditions and the boundary matrices to control unstable modes at $\pm\infty$.
- The freezing method generalizes to abstract equivariant evolution equations posed on a Banach manifold.
- The method successfully freezes waves in the quintic-cubic Ginzburg Landau equation that rotate and travel simultaneously.

3 Patterns in hyperbolic and hyperbolic-parabolic systems

The freezing method discussed in lecture 2, leads to challenging problems, both numerically and theoretically, when applied to hyperbolic or hyperbolic-parabolic systems.

A famous example of this type are the Hodgkin-Huxley equations for the propagation of signals in nerve axons. We will use them, both for illustrating the analytical difficulties and for showing numerical applications. In this section we survey results due to J. Rottmann-Matthes [56] on the stability of the freezing method for hyperbolic-parabolic mixed systems of rather general type. The main difficulty arises from the fact that such mixed systems generate only C^0- semigroups so that the techniques for analytic semigroups do no longer apply. Moreover, as in the Hodgkin-Huxley example, nonstrictly hyperbolic parts occur which make the stability analysis even more delicate. The essential tool in resolving these problems is the vector valued Laplace transform applied directly to the PDAE formulation and combined with rather sophisticated resolvent estimates.

We also show an application of the freezing method to Burgers equation for which equivariance includes scalings of the variables. It is then possible to freeze similarity solutions such as N-waves. However the stability of the method for this case, and for conservation laws in general, is largely unsolved.

3.1 Mixed systems and the Hodgkin-Huxley example

The spatially extended version of the Hodgkin-Huxley model from 1952 [41] serves as our standard example,

$$\begin{aligned} V_t &= \frac{a}{2R} V_{xx} - \bar{g}_K n^4 (V - V_K) - \bar{g}_{Na} m^3 h (V - V_{Na}) - \bar{g}_l (V - V_l) \\ n_t &= \alpha_n(V)\,(1-n) - \beta_n(V)\,n \\ m_t &= \alpha_m(V)\,(1-m) - \beta_m(V)\,m \\ h_t &= \alpha_h(V)\,(1-h) - \beta_h(V)\,h, \end{aligned} \tag{80}$$

The system models electric signalling in nerve cells and we refer to [41, 44]) for details of the modelling, in particular for the special form of the nonlinearities $\alpha_n, \alpha_m, \alpha_h, \beta_n, \beta_m, \beta_h$. We note that the system consists of a parabolic PDE that is coupled nonlinearly to a system of three nonlinear ODEs. It is well-known that there exists a traveling wave solution (see for example [38]), a plot of the traveling pulse is given in Figure 16.

In a co-moving frame, see (16), a term μV_x is added to the first equation, a term μn_x to the second equation and so forth. The resulting system is then **parabolic-hyperbolic**, with a hyperbolic part that is not strictly hyperbolic because of the common factor μ in the convection terms.

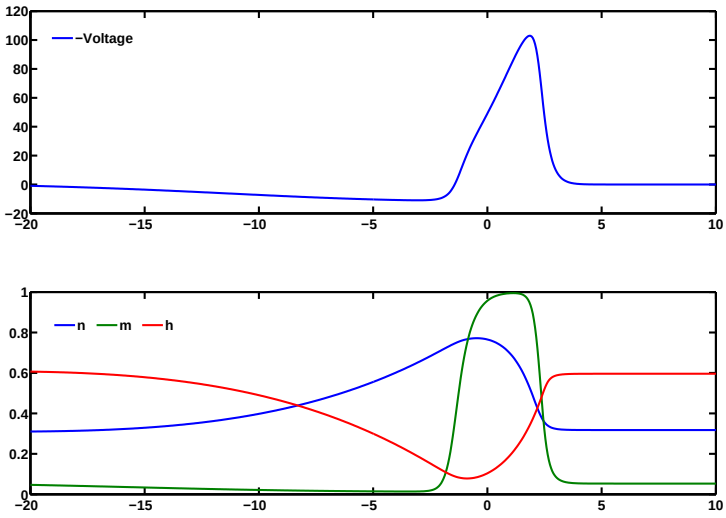

Fig. 16 Traveling pulse of the Hodgkin-Huxley equations.

In the following we analyze the asymptotic stability of traveling waves for mixed systems of the general form

$$\begin{aligned} u_t &= Au_{xx} + g(u,v)_x + f_1(u,v), \quad u(x,0) = u_0(x), \\ v_t &= Bv_x + f_2(u,v), \qquad\qquad\quad v(x,0) = v_0(x), \end{aligned} \tag{81}$$

where $u(x,t) \in \mathbb{R}^n$, $v(x,t) \in \mathbb{R}^m$. Note that (81) includes the Hodgkin-Huxley system. The following conditions are imposed on (81).

Basic Assumptions

(i) $g, f_1 \in C^3(\mathbb{R}^{n+m}, \mathbb{R}^n)$ $f_2 \in C^3(\mathbb{R}^{n+m}, \mathbb{R}^m)$,
(ii) the u–equation is parabolic, i.e. $A \in \mathbb{R}^{n,n}$ satisfies $A + A^\top \geq \alpha > 0$ in the sense of inner products,
(iii) the v–equation is hyperbolic, i.e. $B \in \mathbb{R}^{m,m}$ is diagonal,
(iv) there exists a traveling wave solution $(u,v)(x,t) = (\overline{u},\overline{v})(x - \overline{\mu}t)$ of the PDE (81) with profile $(\overline{u},\overline{v}) \in C_b^1(\mathbb{R}, \mathbb{R}^{n+m})$ and $\overline{u}_x, \overline{v}_x \in H^2(\mathbb{R}, \mathbb{R}^{n+m})$.

Remark 2. (a) In general, hyperbolicity of the second equation in (81) means that the matrix B is real diagonalizable. By a similarity transformation we can put B into diagonal form and hence assume (iii) without loss of generality.
(b) Note that assumption (iv) allows for pulse as well as front solutions.

Before proving stability of traveling waves for (81), we need existence and uniqueness of solutions to the Cauchy problem, when the initial data belong to a proper neighborhood of the traveling wave.

Theorem 5 ([56, Thm. 2.5]). *Let the **Basic Assumptions** (i)-(iv) hold. Then for all $u_0 \in \overline{u} + H^1, v_0 \in \overline{v} + H^1$ there exists a unique maximal solution of* (81)*. More precisely, there exists $T^* \in (0,\infty]$ and (u^*,v^*) such that $u = u^*|_{[0,T]}$ and $v = v^*|_{[0,T]}$ satisfy* (81) *in $L^2 \times L^2$ for a.e. $t \in [0,T]$, $0 < T < T^*$, and*

$$\begin{aligned} &u \in C([0,T]; \overline{u} + H^1) \cap L^2(0,T; \overline{u} + H^2) \cap H^1(0,T; \overline{u} + H^1), \\ &v \in C([0,T]; \overline{v} + H^1) \cap H^1(0,T; \overline{v} + H^1). \end{aligned} \tag{82}$$

Conversely, any pair (u,v) for which (82) *holds and which solves* (81) *in $L^2 \times L^2$ for a.e. $t \in [0,T]$, satisfies $u = u^*|_{[0,T]}$ and $v = v^*|_{[0,T]}$. Moreover,*

$$\textbf{\textit{either}}\ T^* = \infty\ \textbf{\textit{or}}\ \ 0 < T^* < \infty \textit{ and } \lim_{t \nearrow T^*} \|u^*(t) - \overline{u}\|_{H^1} + \|v^*(t) - \overline{v}\|_{H^1} = \infty.$$

Due to its importance, nonlinear stability of traveling waves in systems of the form (81) has been considered by many authors. We just mention a few: In a series of papers [24, 25, 26, 27] J.W. Evans presented a full analysis of Hodgkin-Huxley type equations. By a dynamical systems approach Bates and Jones [7] were able to discuss the stability of systems of the general form (81) without the $g(u,v)_x$ term. But due to a compactness argument, their result does not include the case of fronts. In [46] Kreiss et al. proved stability of traveling waves in systems of the form (81)

but they assumed strict hyperbolicity which is not satisfied for the Hodgkin-Huxley model in a co-moving frame. Finally, we mention [35], where parabolic-hyperbolic systems are considered. There the authors allow the spectrum to touch the imaginary axis, but they assume $g(u,v)_x = \widetilde{a}u_x$ for a constant matrix $\widetilde{a}$ and the v-equation is simply an ODE.

We consider (81) in a moving coordinate frame, see (16). The traveling wave then becomes a steady state of

$$\begin{aligned} u_t &= Au_{xx} + \big(g(u,v) + \overline{\mu}u\big)_x + f_1(u,v), \\ v_t &= \big(B + \overline{\mu}\big)v_x + f_2(u,v). \end{aligned} \tag{83}$$

As in Sect. 1.4, we expect stability with asymptotic phase. For notational convenience we denote $(u,v)^\top = U$ and $(\overline{u},\overline{v})^\top = \overline{U}$ and write (83) in the short form

$$U_t = F(U).$$

We aim at a result in the spirit of Theorem. 3. The linearization of (83) about the profile reads

$$\begin{aligned} u_t &= Au_{xx} + (\partial_1\overline{g} + \overline{\mu})u_x + \partial_2\overline{g}v_x + (\partial_1\overline{g}_x + \partial_1\overline{f}_1)u + (\partial_2\overline{g}_x + \partial_2\overline{f}_1)v, \\ v_t &= (B + \overline{\mu})v_x + \partial_1\overline{f}_2 u + \partial_2\overline{f}_2 v, \end{aligned} \tag{84}$$

where we abbreviate $\overline{g}(x) = g(\overline{u}(x),\overline{v}(x))$, $\partial_1\overline{g}(x) = g_u(\overline{u}(x),\overline{v}(x))$, etc.. The linear operator Λ on the right hand side of (84) has the following block structure

$$\Lambda \begin{pmatrix} u \\ v \end{pmatrix} = \begin{pmatrix} A & 0 \\ 0 & 0 \end{pmatrix} \begin{pmatrix} u \\ v \end{pmatrix}_{xx} + \begin{pmatrix} B_{11} & B_{12} \\ 0 & B_{22} \end{pmatrix} \begin{pmatrix} u \\ v \end{pmatrix}_x + \begin{pmatrix} C_{11} & C_{12} \\ C_{21} & C_{22} \end{pmatrix} \begin{pmatrix} u \\ v \end{pmatrix}. \tag{85}$$

For simplicity we abbreviate

$$\widetilde{A} := \begin{pmatrix} A & 0 \\ 0 & 0 \end{pmatrix}, \quad \widetilde{B} := \begin{pmatrix} B_{11} & B_{12} \\ 0 & B_{22} \end{pmatrix}, \quad \widetilde{C} := \begin{pmatrix} C_{11} & C_{12} \\ C_{21} & C_{22} \end{pmatrix}.$$

As we already saw in Sect. 1.5 shift equivariance implies $(\overline{u}_x,\overline{v}_x)^\top \in \mathcal{N}(\Lambda)$.

3.2 The stability theorem

Similar to Section 1 we impose the following conditions on the operator Λ.
Linear Assumptions:

(i) $A \in \mathbb{R}^{n,n}$ satisfies $A + A^\top > 0$,
(ii) $B_{22} = B + \overline{\mu}I \in \mathbb{R}^{m,m}$ is invertible,
(iii) $\widetilde{B},\widetilde{C}$ are continuously differentiable with bounded derivatives,
(iv) the limits $\lim_{x\to\pm\infty}\widetilde{B} = \widetilde{B}_\pm$ and $\lim_{x\to\pm\infty}\widetilde{C} = \widetilde{C}_\pm$ exist,

(v) if $s \in \mathbb{C}$ satisfies $\det\big(-\omega^2\widetilde{A} + i\omega\widetilde{B}_\pm + \widetilde{C}_\pm - sI\big) = 0$ for some $\omega \in \mathbb{R}$, then $\operatorname{Re} s < -\delta < 0$,

(vi) $\sigma_{\text{point}}(\Lambda) \cap \{\operatorname{Re} s \geq -\delta\} = \{0\}$ and 0 is a simple eigenvalue of Λ.

Note that assumptions (i), (iii), (iv) are already implied by our **Basic Assumptions**, assumption (v) is related to the spectral condition **SC**, and (vi) is just the eigenvalue condition **EC** from Sect. 1.5. The stability of traveling waves in parabolic-

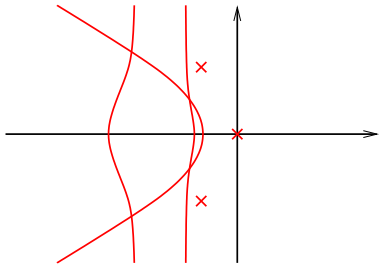

Fig. 17 Sketch of the spectrum of Λ satisfying the **Linear Assumptions**.

hyperbolic systems is the main result of the following theorem.

Theorem 6 (Stability with asymptotic phase [56, Thm. 6.1]). *Assume that the **Basic Assumptions** hold for* (81) *and the linearization Λ about the traveling wave (see* (84), (85)*) satisfies the **Linear Assumptions**.*
Then, for all $0 < \delta_0 < \delta$ there exists $\rho = \rho(\delta_0) > 0$ such that for all initial data with $\|u_0 - \overline{u}\|_{H^2}^2 + \|v_0 - \overline{v}\|_{H^2}^2 \leq \rho$ there is a unique global solution (u^*, v^*) with $T^* = \infty$ for the system (81)*.*
Moreover, there are $C = C(\delta_0), \gamma_\infty = \gamma_\infty(u_0, v_0) \in \mathbb{R}$ with

$$|\gamma_\infty|^2 \leq C\big(\|u_0 - \overline{u}\|_{H^2}^2 + \|v_0 - \overline{v}\|_{H^2}^2\big)$$

so that for all $t \geq 0$ the following estimate holds:

$$\begin{aligned} \|u^*(t) - \overline{u}(\cdot - \overline{\mu}t - \gamma_\infty)\|_{H^1}^2 + \|v^*(t) - \overline{v}(\cdot - \overline{\mu}t - \gamma_\infty)\|_{H^1}^2 \\ \leq C\big(\|u_0 - \overline{u}\|_{H^2}^2 + \|v_0 - \overline{v}\|_{H^2}^2\big) e^{-2\delta_0 t}. \end{aligned} \tag{86}$$

As is typical for hyperbolic equations, the initial data are measured in a stronger norm than the solution as $t \to \infty$.

3.3 Central ideas of the stability proof

The proof of Thm. 6 is quite involved and proceeds in four major steps. We only describe the main ideas and refer to [55, 56] for the details. Without loss of general-

ity we assume that the problem is posed in a co-moving frame so that the traveling wave is a steady state.

Step 1 [Nonlinear coordinates]: Use a nonlinear change of coordinates, in the spirit of Henry [39]: Choose a linear functional $\psi : H^{-1}(\mathbb{R},\mathbb{C}^{n+m}) \to \mathbb{R}$ that satisfies the **nondegeneracy assumption** $\psi(\overline{U}_x) \neq 0$ and write the solution in the form

$$U(t) = \widetilde{U}(t) + \overline{U}\big(\cdot - \gamma(t)\big), \quad \text{where} \quad \widetilde{U}(t) \in \mathcal{N}(\psi).$$

This leads to a **partial differential algebraic equation** (PDAE) for $\widetilde{U}$:

$$\begin{aligned} \widetilde{U}_t &= F\big(\widetilde{U} + \overline{U}(\cdot - \gamma)\big) + \gamma_t \overline{U}_x(\cdot - \gamma), \\ 0 &= \psi(\widetilde{U}). \end{aligned} \tag{87}$$

This change of coordinates is justified because the original PDE problem (83) and the PDAE reformulation (87) are equivalent for U close to $\overline{U}$ and $(\widetilde{U},\gamma)$ close to zero, see [56, Thm. 3.5]. Therefore, it suffices to show that the solution of (87) with transformed initial data $\widetilde{U}(0) = \widetilde{U}_0$, $\gamma(0) = \gamma_0$ converges exponentially fast.

Step 2 [Linearization]: We introduce $\mu = \gamma_t$ as a new variable. Then the PDAE (87) can be written in the form

$$\begin{aligned} \gamma_t &= \mu, && \gamma(0) = \gamma_0, \\ \widetilde{U}_t &= F(\widetilde{U} + \overline{U}(\cdot - \gamma)) + \gamma_t \overline{U}_x(\cdot - \gamma) \\ &= \Lambda \widetilde{U} + \overline{U}_x \mu + Q(\widetilde{U},\gamma,\mu), && \widetilde{U}(0) = \widetilde{U}_0, \\ 0 &= \psi(\widetilde{U}). \end{aligned} \tag{88}$$

Note that in (88) the initial value for μ_0 is given by hidden constraints. The remainder term $Q(\widetilde{U},\gamma,\mu)$ in (88) is of the form

$$Q = \begin{pmatrix} (G_1 + G_2)_x + F_{11} + F_{12} + R_1 \\ F_{21} + F_{21} + R_2 \end{pmatrix},$$

and has estimates which are quadratic in its arguments. For example, we have

$$\begin{aligned} G_1 &= -\int_0^1 D^2 g(\overline{U}(\cdot - s\gamma))\big[\overline{U}_x(\cdot - s\gamma), \gamma\widetilde{U}\big]\, ds, \\ G_2 &= \int_0^1 (1-s) D^2 g(\overline{U}(\cdot - \gamma) + s\widetilde{U})\big[\widetilde{U},\widetilde{U}\big]\, ds, \end{aligned}$$

and similar expressions for F_{ij}. The R_i are quadratic terms in μ and γ.

To prove stability for the nonlinear PDAE problem (88) we treat the higher order terms as inhomogeneities for the linear problem which then reads

$$\begin{aligned}\gamma_t &= \mu,\\ \widetilde{U}_t &= \Lambda\widetilde{U} + \overline{U}_x\mu + \begin{pmatrix} F_1 + G_x \\ F_2 \end{pmatrix},\\ 0 &= \psi(\widetilde{U}).\end{aligned} \tag{89}$$

In (89) the first equation decouples from the other two equations and can be solved in an additional step. Therefore, we consider only the linear, inhomogeneous PDAE

$$\begin{aligned}\widetilde{U}_t &= \Lambda\widetilde{U} + \overline{U}_x\mu + \begin{pmatrix} F_1 + G_x \\ F_2 \end{pmatrix}\\ 0 &= \psi(\widetilde{U}),\end{aligned} \tag{90}$$

subject to consistent initial data $\widetilde{U}(0) = (\widetilde{u}(0), \widetilde{v}(0)) \in H^2 \times H^2$, $\mu(0) \in \mathbb{R}$.

The following linear stability result is the key to nonlinear stability.

Theorem 7 (Linear PDAE stability ([56, Thm. 5.1])). *Let the assumptions be as above and assume $F_1 \in C([0,\infty); L^2)$, $G, F_2 \in C([0,\infty); H^1)$. Then there exists a unique solution (u, v, μ) of* (90)*, and it satisfies*

$$\begin{aligned}&\|u(t)\|_{H^1}^2 + \|v(t)\|_{H^1}^2 + e^{-2\delta_0 t}\int_0^t e^{2\delta_0\tau}\left\{\|u\|_{H^1}^2 + \|v\|_{H^1}^2 + |\mu|^2\right\} d\tau\\ &\quad\le Ce^{-2\delta_0 t}\Big[\|\widetilde{u}_0\|_{H^2}^2 + \|\widetilde{v}_0\|_{H^2}^2 + \int_0^t e^{2\delta_0\tau}\left\{\|G\|_{H^1}^2 + \|F_1\|^2 + \|F_2\|_{H^1}^2\right\} d\tau\Big].\end{aligned} \tag{91}$$

The proof of this theorem will be indicated in **Step 4** below.

Step 3 [From linear to nonlinear stability]: Nonlinear stability of the PDAE (87) can be obtained from Theorem 7 by the following steps:

- Show local existence and uniqueness for (88) for small initial data $\widetilde{U}_0$, $\gamma(0)$.
- Consider $Q(\widetilde{U}, \gamma, \mu)$ in (88) as inhomogeneity in (90) and use the linear result, Theorem 7, to obtain a priori estimates for the local solution.
- Use the a priori estimate in a bootstrapping argument to show that the solution can be extended to all positive times and decays exponentially.

Since the PDAE problem (87) and the PDE problem (83) are locally equivalent, this proves Theorem 6.

Step 4 [Proof of linear stability via Laplace-technique]: We indicate the main steps in the proof of Theorem 7. A crucial step is to use the Laplace-technique which, in simple terms, translates resolvent estimates via the Theorem of Plancherel into decay estimates. Using Laplace-transform for stability proofs is standard, but applying the technique in the context of PDAEs such as (90) is a novel approach, see [54].

By homogenizing the initial data, we may assume without loss of generality $\widetilde{u}(0) = 0, \widetilde{v}(0) = 0$ in (90). More precisely, one writes the equations in terms of the new functions $\widetilde{u} - e^{-2\delta t}\widetilde{u}_0$ and $\widetilde{v} - e^{-2\delta t}\widetilde{v}_0$. This adds a term of the form

$e^{-2\delta t}\Lambda(\widetilde{u}_0,\widetilde{v}_0)^\top$ to the inhomogeneity (see [54, Thm. 5.3]). The linear inhomogeneous problem is exponentially well-posed so that Laplace transformation of (90) is justified for spectral values s with $\mathrm{Re}\, s \geq \alpha$ for some sufficiently large α (see [56]). This leads to the following resolvent equation which we write in operator matrix form:

$$\mathscr{A}(s)\begin{pmatrix}\widehat{u}\\ \widehat{v}\\ \widehat{\mu}\end{pmatrix} = \begin{pmatrix}(sI-\Lambda) & -\begin{pmatrix}\overline{u}_x\\ \overline{v}_x\end{pmatrix}\\ \psi & 0\end{pmatrix}\begin{pmatrix}\widehat{u}\\ \widehat{v}\\ \widehat{\mu}\end{pmatrix} = \begin{pmatrix}\widehat{F}_1+\widehat{G}_x\\ \widehat{F}_2\\ 0\end{pmatrix}. \tag{92}$$

Here $\mathscr{A}(s)$ is an operator on $L^2\times L^2\times\mathbb{C}$ with domain $H^2\times H^1\times\mathbb{C}$.

We first show how resolvent estimates, i.e. solution estimates for (92) lead to stability. By Plancherel's Theorem we have for $\eta\geq\alpha$,

$$\int_0^\infty e^{-2\eta\tau}\|(\widetilde{u},\widetilde{v},\mu)^\top(\tau)\|_{H^1}^2\,d\tau = \frac{1}{2\pi}\int_{-\infty}^{\infty}\|(\widehat{u},\widehat{v},\widehat{\mu})^\top(\eta+i\xi)\|_{H^1}^2 d\xi, \tag{93}$$

where $\|(\widehat{u},\widehat{v},\widehat{\mu})^\top\|_{H^1}^2 = \|\widehat{u}\|_{H^1}^2+\|\widehat{v}\|_{H^1}^2+|\mu|^2$. In **Step 6** below, we show estimates for solutions of (92) which hold uniformly in $\{\mathrm{Re}\, s\geq-\delta_0\}$ for a fixed $\delta_0<\delta$,

$$\|(\widehat{u}(s),\widehat{v}(s),\widehat{\mu}(s))^\top\|_{H^1}^2 \leq C\|(\widehat{F}_1(s),\widehat{G}(s),\widehat{F}_2(s))^\top\|_{L^2,H^1}^2. \tag{94}$$

Here we used the norm $\|(\widehat{F}_1,\widehat{G},\widehat{F}_2)^\top\|_{L^2,H^1}^2 = \|\widehat{F}_1\|_{L^2}^2+\|\widehat{G}\|_{H^1}^2+\|\widehat{F}_2\|_{H^1}^2$. Note that $\widehat{u},\widehat{v},\widehat{\mu}$ in equation (92) are analytic functions, given as the Laplace transforms of $\widetilde{u},\widetilde{v},\mu$, which is only justified in $\{\mathrm{Re}\, s\geq\alpha\}$. But the resolvent equation (92) is in fact uniquely solvable in the larger domain $\{\mathrm{Re}\, s>-\delta\}$ and the solution depends analytically on s in this region. Therefore, $\widehat{u},\widehat{v},\widehat{\mu}$ in (94) coincide with the analytic continuations of the Laplace transforms. By [4, Thm. 4.4.13] this implies that the Laplace transforms of $\widetilde{u},\widetilde{v},\mu$ even exist in the larger domain $\{\mathrm{Re}\, s>-\delta\}$. Then the Payley-Wiener and Plancherel Theorem [4, Sect. 1.8] show that (93) even holds for $\eta\geq-\delta_0>-\delta$. This crucial step of shifting contours in the Laplace transform to the left is illustrated in Figure 18.

We use (93) for $\eta=-\delta_0$, insert estimate (94) into the right hand side and finally use Plancherel's Theorem for the inhomogeneities to obtain

$$\begin{aligned}\int_0^\infty e^{-2\eta\tau}\|(\widetilde{u},\widetilde{v},\mu)^\top(\tau)\|_{H^1}^2\,d\tau &\leq \frac{1}{2\pi}\int_{-\infty}^{\infty} C\|(\widehat{F}_1,\widehat{G},\widehat{F}_2)^\top(\eta+i\xi)\|_{L^2,H^1}^2\,d\xi\\ &= C\int_0^\infty e^{-2\eta\tau}\|(F_1,G,F_2)^\top(\tau)\|_{L^2,H^1}^2\,d\tau.\end{aligned} \tag{95}$$

This estimate proves the linear stability result and leads to the estimate (91).

Step 5 [Fredholm-properties]: It remains to analyze (92) and show (94). We begin with Fredholm properties of $\mathscr{A}(s)$. For this rewrite the second order operator $sI-\Lambda: H^2\times H^1\to L^2\times L^2$ as a first order operator by introducing $z=(u,Au_x,v)^\top$. This leads to an operator $L(s): H^2\times H^1\times H^1\to H^1\times L^2\times L^2$ given by

$$L(s)z = z_x - M(x,s)z,$$

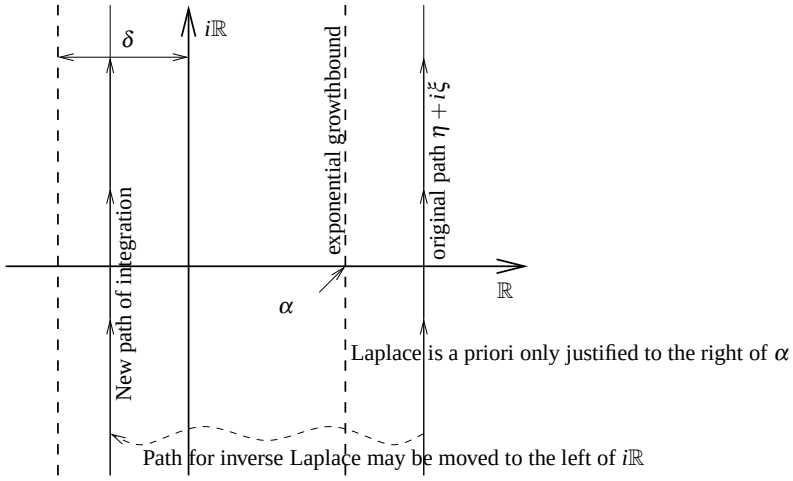

Fig. 18 Initially, equality (93) only holds for a path of integration to the right of α. Then it is justified in a much larger region, and the line of integration is shifted from the right of α to the left of $i\mathbb{R}$.

where the matrix valued function $M(x,s) \in \mathbb{C}^{2n+m}$ reads

$$M(x,s) = \begin{pmatrix} 0 & A^{-1} & 0 \\ sI + B_{12}B_{22}^{-1}C_{21} - C_{11} & -B_{11}A^{-1} & -B_{12}B_{22}^{-1}(sI - C_{22}) - C_{12} \\ -B_{22}^{-1}C_{21} & 0 & B_{22}^{-1}(sI - C_{22}) \end{pmatrix}.$$

We employ the following Lemma from [11].

Lemma 1. *The second order operator $sI - \Lambda$ on $L^2 \times L^2$ with domain $H^2 \times H^1$ is Fredholm if and only if the first order operator $L(s)$ on $H^1 \times L^2 \times L^2$ with domain $H^2 \times H^1 \times H^1$ is Fredholm. In this case the Fredholm indices as well as the dimensions of the nullspaces of the two operators coincide.*

It is not difficult to show that the assumptions on the coefficients of the linear operator, in particular **Linear Assumptions** parts (iv) and (v), imply that the limit matrices $\lim_{x\to\pm\infty} M(x,s) = M_\pm(s)$ exist and are hyperbolic matrices. Moreover, the dimensions of the generalized eigenspaces for eigenvalues with real part less than zero is the same for $M_-(s)$ and $M_+(s)$, see [56, App. A]. By classical results of Coppel [21], the linear first order operator $L(s)$ has exponential dichotomies on $\mathbb{R}_\pm$, and a result of Palmer [50] shows the following,

Lemma 2. *For $\operatorname{Re} s > -\delta$ the operator $L(s)$ is Fredholm of index 0 and $\dim \mathscr{N}(L(0)) = \operatorname{codim} \mathscr{R}(L(0)) = 1$.*

Using the bordering lemma, e.g. [8], this proves that the original operator $\mathscr{A}(s)$ is Fredholm of index zero for all $\operatorname{Re} s > -\delta$.

Step 6 [Resolvent estimates]: After these preliminaries, the resolvent estimates are shown separately in the following three regions of the complex plane:

Region I: $\{s \in \mathbb{C} : \mathrm{Re}\, s \geq -\delta_0, |s| \gg 0\}$,
here the parabolic-hyperbolic structure dominates, the **dispersion relation** is crucial for the estimates (this is different from the purely parabolic case!).

Region II: $\Omega \subset \rho(\Lambda) \cap \{\mathrm{Re}\, s > -\delta_0\}$ compact.

Region III: $\{s \in \mathbb{C} : |s| \ll 1\}$,
here the PDAE formulation removes 0 from the spectrum and leads to appropriate estimates.

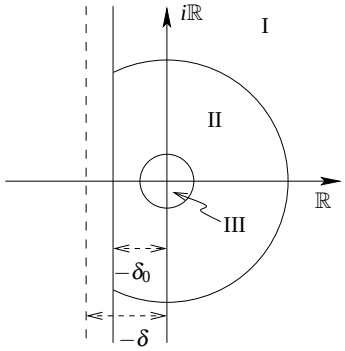

Since Region II is compact in the resolvent sent, the estimates are obvious. In Region I we assume $|s|$ to be large. The **Linear Assumption** (v) then states that

$$s \in \sigma \begin{pmatrix} -\omega^2 A + i\omega B_{11} + C_{11} & i\omega B_{12} + C_{12} \\ C_{21} & i\omega B_{22} + C_{22} \end{pmatrix},$$

for some $\omega \in \mathbb{R}$ implies $\mathrm{Re}\, s < -\delta$. Here and in the following we drop the index $\pm$ for simplicity. By a matrix perturbation result, e.g. from [65], there is $\omega_0 > 0$ so that the matrix is similar to

$$\begin{pmatrix} -\omega^2 A + i\omega B_{11} + C_{11} + \mathscr{O}(|\omega|^{-1}) & i\omega B_{12} + C_{12} \\ 0 & i\omega B_{22} + C_{22} + \mathscr{O}(|\omega|^{-1}) \end{pmatrix}.$$

for all $|\omega| \geq \omega_0$. Together with the **dispersion relation** this shows

Lemma 3. *For every $0 < \delta' < \delta$ there is ω_1 so that for all $\omega \in \mathbb{R}$, $|\omega| > \omega_1$ holds the* hyperbolic dispersion relation

$$s \in \sigma(i\omega B_{22} + C_{22}) \Rightarrow \mathrm{Re}\, s < -\delta'. \tag{96}$$

For the hyperbolic part we have the following result from [54]:

Proposition 1. *For every $\delta_0 < \delta$ there exist constants $\rho_0, K > 0$ such that the equation*

$$(sI - B_{22}\partial_x - C_{22}(x))v = F \quad \text{in } L^2(\mathbb{R}, \mathbb{C}^m),$$

has a unique solution $v \in H^1$ for all $F \in H^1$ and for all s with $\mathrm{Re}\, s \geq -\delta_0$, $|s| > \rho_0$. The solution satisfies the estimate

$$\|v\|_{L^2}^2 \leq K\|F\|_{L^2}^2, \quad \|v\|_{H^1}^2 \leq K\|F\|_{H^1}^2.$$

A corresponding result for the parabolic part is proved in [46]:

Proposition 2. *There are constants $c_1, K, \varepsilon > 0$ so that for all $s = re^{2i\theta}$, $r \geq c_1$, $|\theta| \leq \pi/4 + \varepsilon$ there exists a unique solution $u \in H^2$ of*

$$su - Au_{xx} - B_{11}u_x - C_{11}u = f + g_x \text{ in } L^2$$

for all $f \in L^2$, $g \in H^1$. *The solution satisfies the estimate*

$$|s|^2\|u\|^2 + |s|\|u_x\|^2 \le K\Big(\|f\|^2 + |s|\|g\|^2\Big).$$

By applying Propositions 1 and 2 to the coupled system

$$\begin{aligned} su - Au_{xx} - B_{11}u_x - C_{11}u &= \big(F_1 + C_{12}v - B_{12,x}v\big) + \big(G + B_{12}v\big)_x, \\ sv - B_{22}v_x - C_{22}v &= F_2 + C_{21}u, \end{aligned}$$

one obtains unique solvability and solution estimates in Region I.

In Region III we benefit from the formulation as a partial differential algebraic equation. First consider $s = 0$ and assume that (W, λ) is in the nullspace of $\mathscr{A}(0)$, i.e.

$$\mathscr{A}(0)\begin{pmatrix} W \\ \lambda \end{pmatrix} = \begin{pmatrix} -\Lambda & -\begin{pmatrix} \overline{u}_x \\ \overline{v}_x \end{pmatrix} \\ \psi & 0 \end{pmatrix}\begin{pmatrix} W \\ \lambda \end{pmatrix} = \begin{pmatrix} 0 \\ 0 \end{pmatrix}.$$

But our assumptions, 0 is a simple eigenvalue and, therefore, $(\overline{u}_x, \overline{v}_x)^\top$ is not in the range of Λ, which enforces $\lambda = 0$. Then W must belong to the kernel of Λ which is the one-dimensional space spanned by $(\overline{u}_x, \overline{v}_x)^\top$. The nondegeneracy assumption on ψ then implies that also W vanishes, so that $\mathscr{A}(0) : H^2 \times H^1 \times \mathbb{C} \to L^2 \times L^2 \times \mathbb{C}$ is a linear homeomorphism due to Fredholm index zero. A perturbation argument then allows to deal with small s-values.

Lemma 4. *There exist* $c_0, K > 0$ *so that for all* $s \in \mathbb{C}$ $|s| < c_0$ *there is a unique solution* $(\widehat{u}, \widehat{v}, \widehat{\lambda}) \in H^2 \times H^1 \times \mathbb{C}$ *of*

$$\begin{pmatrix} (sI - \Lambda) & -\begin{pmatrix} \overline{u}_x \\ \overline{v}_x \end{pmatrix} \\ \psi & 0 \end{pmatrix}\begin{pmatrix} \widehat{u} \\ \widehat{v} \\ \widehat{\lambda} \end{pmatrix} = \begin{pmatrix} \widehat{F}_1 + \widehat{G}_x \\ \widehat{F}_2 \\ 0 \end{pmatrix},$$

and the solution satisfies

$$\|\widehat{u}\|_{H^2} + \|\widehat{v}\|_{H^1} + |\widehat{\lambda}| \le K\big(\|\widehat{F}_1\| + \|\widehat{G}\|_{H^1} + \|\widehat{F}_2\|\big).$$

This finishes the proof of Theorem 7.

3.4 Freezing waves in hyperbolic-parabolic systems

In this section we consider the freezing method when solving hyperbolic-parabolic systems in the neighborhood of traveling waves. Recall the general form (61) of the freezing method for a shift-equivariant evolution equation $U_t = F(U)$,

$$V_t = F(V) + \mu V_x, \tag{Fr$_1$}$$
$$0 = \psi(V,\mu), \tag{Fr$_2$}$$

where (Fr$_2$) is the phase condition. Further recall the two standard choices for phase conditions from Section 2.1:

Fixed phase condition: Given a template function $\hat{V}$, force the solution of (Fr$_1$) to align best under all shifts of $\hat{V}$ with the unshifted template function $\hat{V}$, i.e.

$$0 = \operatorname{argmin}_{\gamma\in\mathbb{R}} \|V - \hat{V}(\cdot - \gamma)\|.$$

If the norm is given by some inner product $(\cdot,\cdot)$ and $\hat{V}$ is sufficiently smooth, the condition above implies $0 = (\hat{V}_x, V - \hat{V})$.

Orthogonal phase condition: Force the time evolution of the solution V of (Fr$_1$) to be orthogonal to the orbit of the spatial shifts of V in the Hilbert space L^2:

$$0 = (V_x, V_t) = (V_x, F(V) + \mu V_x).$$

For a sketch of these conditions see Figure 19.

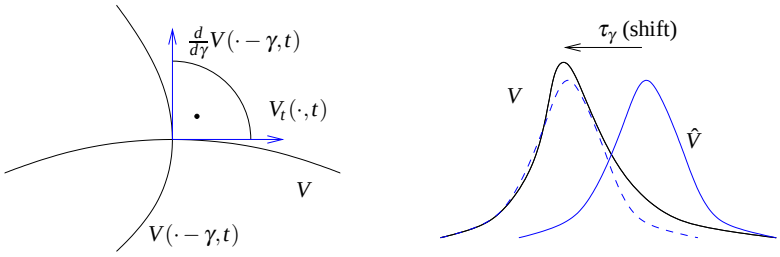

Fig. 19 Geometric interpretation of the orthogonal phase condition (left) and of the fixed phase condition (right).

Example 9 (FitzHugh-Nagumo system). Recall the FitzHugh-Nagumo equation from Example 4 with parameters $a = 0.7$, $b = 3$, $\phi = 0.08$. We set $\varepsilon = 0$, so that we have the hyperbolic-parabolic mixed case as in [57]. The system reads

$$\begin{aligned} u_t &= u_{xx} + u - \tfrac{1}{3}u^3 - v, \quad & u(x,0) &= u_0(x), \\ v_t &= \phi(u + a - bv), & v(x,0) &= v_0(x), \end{aligned} \tag{97}$$

Figure 20 shows a colorplot of the time-evolution of u and v for the frozen system. The initial data are chosen as a jump function, which equals the rest state at $-\infty$ for $x \le 0$ and the rest state at $+\infty$ for $x > 0$. A plot of the asymptotic profile, calculated by the solution of a boundary value problem, is given in the left frame of Figure 21. We indicate the rate at which the solution to the freezing method converges to the asymptotic profile by plotting the L^2-norm of the time-derivative in the right frame

of Figure 21. In [57] this behavior is related to the spectral gap of the linearized operator.

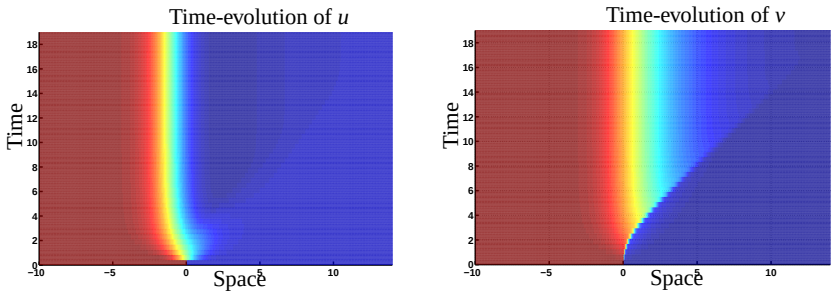

Fig. 20 Plot of frozen FitzHugh-Nagumo solutions $u(x,t)$ (left) and $v(x,t)$ (right). Note that u appears to be smooth immediately, while v exhibits a discontinuity that decays with time.

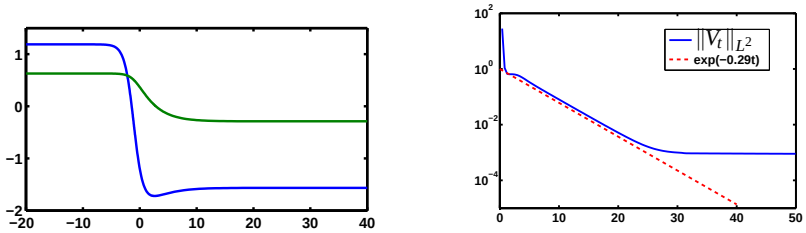

Fig. 21 Space dependence of FitzHugh Nagumo solutions $u(x,t)$ $v(x,t)$ (left) and temporal decay of $\|(u_t, v_t)\|_{L^2}$ with time (right)

Example 10 (Hodgkin-Huxley system). As a second example we use the freezing method for a long-time simulation of the Hodgkin-Huxley system (80). For suitable initial data, which are chosen as a simple jump in the voltage, the long-time simulation approximates the traveling pulse. The result of one such long-time simulation was used as initial guess to calculate the traveling pulse shown in Figure 16 from a boundary value problem (cf. (12)). We sketch the numerical spectrum of the linearization about the traveling pulse in Figure 22.

3.5 Stability theorem for the freezing method

An obvious question is, whether stability with asymptotic phase for traveling waves in hyperbolic-parabolic problems translates into stability of equilibria for the freezing method. This is in fact true, as the following result will show.

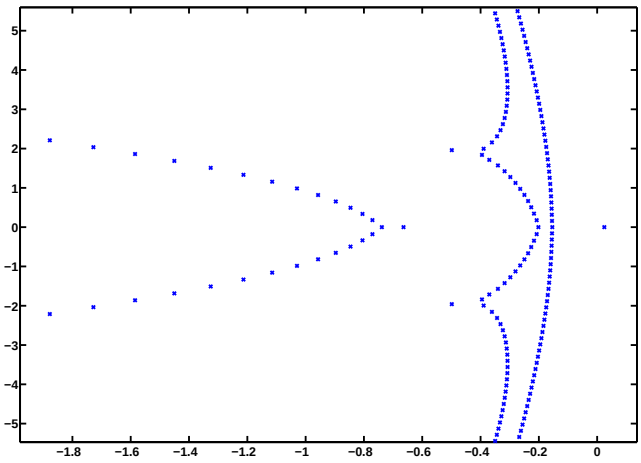

Fig. 22 Numerical approximation of the spectrum near zero for the linearization of the co-moved Hodgkin-Huxley equations about the traveling pulse.

Consider a hyperbolic-parabolic partial differential equation of the general form (81). The freezing method for this system is

$$\begin{aligned} u_t &= Au_{xx} + g(u,v)_x + f_1(u,v) + \mu u_x, \\ v_t &= Bv_x + f_2(u,v) + \mu v_x, \\ 0 &= \psi(\hat{u}-u, \hat{v}-v). \end{aligned} \tag{98}$$

We impose the **Basic Assumption** from Sect. 3.1 for and the **Linear Assumptions** from Sect. 3.2. In addition, we require for the phase condition:

(i) $\hat{u}-\overline{u},\ \hat{v}-\overline{v} \in H^1$,
(ii) $\psi(\hat{u}-\overline{u}, \hat{v}-\overline{v}) = 0$,
(iii) $\psi(\overline{u}_x, \overline{v}_x) \neq 0$. (non-degeneracy condition)

Condition (ii) implies that $(\overline{u}, \overline{v}, \overline{\mu})$ is a steady state of (98). With these assumptions the following result holds.

Theorem 8 ([55], [57]). *For all $0 < \delta_0 < \delta$ there exists $\rho_0 > 0$ such that for all consistent initial data of* (98) *with $\|u_0-\overline{u}\|^2_{H^2} + \|v_0-\overline{v}\|^2_{H^2} \leq \rho_0$ there is a unique global solution (u,v,μ) of the freezing equation* (98)*. The solution satisfies*

$$\begin{aligned} &u-\overline{u} \in C([0,T];H^1) \cap L^2(0,T;H^2) \cap H^1(0,T;L^2), \\ &v-\overline{v} \in C([0,T];H^1) \cap H^1(0,T;L^2), \quad \mu \in C([0,T];\mathbb{R}), \end{aligned}$$

and converges exponentially fast to the asymptotic profile and to the speed of the traveling pulse. More precisely, there is $C = C(\delta_0)$ such that for all $t \geq 0$,

$$\|u(t) - \overline{u}\|_{H^1}^2 + \|v(t) - \overline{v}\|_{H^1}^2 + |\mu(t) - \overline{\mu}|^2 \leq C\big(\|u_0 - \overline{u}\|_{H^2}^2 + \|v_0 - \overline{v}\|_{H^2}^2\big)e^{-2\delta_0 t}.$$

It is worth noting, that the result also applies to viscous conservation laws with a source term. The following numerical experiment shows an example of this type.

Example 11 (Burgers' equation). Consider Burgers' equation with a source term,

$$u_t + \big(\tfrac{1}{2}u^2\big)_x = 0.1u_{xx} + u(1-u)(u-\tfrac{1}{4}). \tag{99}$$

The following results are taken from [53]. Figure 23 shows the result of a numerical simulation of (99) with the freezing method. The left plot in Figure 24 shows the

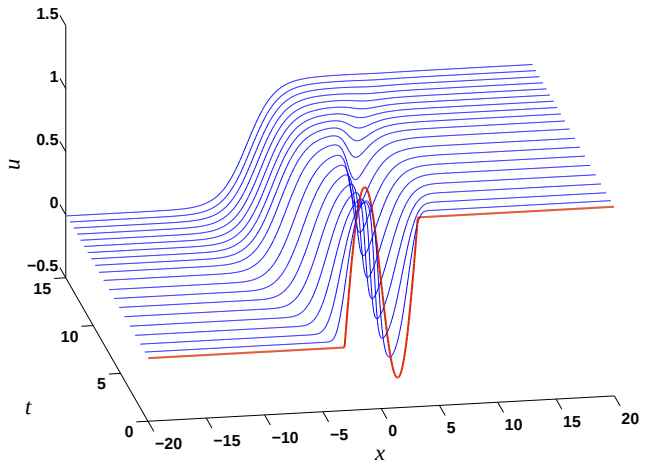

Fig. 23 Numerical simulation of (99) with the freezing method. The bold line indicates the initial data (cf. [53]).

dispersion curves and the right plot shows a numerical approximation of the spectrum for the operator linearized about the traveling wave. In numerical experiments one observes an approximate rate of convergence $e^{-0.2t}$ as $t \to \infty$.

Example 12. We present results for hyperbolic systems without a parabolic part. This was first analyzed in [54] and [55]. A large number of examples of such systems are obtained by using the so-called Cattaneo-Maxwell flux instead of the usual Fickian law:

Consider a system of reaction diffusion equations

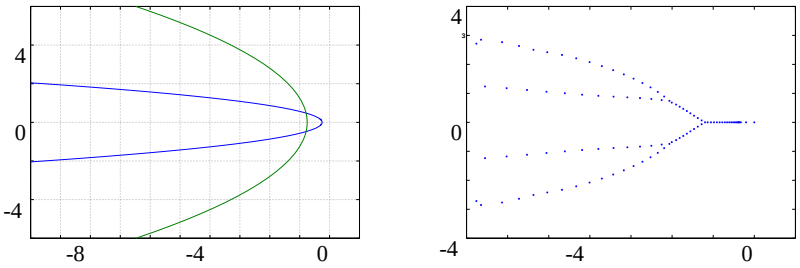

Fig. 24 Dispersion relation for Burgers' equation with a source term (left), plot of a numerical approximation for the spectrum of the linearized operator (right).

$$v_t + q_x = r(v),$$

where v denotes the concentrations of the substrates, q stands for the fluxes of the substrates, and r contains reactions terms for the substrates. Usually the fluxes are given by the Fickian law ($q = -Dv_x$), but this leads to the unphysical phenomenon of infinite speed of propagation of the substrates. Cattaneo [19] proposed a different flux law for the case of heat transfer. He added a damping term to the Fickian law which reads

$$Tq_t + q = -v_x.$$

This leads to the following semilinear hyperbolic problem

$$\begin{pmatrix} v \\ q \end{pmatrix}_t + \begin{pmatrix} q \\ \frac{1}{T}v \end{pmatrix}_x = \begin{pmatrix} r(v) \\ -\frac{1}{T}q \end{pmatrix}.$$

As is well-known, solutions to hyperbolic problems have a finite speed of propagation. This removes the apparent paradox of infinite speed of propagation for the substrates. Moreover, the Fickian law appears as a singularly perturbed limit if the parameter T becomes large.

In [55] we consider a hyperbolic variant of the Hodgkin-Huxley equations (80) by using the Cattaneo-Maxwell flux. The system then becomes

$$\begin{aligned} V_t &= \frac{a}{2R}q_x - \bar{g}_K n^4 (V - V_K) - \bar{g}_{Na} m^3 h (V - V_{Na}) - \bar{g}_l (V - V_l), \\ q_t &= -V_x - q, \\ n_t &= \alpha_n(V)(1-n) - \beta_n(V)\, n, \\ m_t &= \alpha_m(V)(1-m) - \beta_m(V)\, m, \\ h_t &= \alpha_h(V)(1-h) - \beta_h(V)\, h, \end{aligned} \tag{100}$$

where the nonlinearities α_n, β_n, etc. are the same as in the original equation (80). The freezing method works for this example just as well as for the original Hodgkin-Huxley system. After a first long-time simulation, one can again use the final state of the initial value problem as initial guess for the boundary value problem and then

do the standard subsequent analysis for the traveling wave such as computing the spectrum, performing parameter continuation, etc..

We plot in Figure 25 the dispersion relation of the steady state problem, i.e. of the problem in a co-moving frame with the correct velocity $\overline{\mu}$ of the traveling wave. Due to the hyperbolic character of the equations, all curves approach vertical lines, for more details we refer to [55, Sect. 8] and [53].

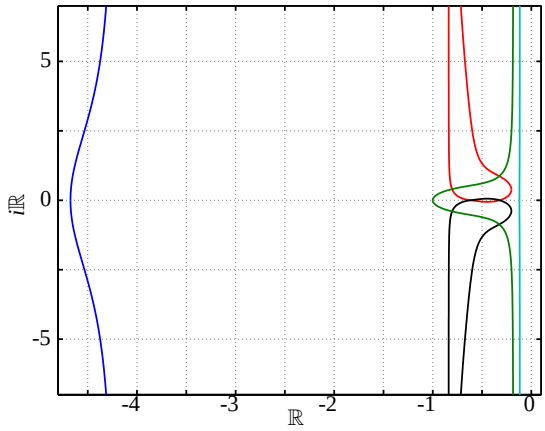

Fig. 25 Dispersion relation for the steady state of the hyperbolic version of the Hodgkin-Huxley equation (cf. [55]).

3.6 Numerical experiments for more general symmetries

Note that equivariance of an evolution equation (43) completely avoids transformation of the time variable. So far we just used equivariance in the form (46) and kept the time variable in the ansatz (71). But it is possible to include more general symmetries that involve the time variable, and this has already been proposed in [58].

As an example we consider the viscous Burgers' equation

$$u_t = -(\tfrac{1}{2}u^2)_x + \nu u_{xx} =: F(u),\ x \in \mathbb{R}, t \geq 0, \tag{101}$$

and take the Lie group

$$G = \mathbb{R}^*_+ \ltimes \mathbb{R},$$

with multiplication for $\gamma, \eta \in G$ given by:

$$(\gamma_1, \gamma_2) \circ (\eta_1, \eta_2) = (\gamma_1 \eta_1, \gamma_2 + \gamma_1 \eta_2), \quad \mathbb{1} = (1, 0).$$

We use the group actions a and m, given by

$$[a(\gamma)u](x) = \frac{1}{\gamma_1} u(\frac{x-\gamma_2}{\gamma_1}), \quad m(\gamma) = \frac{1}{\gamma_1^2}.$$

A simple computation shows that for sufficiently smooth functions u,

$$F(a(\gamma)u) = m(\gamma)a(\gamma)F(u). \tag{102}$$

Note that, instead of commuting F and $a(\gamma)$ as in (46), we have an additional factor $m(\gamma)$. This factor leads to a time scaling as we will see in the following discussion.

We replace (71) by the following **ansatz:**

$$u(t) = a(\gamma(\tau))v(\tau), \tag{103}$$

where γ is a smooth curve in G, v is a smooth curve in the domain of F and $\tau = \tau(t)$ is a smooth real valued function of t.

Using the symmetry property (102) in the evolution equation (101), we arrive at the following:

$$\begin{aligned} &u_t = F(u) = F\big(a(\gamma(\tau))v(\tau)\big) = m(\gamma)a(\gamma)F(v), \text{ and also} \\ &u_t = a(\gamma)d[a(\mathbb{1})v]dL_{\gamma^{-1}}(\gamma)\gamma_\tau\tau_t + a(\gamma)v_\tau\tau_t. \end{aligned} \tag{104}$$

If we choose τ to satisfy the ordinary differential equation $\tau_t = m(\gamma(\tau))$, then (104) leads to the system

$$v_\tau = F(v) - d[a_\gamma(\mathbb{1})v]\mu, \tag{105}$$

$$\tau_t = m(\gamma(\tau)), \tag{106}$$

$$\gamma_\tau = dL_\gamma(\mathbb{1})\mu. \tag{107}$$

Note that it is not necessary to solve (105)–(107) simultaneously. In fact, equations (106) and (107) are only needed for reconstruction, i.e. to obtain the solution in the original coordinates. The relative equilibrium is completely described by a steady solution of (105). For the simulation of (105) the same ideas as in Section 2 apply. We only present the results of one simulation in Figure 26. Looking at the scales in Figure 26 it is nice to observe that the solution decays to zero in the original variables and spreads to infinity. In the transformed variables however, the solution becomes a steady state. Moreover, using the freezing method, one is able to directly observe a transient behavior: For a very long time (in the original time variable) the solution is close to what is called an N-wave in the theory of hyperbolic conservation laws, before it finally approaches the correct viscosity wave. This behavior has been observed already in [45], but there the authors used that the asymptotic values for $\overline{\mu}$ and, therefore, a correct asymptotic scaling of space and time are known. Our method applies also to systems where the asymptotic scalings are not easily found and, moreover, the method yields these asymptotic scalings as part of its solution.

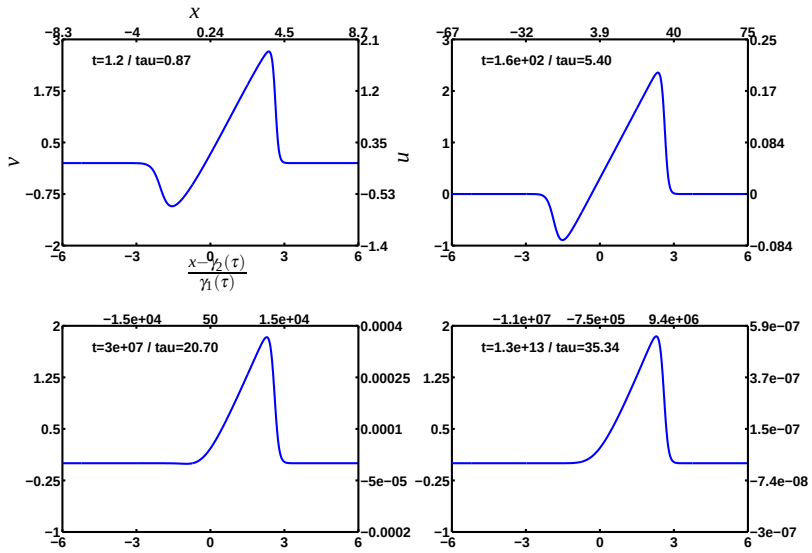

Fig. 26 Result of the freezing method for the viscous Burgers' equation at four different times. In each of the four plots the scale on top is for the original space variable x, the bottom scale is in the transformed variable $\xi = \frac{x-\gamma_2(\tau)}{\gamma_1(\tau)}$, the scale on the left is for the transformed dependent variable $v(\xi,\tau)$ and the scale on the right is for the original dependent variable $u(x,t)$. In each plot we also give the actual original time t and the transformed time $\tau(t)$ (see [53]).

3.7 Summary

A summary of the results of this section is the following:

- Stability with asymptotic phase for general coupled parabolic-hyperbolic systems can be proved under the assumption that the spectrum of the linearization lies strictly to the left of the imaginary axis except for a simple zero eigenvalue,
- The idea of the proof is to use Laplace-transform and derive uniform resolvent estimates for the transformed equation,
- For large spectral values, resolvent estimates are obtained from the parabolic-hyperbolic structure and the dispersion relation,
- For small spectral values, the zero-eigenvalue is removed from the spectrum by the phase condition which appears in the PDAE formulation,
- Numerical experiments confirm the predicted exponential rates,
- The freezing method applies to the computation of similarity solutions.

4 Rotating patterns in two and three space dimensions

While the previous lectures were restricted to patterns in one space dimension, we will progress in this section to nonlinear waves in two and three space dimensions. Since the freezing method is formulated in abstract terms it is rather straightforward to make it work for equivariant parabolic systems in $d \geq 2$ dimensions, where the Lie group is now the d-dimensional Euclidean group or consists of products or subgroups thereof. It is much harder, however, to prove nonlinear stability of such patterns under reasonable assumptions on the associated spectra. In this section we discuss the stability result from [9] which applies to two-dimensional rotating patterns that are localized, i.e. which decay at infinity. Again, as in Section 3 a major difficulty results from the fact that, due to the angular modes, the linearized operators only lead to C^0-semigroups. Moreover, due to equivariance with respect to the two-dimensional Euclidean group, three eigenvalues now appear on the imaginary axis. We show how to obtain exponential decay of the semigroup in a subspace complementary to the eigenvectors that belong to these three eigenvalues. Then stability with asymptotic phase follows in a suitable Sobolev space. We also show some simulations of the freezing method for cases where the theory does currently not apply: two-dimensional rotating spirals for Barkley's excitable system (see [6]) and three dimensional spinning solitons for the quintic-cubic Ginzburg-Landau equation.

4.1 Reaction diffusion systems in $\mathbb{R}^2$ and the freezing method

We apply the abstract freezing approach from Section 2.4 to reaction diffusion systems in two dimensions

$$u_t = A\Delta u + f(u),\ t \geq 0,\ x \in \mathbb{R}^2, \quad u(\cdot,0) = u_0, \tag{108}$$

where $u(x,t) \in \mathbb{R}^m$ and $A \in \mathbb{R}^{m,m}$ is positive definite. The system (108) is equivariant with respect to the Euclidean group $G = SE(2)$ under the action $a(\gamma)$, given for $\gamma = (\theta,\tau) \in S^1 \ltimes \mathbb{R}^2$ by

$$a(\gamma)v(x) = v(R_{-\theta}(x-\tau)),\ x \in \mathbb{R}^2, \quad R_\theta = \begin{pmatrix} \cos(\theta & -\sin(\theta) \\ \sin(\theta) & \cos(\theta) \end{pmatrix}. \tag{109}$$

Here we used the representation of $SE(2)$ as a semi-direct product of S^1 and $\mathbb{R}^2$ with the group operation defined through

$$(\theta_1,\tau_1) \circ (\theta_2,\tau_2) = (\theta_1+\theta_2, R_{\theta_2}\tau_2 + \tau_1). \tag{110}$$

The derivative of $a(\gamma)v$ with respect to $\gamma \in G$ turns out to be

$$d[a(\mathbb{1})v]\mu = \mu_1 D_\theta v + \mu_2 D_1 v + \mu_3 D_2 v, \quad \mu = (\mu_1,\mu_2,\mu_3) \in \mathscr{A} = se(2), \tag{111}$$

where $D_\theta v(x) = x_2 D_1 v(x) - x_1 D_2 v(x)$ is the angular derivative and $v : \mathbb{R}^2 \to \mathbb{R}^m$ is assumed to be sufficiently smooth.

Therefore, the freezing system (73) associated with (108) reads as follows

$$\begin{aligned} v_t &= A\Delta v + f(v) + \mu_1 D_\theta v + \mu_2 D_1 v + \mu_3 D_2 v, \quad v(\cdot,0) = u_0 \\ 0 &= (D_\theta \hat{v}, v - \hat{v})_{L^2} = (D_1 \hat{v}, v - \hat{v})_{L^2} = (D_2 \hat{v}, v - \hat{v})_{L^2}, \\ \gamma_t &= \begin{pmatrix} \theta \\ \tau \end{pmatrix}_t = \begin{pmatrix} 1 & 0 \\ 0 & R_\theta \end{pmatrix} \mu, \quad \gamma(0) = \begin{pmatrix} 0 \\ 0 \end{pmatrix}. \end{aligned} \tag{112}$$

A **rotating wave** solution of (108) is of the form

$$u(x,t) = u_*(R_{-ct}x), \quad x \in \mathbb{R}^2, \quad t \in \mathbb{R}, \tag{113}$$

where u_* denotes the profile and c denotes the angular velocity of the wave. In terms of the group action we may write such a solution as $u(t) = a(ct,0)u_*$, $t \in \mathbb{R}$ which is a relative equilibrium of (108). For any $\theta \in S^1, \tau \in \mathbb{R}^2$ the function $a((\theta,\tau)\circ(ct,0))u_*(x) = u_*(R_{-ct-\theta}(x-\tau))$ is then also a rotating wave, but with phase shift θ and with center of rotation at τ. These solutions are equilibria of the first equation in (112) and solve the reconstruction equation in (112) with initial data $\gamma(0) = (\theta,\tau)$.

Example 13 (Quintic-cubic Ginzburg-Landau equation (QCGL)). Consider the QCGL in two space dimensions (compare Example 5):

$$u_t = \alpha\Delta u + (\delta + \beta|u|^2 + \gamma|u|^4)u, \quad x \in \mathbb{R}^2, \quad u(x,t) \in \mathbb{C}, \tag{114}$$

with parameters $\alpha,\beta,\gamma,\delta \in \mathbb{C}, \operatorname{Re}\alpha > 0$. In real coordinates $u = u_1 + iu_2$ this leads to a parabolic system of the type (108). According to [22] the system (114) has so called spinning soliton solutions for parameter values

$$\alpha = \frac{1}{2}(1+i), \quad \beta = \frac{5}{2} + i, \quad \gamma = -1 - \frac{i}{10}, \quad \delta = -\frac{1}{2}. \tag{115}$$

Figure 27 shows the result of the numerical computation for these parameter values, both for the given system (108) and for the frozen system (112). The computations were done with COMSOL Multiphysics^{TM} on a ball of radius 20 and with Neumann boundary conditions. Figure 27(c) shows the final profile of the spinning soliton. In Figure 27 we plot the time dependence of $\operatorname{Re} u(\cdot,0,t)$ at the cross-section $x_2 = 0$ both for the nonfrozen system 27(a) and the frozen system 27(b). The time evolution of the velocities $\mu(t) = (\mu_1(t),\mu_2(t),\mu_3(t))$ are shown in Figure 27(d).

The system (114) is in fact equivariant with respect to the 4-dimensional group $G = S^1 \times SE(2)$ where (109) is replaced by the action $a(\gamma)v(x) = e^{i\varphi}v(R_{-\theta}(x-\tau)), x \in \mathbb{R}^2$ for $\gamma = (\varphi,\theta,\tau) \in G$. It turns out that the spinning solitons $u(x,t)$ considered here are symmetric in the following sense: $e^{i\varphi}u_*(x) = u_*(R_\varphi x)$. Then there is a nontrivial isotropy subgroup $G(u_*) = \{g \in G : a(g)u_* = u_*\}$ and the linear map $d[a(\mathbb{1})u_*] : \mathscr{A} \to Y$ is no longer one-to-one. This causes problems with the phase conditions (76),(77) which become ill-posed with respect to the parameter μ. In the

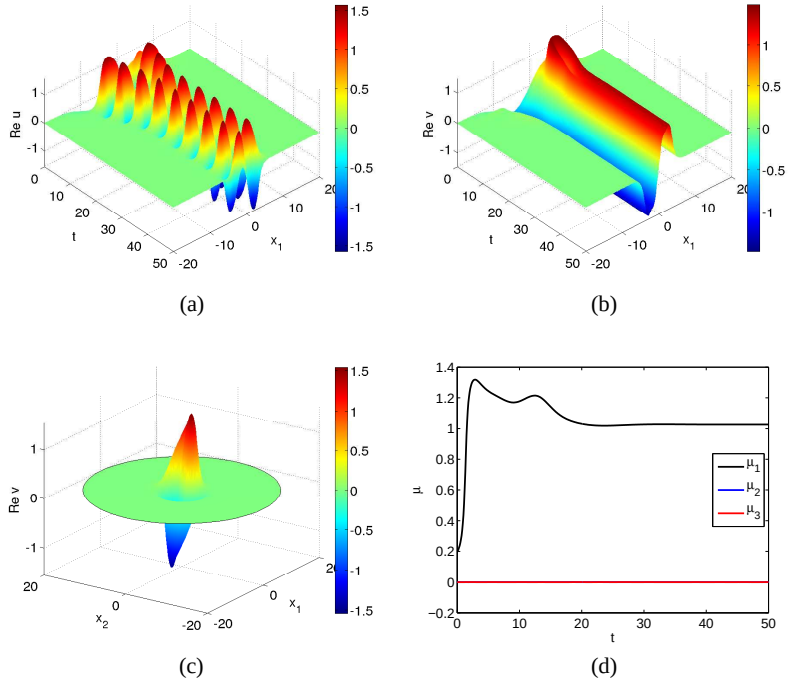

Fig. 27 Spinning solitons in the quintic-cubic Ginzburg-Landau equation. Cross-section at $x_2 = 0$ for the real part of solutions to the nonfrozen system (114) (a) and to the frozen system (112) (b). Profile $\overline{v}$ of the spinning soliton (c) and time-dependence of velocities (μ_1, μ_2, μ_3) (d). All solutions obtained by Comsol Multiphysics with piecewise linear finite elements and Neumann boundary conditions. A fixed phase condition as in (112) was used with template function $\hat{v}$ taken from the solution of the nonfrozen system at time $t = 50$. Parameter-values are given by (115).

current example we avoided such complications by considering equivariance only with respect to the three-dimensional group $SE(2)$. In this smaller group the isotropy subgroup becomes trivial.

4.2 Spectra of 2D rotating waves: essential and point spectrum

In the following we discuss the behavior of the spectrum of the linear differential operator obtained by linearizing about a rotating wave of the parabolic system (108). We consider a localized rotating wave (113). By this we mean that the profile converges to a zero v_∞ of f as $|x| \to \infty$ and that all derivatives up to order 2 converge to zero. By shifting v_∞ into the origin we may assume $f(0) = 0$ and hence

$$\sup_{|x| \geqslant r} |D^\alpha u_*(x)| \to 0 \quad \text{as} \quad r \to \infty \quad \text{for} \quad |\alpha| \leqslant 2. \tag{116}$$

We transform (108) into rotating coordinates via $u(x,t) = v(R_{-ct}x,t)$ and obtain

$$v_t = A\triangle v + cD_\phi v + f(v), \text{ with } D_\phi v = -x_2 D_1 v + x_1 D_2 v. \tag{117}$$

Linearizing at the steady state $v = u_*$ of (117) yields the operator

$$\mathscr{L}u = A\triangle u + cD_\phi u + B(x)u, \quad B(x) = f'(u_*(x)),\ x \in \mathbb{R}^2. \tag{118}$$

Applying D_1, D_2, D_ϕ to $A\triangle u_* + cD_\phi u_* + f(u_*) = 0$ and using the commutator relations $[D_1, D_\phi] = D_2$, $[D_2, D_\phi] = -D_1$, $[D_\phi, \triangle] = 0$ leads to the equations

$$0 = \mathscr{L}D_\phi u_* = \mathscr{L}(D_1 u_*) + cD_2 u_* = \mathscr{L}(D_2 u_*) - cD_1 u_*, \tag{119}$$

in particular, $\mathscr{L}(D_1 u_* \pm iD_2 u_*) = \pm ic(D_1 u_* \pm iD_2 u_*)$. Therefore, the operator $\mathscr{L}$ has at least the three eigenvalues $0, \pm ic$ in its spectrum (see Figure 28(a)) provided the functions $D_1 u_*, D_2 u_*, D_\theta$ lie in the function space under consideration. Next we

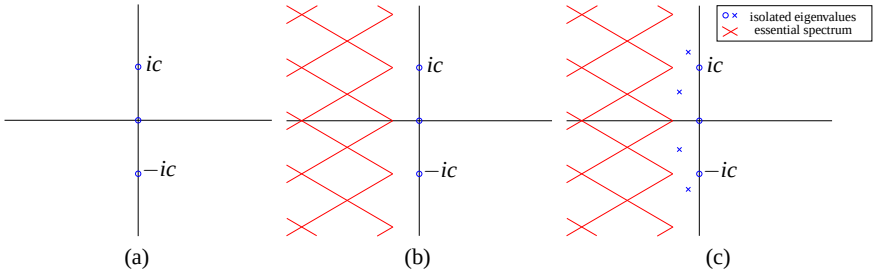

Fig. 28 Critical eigenvalues $0, \pm ic$ for a linearized rotating wave (a), essential spectrum for QCGL from Example 13: $s = inc + \delta - \kappa^2(\alpha_1 \pm i\alpha_2)$, $\kappa \in \mathbb{R}$, $n \in \mathbb{Z}$ with parameter values from (115) (b), Schematic picture of essential spectrum, critical eigenvalues, and further isolated eigenvalues for the QCGL from Example 13 (d).

discuss the essential spectrum of $\mathscr{L}$. In polar coordinates the operator reads

$$\mathscr{L} = A\left(D_r^2 + \frac{1}{r}D_r + \frac{1}{r^2}D_\theta^2\right) + cD_\theta + f'(u_*(r,\theta)). \tag{120}$$

As $r \to \infty$ we find the constant coefficient operator

$$\mathscr{L}_\infty = AD_r^2 + cD_\theta + f'(0) \tag{121}$$

With $u(r,\theta) = e^{in\theta}e^{i\kappa r}u_\infty$ we obtain $s \in \sigma(\mathscr{L}_\infty)$, if s satisfies for some $\kappa \in \mathbb{R}$ and $n \in \mathbb{Z}$ the **dispersion relation**

$$\det(-\kappa^2 A + inc + f'(0) - s) = 0. \tag{122}$$

For the quintic-cubic Ginzburg-Landau equation from Example 13 the curves from (122) turn out to be infinitely many copies of two half lines shifted along the imaginary axis, see Figure 28(b),

$$s = -\kappa^2\alpha + inc + \delta, \quad s = -\kappa^2\bar{\alpha} + inc + \bar{\delta}, \quad \kappa \in \mathbb{R}, \quad n \in \mathbb{Z}. \tag{123}$$

We indicate why these curves belong to the essential spectrum of the variable coefficient operator $\mathscr{L}$, i.e. $\sigma(\mathscr{L}_\infty) \subset \sigma_{\mathrm{ess}}(\mathscr{L})$. With the eigenfunctions above let

$$u_R(r,\theta) = \psi_R(r)\left(e^{in\theta}e^{i\kappa r}u_\infty\right)$$

where ψ_R is a smooth cut-off function such that

$$\psi_R(r) = \begin{cases} 1 & , R \leqslant r \leqslant 2R, \\ 0 & , 0 \leqslant r \leqslant R-1, 2R+1 \leqslant r. \end{cases}$$

By a straightforward computation one shows

$$\|u_R\|_{L^2}^2 \geqslant CR^2, \quad \|(\mathscr{L}-s)u_R\|_{L^2}^2 \leqslant C\left(R + R^2\varepsilon_R^2\right),$$

where $\varepsilon_R = \sup_{r\geqslant R,\theta} |f'(u^*(r,\theta)) - f'(0)| \to 0$ as $R \to \infty$. This contradicts the continuity of $(\mathscr{L}-s)^{-1}$ with respect to $\|\cdot\|_{L^2}$, i.e. $\|u_R\|_{L^2} \leqslant C\|(\mathscr{L}-s)u_R\|_{L^2}$. For the QCGL from Example 13 we expect further isolated eigenvalues to the right of the essential spectrum, see Figure 28(c) for a schematic drawing.

Clearly, since the spectrum of $\mathscr{L}$ is not contained in a sector, we expect the semigroup $e^{t\mathscr{L}}$ to be continuous but not analytic. This has serious implications for the nonlinear stability theory to be discussed in the next subsection.

Figure 29 shows details of the numerical spectrum that is found for a numerical discretization of $\mathscr{L}$ of size 10^4. The detail shows about 400 eigenvalues lying in a ball centered at 3. It turns out that, in addition to the three eigenvalues $0, \pm ic$ on the imaginary axis, there are clusters of eigenvalues which approximate the essential spectrum from Figure 28(b), and there is a total of 8 pairs of complex conjugate eigenvalues (indicated by crosses in Figure 29) between the imaginary axis and the essential spectrum. The contour plots of the associated eigenfunctions (see [9, Figure 3]) show that these eigenfunctions are actually localized, i.e. we assume their continuous counterparts to lie in $L^2(\mathbb{R}^2,\mathbb{C})$. On the contrary, the numerical eigenfunctions found for eigenvalues within the clusters, are easily recognized as being non-localized (cf. [9, Figure 3]).

4.3 A nonlinear stability theorem

In this section we outline the nonlinear stability theory for rotating patterns following [9]. We mention the alternative approach of [62] which uses center manifold

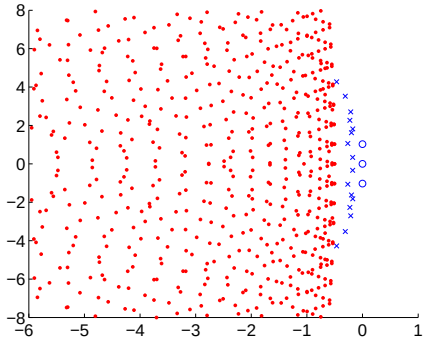

Fig. 29 Plot of numerical spectrum for the QCGL from Example 13 with parameter values from (115). In addition to 3 eigenvalues on the imaginary axis and the clusters approximating the essential spectrum from Figure 28(b), one finds additional pairs of isolated eigenvalues indicated by the blue crosses.

reductions. Recall the Sobolev spaces $H^j = H^j(\mathbb{R}^2,\mathbb{R}^m)$, $j = 0,1,2$ and the Sobolev embedding $H^2(\mathbb{R}^2) \subset L^\infty(\mathbb{R}^2) \cap C(\mathbb{R}^2)$ and introduce the subspace

$$H^2_{\mathrm{Eucl}} = H^2_{\mathrm{Eucl}}(\mathbb{R}^2,\mathbb{R}^m) = \{u \in H^2 : D_\theta u \in L^2(\mathbb{R}^2,\mathbb{R}^m)\}.$$

As above we assume the existence of a rotating wave (113) for the system (108) with nonvanishing velocity $c \neq 0$, and we impose the following

Wave conditions

(i) $f \in C^4(\mathbb{R}^m,\mathbb{R}^m)$ and $f(0) = 0$,
(ii) $\sup_{|x|\geqslant r,|\alpha|\leqslant 2}|D^\alpha u_*(x)| \to 0$ as $r \to \infty$.
(iii) $f'(0) \leqslant -2\beta I$ for some $\beta > 0$.
(iv) The eigenvalues $0, \pm ic$ have eigenfunctions $D_\theta u_*, D_1 u_* \pm iD_2 u_*$ in H^2_{Eucl}, and they are algebraically simple for the operator $\mathscr{L} = A\triangle + cD_\theta + f'(u_*)$ in H^2_{Eucl}.
(v) There are no further eigenvalues $s \in \mathbb{C}$ for $\mathscr{L}$ with $\mathrm{Re}\,(s) \geqslant -2\beta$.

Theorem 9. *([9]) Under the wave conditions (i)-(v) above, there exists an $\varepsilon > 0$ such that for any solution of* (108) *satisfying $\|u(0) - u_*\|_{H^2} \leqslant \varepsilon$ there is a C^1-function $\gamma(t) = (\theta(t),\tau(t)) \in SE(2)$, $t \geq 0$ and some $(\theta_\infty,\tau_\infty) \in SE(2)$ such that for $t \geq 0$,*

$$\begin{aligned} \|u(\cdot,t) - a(\gamma(t))u_*\|_{H^2} &\leqslant Ce^{-\beta t}\|u(0) - u_*\|_{H^2}, \\ |\theta(t) + ct - \theta_\infty| + |\tau(t) - \tau_\infty| &\leqslant Ce^{-\beta t}\|u(0) - u_*\|_{H^2}. \end{aligned} \tag{124}$$

Note that this theorem states **stability with asymptotic phase**, as we know it for traveling waves from Theorems 3 and 6.

In the following we provide some ingredients from the proof. First we transform into rotating coordinates (117).

Step 1 [Nonlinear coordinates]:
Decompose the solution of (117) and the initial value $v(0) = u_0$ in a way analogous

to (87) (see Figure 4.3 for an illustration):

$$\begin{aligned} v(t) &= a(\gamma(t))u_* + w(t), \quad \gamma(t) = (\theta(t), \tau(t)) \in S^1 \ltimes \mathbb{R}^2, \\ u_0 &= a(\gamma_0)u_* + w_0, \quad \gamma(0) = (\theta_0, \tau_0), \end{aligned} \tag{125}$$

where $w(t), w_0$ lie in the subspace $W = \{\psi_1, \psi_2, \psi_3\}^\perp$ of H^2. Here, orthogonality holds with respect to $(\cdot,\cdot)_{L^2}$, and the functions $\psi_1 \pm i\psi_2, \psi_3 \in H^2_{\text{Eucl}}$ are eigenfunctions of the adjoint operator $\mathscr{L}^*$ corresponding to the eigenvalues $\pm ic, 0$ (cf. wave condition (iv)).

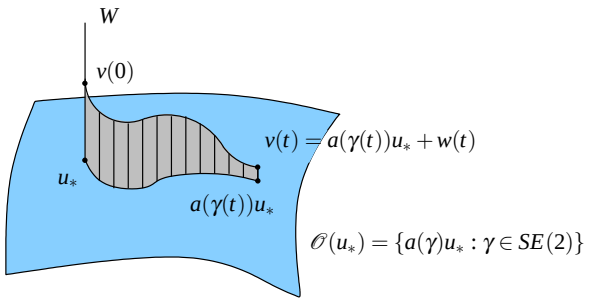

Fig. 30 Decomposition of dynamics near a two-dimensional group orbit

Step 2 [The decomposed system]: Inserting (125) into (117), expanding the nonlinearities and inverting the linear parts leads to the following system of coupled integral equations for the new variables $w(t), \gamma(t)$:

$$\begin{aligned} w(t) &= e^{t\mathscr{L}} w_0 + \int_0^t e^{(t-\tau)\mathscr{L}} \rho^{[w]}(w(\tau), \gamma(\tau)) d\tau, \\ \gamma(t) &= e^{tE_c} \gamma_0 + \int_0^t e^{(t-\tau)E_c} \rho^{[\gamma]}(w(\tau), \gamma(\tau)) d\tau, \end{aligned} \tag{126}$$

where E_c has the matrix representation $E_c = \begin{pmatrix} 0 & c & 0 \\ -c & 0 & 0 \\ 0 & 0 & 0 \end{pmatrix}$ and $\rho^{[\gamma]}, \rho^{[w]}$ are quadratic remainder terms.

Step 3 [From linear to nonlinear decay estimates]:
The crucial step in the proof is the linear decay estimate

$$\|e^{t\mathscr{L}} w\|_{H^2} \leqslant Ce^{-\beta t} \|w\|_{H^2} \quad \text{for} \quad w \in W, \tag{127}$$

which will be discussed in more detail in Step 4 below. The nonlinear estimate (124) is obtained by using Gagliardo Nirenberg type estimates for the remainders $\rho^{[w]}$ resp. $\rho^{[\gamma]}$ and combining them with the linear estimate (127).

Step 4 [Exponential decay of a C^0-semigroup]:
We collect the available information for the variable coefficient operator $\mathscr{L}$ from

(119) and the constant coefficient operator (121). The wave condition (ii) guarantees $\mathrm{Re}\,(\sigma(\mathscr{L}_\infty)) \leqslant -\beta$. Using condition (iii) one can also prove that $\mathscr{L} = \mathscr{L}_\infty + (f'(u_*) - f'(0)) : H^2_{Eucl} \to L^2$ is a relatively compact perturbation of $\mathscr{L}_\infty$, which by Theorem 2 shows $\mathrm{Re}\,\sigma_{ess}(\mathscr{L}) \leq -\frac{\beta}{2} < 0$. But now the problem arises that the spectral mapping theorem for C^0-semigroups holds for the point spectrum, but in general not for the essential spectrum, see [51],[28]. That is, $\exp(\sigma(\mathscr{L})) = \sigma(\exp(\mathscr{L}))$ holds for $\sigma = \sigma_{\mathrm{point}}$ (up to the number 0) but not for σ_{ess}.

However, it turns out that, instead of Theorem 2 one can use the following Theorem on relatively compact perturbation of the semigroup itself.

Theorem 10. *Let $A : D(A) \subset X \to X$ denote the generator of a C^0-semigroup e^{tA} of type*

$$\omega(A) = \inf_{t>0} t^{-1} \log \left\| e^{tA} \right\| = \lim_{t\to\infty} t^{-1} \log \left\| e^{tA} \right\|,$$

and let $B \in L[X]$ be linear, bounded such that

$$Be^{tA} \quad \textit{is compact for all} \quad t > 0.$$

Then $A + B : D(A) \to X$ generates a C^0-semigroup $e^{t(A+B)}$ with

$$\left|\sigma_{\mathrm{ess}}(e^{A+B})\right| \leqslant e^{\omega(A)}. \tag{128}$$

Moreover, $\mathrm{Re}\left[\sigma_{\mathrm{point}}(A+B)\right] \leqslant \omega_+$ *implies* $\omega(A+B) \leqslant \max\{\omega(A), \omega_+\}$.

For a proof of the theorem we refer to [9, Appendix], and we note that it can also be derived by combining several results from [28]. In our situation we can apply the theorem to the operators $A = \mathscr{L}_\infty$, $A + B = \mathscr{L}$, $B = f'(u_*) - f'(0)$ since $(f'(u_*) - f'(0))e^{t\mathscr{L}_\infty}$ is compact in H^2. Equation (128) then leads to an exponential estimate for $\sigma_{\mathrm{ess}}(e^{t\mathscr{L}})$, in particular $|\sigma_{\mathrm{ess}}(e^{\mathscr{L}})| < 1$. Now one restricts $\mathscr{L}$ to the subspace W which is invariant under $\exp\mathscr{L}$ (but not under $e^{\mathscr{L}_\infty}$!) and applies the spectral mapping theorem to find $|\sigma_{\mathrm{point}}(e^{L_{|W}})| < 1$ from wave condition (v). Combining both results, finally proves the estimate (127).

4.4 Further experiments with waves in 2D and 3D

We finish this section with numerical experiments in two and three space dimensions. We note that for these non-localized waves, there is currently no rigorous nonlinear stability analysis available.

Example 14 (Barkley model). The frozen version (112) of the well-known Barkley spiral system [6] reads

$$
\begin{aligned}
u_t &= \triangle u + \frac{1}{\varepsilon} u(1-u)(u - \frac{v+b}{a}) + \mu_1(x_2 u_{x_1} - x_1 u_{x_2}) + \mu_2 u_{x_1} + \mu_3 u_{x_2}, \\
v_t &= u - v + \mu_1(x_2 v_{x_1} - x_1 v_{x_2}) + \mu_2 v_{x_1} + \mu_3 v_{x_2}, \\
0 &= (x_2 u_{0,x_1} - x_1 u_{0,x_2}, u - u_0)_{L^2} + \left(x_2 v^0_{x_1} - x_1 v^0_{x_2}, v - v^0\right)_{L^2}, \\
0 &= (u_{0,x_1}, u - u_0)_{L^2} + \left(v^0_{x_1}, v - v^0\right)_{L^2} = (u_{0,x_2}, u - u_0)_{L^2} + \left(v^0_{x_2}, v - v^0\right)_{L^2}.
\end{aligned}
$$

For parameter values

$$
\varepsilon = \frac{1}{50}, \quad a = 0.75, \quad b = 0.01, \tag{129}
$$

Figure 31(d) shows the behavior of the 3 group velocities of a frozen spiral.

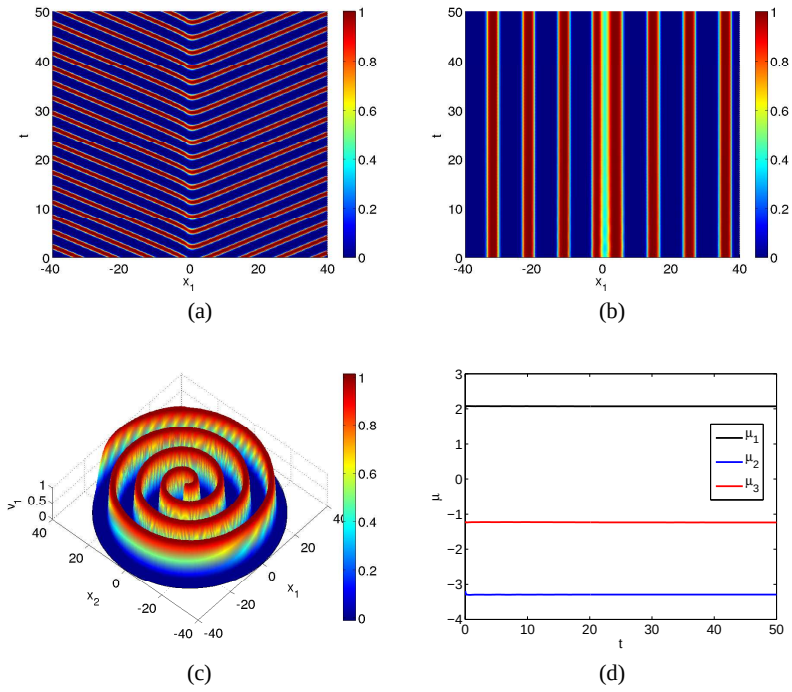

Fig. 31 Cross-section at $x_2 = 0$ for the first component of the Barkley spiral $u(x,t)$ of the nonfrozen system (a) and of the frozen system (b). First component of the profile $\bar{v}$ of the Barkley spiral (c) and time-dependence of velocities (μ_1, μ_2, μ_3) (d). Solution by Comsol Multiphysics with piecewise linear finite elements, Neumann boundary conditions, fixed phase condition with template function $\hat{v}$ taken from the solution of the nonfrozen system at time $t = 150$ and parameter values from (129).

Let us compute the motion $\gamma(t) = (\theta(t), \tau(t))$ in the group when the solution has reached its relative equilibrium, i.e. we determine $\gamma(t) = \exp(t\bar{\mu}) \in G$ for a given $\bar{\mu} \in \mathscr{A}$ from the reconstruction equation

$$\dot{\gamma} = dL_\gamma(\mathbb{1})\bar{\mu} = \begin{pmatrix} 1 & 0 \\ 0 & R_\theta \end{pmatrix} \bar{\mu}, \quad \gamma(0) = 0. \tag{130}$$

The solution is

$$\bar{\gamma}(t) = \begin{pmatrix} \theta(t) \\ \tau(t) \end{pmatrix} = \begin{pmatrix} \bar{\mu}_1 t \\ (I - R_{\bar{\mu}_1 t}) x_c \end{pmatrix}, \quad \text{where} \quad x_c = \frac{1}{\bar{\mu}_1} \begin{pmatrix} -\bar{\mu}_3 \\ \bar{\mu}_2 \end{pmatrix}. \tag{131}$$

Note that $\tau(t)$ moves on a circle of radius $\|x_c\|$ centered at x_c. Inserting this into the profile u_* we obtain the solution

$$\bar{u}(x,t) = u_*(R_{-\bar{\mu}_1 t}(x + (R_{\bar{\mu}_1 t} - I)x_c)) = u_*(R_{-\bar{\mu}_1 t}(x - x_c) + x_c). \tag{132}$$

If a specific point $\bar{x}$ of the profile u_* is of interest, e.g. the tip of a spiral, then this point will be visible at position $x(t)$ with $\bar{x} = R_{-\bar{\mu}_1 t}(x(t) - x_c) + x_c$, i.e. on the circle given by $x(t) = R_{\bar{\mu}_1 t}(\bar{x} - x_c) + x_c$. Our conclusion is that the freezing method gives the information about the center x_c and the speed of rotation $\bar{\mu}_1$ for free. There is no need to use ad-hoc definitions for locating the tip of a spiral, for example. A comparison of this method with traditional ways of following the tip of a spiral from a direct simulation of the given system is provided in [14]. However, we note that it can be useful to impose such spiral tip conditions if one aims at phase conditions that lead to global sections. In [34] such an approach is used for freezing not only rigidly rotating spirals (relative equilibria) but also to recognize meandering spirals (relative periodic orbits). The work [40] contains another interesting application of the freezing methodology, namely to follow the large core limit of spiral waves, i.e. to observe the behavior $\mu_1 \to 0$ or $x_c \to \infty$ under parametric perturbations, without solving the equations on extremely large domains.

Example 15 (Quintic-cubic Ginzburg-Landau equation). We continue the QCGL equations from Example 13 in three space dimensions

$$u_t = \alpha \Delta u + (\delta + \beta|u|^2 + \gamma|u|^4)u, \quad x \in \mathbb{R}^3, \quad u(x,t) \in \mathbb{C}, \tag{133}$$

and look for $3D$ spinning solitons. The system is equivariant with respect to the action of the 6-dimensional Euclidean group $G = SE(3) = SO(3) \ltimes \mathbb{R}^3$, given by

$$[a(\gamma)v](x) = v(R^{-1}(x - \tau)), \quad \gamma = (R, \tau) \in SE(3). \tag{134}$$

Recall that the group operation in this representation is $\gamma \circ \tilde{\gamma} = (R\tilde{R}, \tau + R\tilde{\tau})$. The freezing method leads to the PDE

$$\begin{aligned} v_t = {} & \alpha \Delta v + (\delta + \beta|u|^2 + \gamma|u|^4)u + \mu_4 v_{x_1} + \mu_5 v_{x_2} + \mu_6 v_{x_3} \\ & + \mu_1(v_{x_2}x_3 - v_{x_3}x_2) + \mu_2(v_{x_3}x_1 - v_{x_1}x_3) + \mu_3(v_{x_1}x_2 - v_{x_2}x_1), \end{aligned} \tag{135}$$

complemented by 6 phase conditions. In Figure 32 we show the results of a simulation of this system for the same parameter values as in (115). Figure 32(a)-(c) shows the spinning solitons for 3 different time instances of the original equation, while Figure 32(d) displays the profile of the frozen solution by showing two iso-

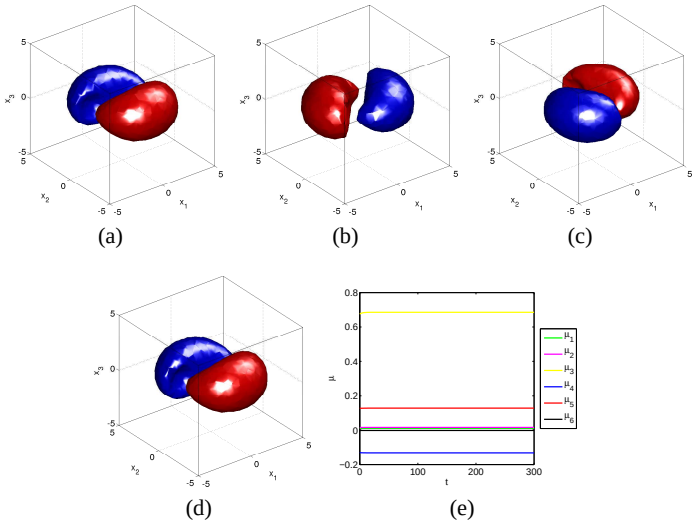

Fig. 32 Isosurfaces $\mathrm{Re}\, u(x_1,x_2,x_3,t) = \pm 0.5$ at times $t = 0$, 3.2, 6.5 (a)-(c), isosurfaces of the real part of the profile $\overline{v}$ and time-dependence of velocities $\mu(t)$ for the three-dimensional QCGL (133)

surfaces of the real part. The behavior of the six algebraic variables $\mu_1,\ldots,\mu_6$ is shown in Figure 32(e). The resulting relative equilibria seem to be localized and stable with asymptotic phase, but we are not aware of any rigorous result in this direction comparable to Theorem 9.

4.5 Summary

Let us summarize the results of this section:

- The freezing method applies to 2D and 3D rotating patterns and automatically generates information about angular velocities and centers of rotation.
- For rotating localized 2D waves one can prove nonlinear stability with asymptotic phase in the Sobolev space H^2 from linear stability.
- Differential operators obtained by linearizing about rotating two-dimensional patterns generate only C^0-semigroups.
- Numerical approximations and convergence of the freezing method are not yet analyzed theoretically. There are also no rigorous theorems on nonlinear stability of nonlocalized rotating patterns such as spiral waves.

5 Decomposition and freezing of multi-structures

Many excitable systems discussed in the first sections admit special solutions that are composed of several waves and thus cannot be frozen in a single coordinate frame. Often such patterns travel at different speeds and either move towards each other (the case of *strong interaction*) or repel each other (the case of *weak interaction*). As long as the patterns do not interact strongly they seem to behave like linear superpositions, though this cannot be true in the strict sense for a nonlinear system. In this section we discuss an extension of the freezing method to handle multiple coordinate frames in which the single profiles can stabilize independently while still capturing their nonlinear interaction. The basic idea is to use dynamic partitions of unity in order to decompose the system into a larger system of PDAEs, the dimension of which is determined by the maximal number of patterns. The basic idea is taken from [12] while we follow here the improvement from [64]. In particular, we explain a highly sophisticated stability result from the thesis [64] which applies to weakly interacting fronts and pulses. We also mention that this numerical approach is closely related to an analytical method developed in [63], [70] where so-called exit and shooting manifolds are constructed which are followed by the multi-structures for a certain time.

5.1 Multi-pulses and multi-fronts

Consider the Cauchy problem for a parabolic (or mixed hyperbolic-parabolic) system in one space variable

$$\begin{aligned} u_t &= Au_{xx} + f(u),\ x \in \mathbb{R}, t \geq 0, \\ u(\cdot,0) &= u_0, \end{aligned} \tag{136}$$

for a function $u(x,t) \in \mathbb{R}^m$ on the real line, where $A \in \mathbb{R}^{m,m}$ is assumed to be positive semidefinite and $f : \mathbb{R}^m \to \mathbb{R}^m$ is assumed to be sufficiently smooth. Multi-pulses and multi-fronts generically appear in a large variety of systems of the form (136) and we mention two standard examples:

Example 16. **FitzHugh-Nagumo system**
Recall the FitzHugh-Nagumo system

$$\begin{aligned} u_t = \begin{pmatrix} u_1 \\ u_2 \end{pmatrix}_t &= \begin{pmatrix} 1 & 0 \\ 0 & \varepsilon \end{pmatrix} u_{xx} + f(u) \\ f\begin{pmatrix} u_1 \\ u_2 \end{pmatrix} &= \begin{pmatrix} u_1 - \frac{1}{3}u_1^3 - u_2 \\ \phi\,(u_1 + a - bu_2) \end{pmatrix}, \quad \phi, a, b > 0, \varepsilon \geqslant 0. \end{aligned}$$

In Example 7 we observed for pulse like initial data the generation of a **double pulse** solution, see Figure 12. More precisely, the solution to the Cauchy problem

develops two pulses, traveling in opposite directions. See Example 7 for the details of the numerical simulation.

We have seen that the numerical method of freezing captures one of the two evolving pulses, while the other leaves the computational domain. In fact, in the numerical experiments the phase condition determined which of the two traveling pulses is captured and which is lost.

Example 17 (Nagumo equation). As an example that generates **double fronts** we consider again the Nagumo equation, compare Example 6,

$$u_t = u_{xx} + u(1-u)(u-a), \quad x \in \mathbb{R},\, t \geq 0, \quad u(\cdot,0) = u_0,$$

with parameter $a = \frac{1}{4}$. As initial condition for the Cauchy problem we choose the piecewise linear function

$$u_0(x) = \mathbf{1}_{(-50,0]}(x) \cdot \frac{x+50}{50} + \mathbf{1}_{(0,50)}(x) \cdot \frac{50-x}{50}, \tag{137}$$

where $\mathbf{1}_M(x) = 1$ for $x \in M$ and $\mathbf{1}_M(x) = 0$ for $x \notin M$ is the indicator function of a set M. The solution to this problem consists of two fronts traveling with the same speed in opposite directions. A numerical solution is shown in Figure 33.

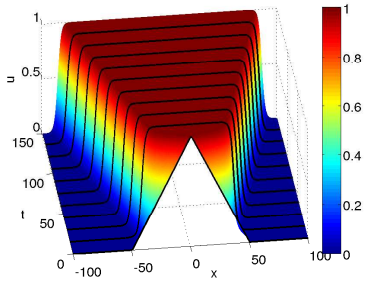

Fig. 33 Space-time diagram of a double front solution to the Nagumo equation for parameter value $\alpha = \frac{1}{4}$ on the domain $\Omega = [-100, 100]$. Solution by Comsol Multiphysics with piecewise linear finite elements, Neumann boundary conditions, $\triangle x = 0.1$, $\triangle t = 0.1$, BDF of order 2 and initial data u_0 from (137).

The above examples show that it is important to be able to capture multi-pulses and multi-fronts. Obviously, this cannot be done by using a single moving frame. For patterns sufficiently far apart, the individual parts of the pattern seem not to influence each other and the multi-structures look like linear superpositions, but due to nonlinearities they cannot be linear superpositions. Nevertheless, in the case of **weak interaction**, i.e. when the patterns are far apart for large times, linear superposition is a good model. Currently, there is no theory available in the case of **strong interaction**, i.e. when the individual parts of the multi-structure get close to each other.

5.2 Decompose and freeze multi-structures

Now consider the Cauchy problem (136) and assume that the solution u consists of N single profiles. To generalize the freezing ansatz to this situation we write the solution as the superposition of N profiles in the following form

$$u(x,t) = \sum_{j=1}^{N} v_j(x - g_j(t), t). \tag{138}$$

Here the function $g_j : [0,\infty[\to \mathbb{R}$ denotes the time dependent position of the j-th profile $v_j : \mathbb{R} \times [0,\infty[\to \mathbb{R}^m$, $(x,t) \mapsto v_j(x,t)$. Of course, due to nonlinearity, the solution u is not just the superposition of N separate profiles as pretended in (138).

To overcome this difficulty and to make use of the fact that well separated profiles basically behave like linear superpositions, we use the idea of partition of unity: Let $\varphi \in C^\infty(\mathbb{R},\mathbb{R})$ be a positive bump function such that the main mass is located near zero and $0 < \varphi(x) \leqslant 1$ for every $x \in \mathbb{R}$. A suitable choice for φ is $\varphi(x) = \operatorname{sech}(\beta x) = \frac{1}{\cosh(\beta x)}$ with $\beta > 0$. Then for $g = (g_1, \ldots, g_N) : [0,\infty) \to \mathbb{R}^N$ and $x \in \mathbb{R}$ the functions

$$Q_j(g(t),x) = \frac{\varphi(x - g_j(t))}{\sum_{k=1}^{N} \varphi(x - g_k(t))},\ j = 1,\ldots,N \tag{139}$$

have non-vanishing denominators and form a time-dependent partition of unity, i.e.

$$1 = \frac{\sum_{j=1}^{N} \varphi(x - g_j)}{\sum_{k=1}^{N} \varphi(x - g_k)} = \sum_{j=1}^{N} Q_j(g,x).$$

We are interested in solutions of (136) of the form (138). In order to investigate such solutions we insert the ansatz (138) into (136) and use the partition of unity (139). Abbreviating $v_k(*) = v_k(\cdot - g_k(t), t)$ this leads to

$$\begin{aligned}
&\sum_{j=1}^{N} [v_{j,t}(*) - v_{j,x}(*) g_{j,t}] = u_t = Au_{xx} + f(u) \\
&= \sum_{j=1}^{N} \left[Av_{j,xx}(*) + Q_j(g,\cdot) f\left(\sum_{k=1}^{N} v_k(*) \right) \right] \\
&= \sum_{j=1}^{N} \left[Av_{j,xx}(*) + f(v_j(*)) + Q_j(g,\cdot) \left\{ f\left(\sum_{k=1}^{N} v_k(*) \right) - \sum_{k=1}^{N} f(v_k(*)) \right\} \right].
\end{aligned} \tag{140}$$

Now, we require that the summands on the left and on the right hand side of (140) coincide for every $j = 1,\ldots,N$. The idea is to consider each of the summands in its own co-moving frame and apply the freezing ansatz: We substitute $\xi = x - g_j(t)$, $\mu_j = g_{j,t}$ and $*_{kj} = \xi - g_k(t) + g_j(t)$, add initial and phase condition for each v_j, $j = 1,\ldots,N$ and obtain the following coupled system for $j = 1,\ldots,N$, $\xi \in \mathbb{R}$, $t \geq 0$

$$\begin{aligned} v_{j,t}(\xi,t) &= Av_{j,\xi\xi}(\xi,t) + v_{j,\xi}(\xi,t)\mu_j(t) + f(v_j(\xi,t)) \\ &\quad + \frac{\varphi(\xi)}{\sum_{k=1}^N \varphi(*_{kj})}\left[f\left(\sum_{k=1}^N v_k(*_{kj},t)\right) - \sum_{k=1}^N f(v_k(*_{kj},t))\right], \\ 0 &= (v_j(\cdot,t) - \hat{v}_j, \hat{v}_{j,x})_{L^2}, \quad v_j(\cdot,0) = v_j^0, \\ g_{j,t} &= \mu_j, \qquad\qquad\qquad\quad g_j(0) = g_j^0. \end{aligned} \tag{141}$$

To enforce that also the initial condition in (136) is satisfied, we additionally require $u_0 = \sum_{j=1}^N v_j^0(\cdot - g_j^0)$. It is easy to see that if (v_j, g_j) solves (141) and satisfies the assumption on the initial condition, then $u(\cdot,t) = \sum_{j=1}^N v_j(\cdot - g_j(t), t)$ solves the Cauchy problem (136). Note that the decomposition is not unique.

In the case of multi-fronts one has different limits at $\pm\infty$ and it is, even in the linear case, not possible to simply add the single profiles as we did in (138). In order to employ the above procedure also in this case, we define

$$u_j^- = \begin{cases} 0 & , j = 1, \\ \lim_{x\to-\infty} w_j(x) & , j \geq 2, \end{cases} \tag{142}$$

where w_j is the expected j-th wave. The situation is depicted in Figure 34, where a double front is considered. Writing the j-th wave as $v_j(\xi,t) + u_j^-$ and following the

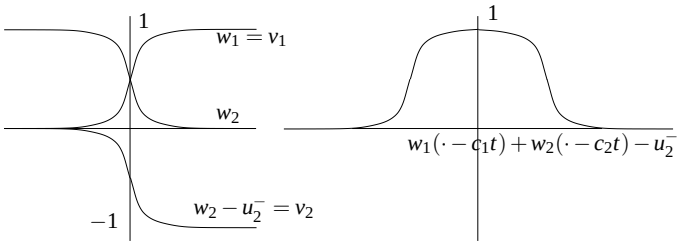

Fig. 34 The sum of two fronts forming a multi-front.

recipe from (140), we obtain the coupled PDAE system for $j = 1,\ldots,N$:

$$\begin{aligned} v_{j,t}(\xi,t) &= Av_{j,\xi\xi}(\xi,t) + v_{j,\xi}(\xi,t)\mu_j(t) + f(v_j(\xi,t) + u_j^-) \\ &\quad + \frac{\varphi(\xi)}{\sum_{k=1}^N \varphi(*_{kj})}\left[f\left(\sum_{k=1}^N v_k(*_{kj},t)\right) - \sum_{k=1}^N f(v_k(*_{kj},t) + u_k^-)\right], \\ 0 &= (v_j(\cdot,t) - \hat{v}_j, \hat{v}_{j,x})_{L^2}, \quad v_j(\cdot,0) = v_j^0, \\ g_{j,t} &= \mu_j, \qquad\qquad\qquad\quad g_j(0) = g_j^0. \end{aligned} \tag{143}$$

Again we require $u_0 = \sum_{j=1}^N v_j^0(\cdot - g_j^0)$, so that a solution (v_j, g_j) to (143) yields a solution of (136) via (138). Note that allowing $u_j^- = 0$, (143) includes the case

of pulses (141) and also the cases of solutions that consist of both, pulse and front solutions.

We just mention, that the PDAE systems (141) and (143) contain nonlinear and nonlocal coupling terms. For solving the PDAE on a bounded domain $J = [x_-, x_+]$, we have to interpolate by the left and the right limit, respectively, whenever $*_{kj} = \xi - g_k(t) + g_j(t) \notin [x_-, x_+]$. Namely, we extend the function v_j to be constant equal to its boundary values.

Example 18 (Nagumo equation). Consider the Nagumo equation from Example 6 with parameter $a = \frac{1}{4}$,

$$u_t = u_{xx} + u(1-u)(u-a), \quad x \in \mathbb{R},\ t \geq 0, \quad u(\cdot,0) = u_0.$$

(a) First consider the case of two repelling fronts. This situation occurs, for example, when the initial data form a hat function as in (137). We use the PDAE system (143) with $N = 2$ and $u_2^- = 1$. As initial data we choose

$$v_1^0(x) = \mathbf{1}_{(-25,25)}(x) \cdot \frac{x+25}{50} + \mathbf{1}_{[25,\infty)}(x), \quad x \in \mathbb{R},$$
$$v_2^0(x) = -\mathbf{1}_{(-25,25)}(x) \cdot \frac{x+25}{50} - \mathbf{1}_{[25,\infty)}(x), \quad x \in \mathbb{R}$$

for the two profiles and $g_1^0 = -25$, $g_2^0 = 25$ for the initial shifts. The simulation is performed on the finite interval $J = [-50, 50]$ with $\varphi(x) = \operatorname{sech}\left(\frac{x}{2}\right)$ and the solutions v_1 and v_2 are assumed to equal their asymptotic values outside the computational domain. The results of a simulation are plotted in Figure 35. The performance of the decompose and freeze method can be demonstrated by plotting the difference of the superposition (138) from the result obtained by a direct simulation of the full system (see [12] for such a comparison).

(b) As a second example we consider the case of two colliding fronts. For this we take initial conditions

$$u_0(x) = 1 - \mathbf{1}_{(-100,0]}(x) \cdot \frac{x+100}{100} + \mathbf{1}_{(0,100)}(x) \cdot \frac{x-100}{100}, \quad x \in \mathbb{R},$$

which we split as follows $u_0 = v_1^0(\cdot - g_1^0) + v_2^0(\cdot - g_2^0)$, with

$$v_1^0(x) = \mathbf{1}_{(-\infty,50)}(x) - \mathbf{1}_{(-50,50)}(x) \cdot \frac{x+50}{100}, \quad x \in \mathbb{R},$$
$$v_2^0(x) = \mathbf{1}_{(-50,50)}(x) \cdot \frac{x+50}{100} + \mathbf{1}_{[50,\infty)}(x), \quad x \in \mathbb{R}.$$

The initial shifts are $g_1^0 = -50$, $g_2^0 = 50$. Note that in this case we have $u_2^- = 0$ and $\varphi(x) = \operatorname{sech}\left(\frac{x}{2}\right)$. A result of the method is shown in Figure 36. Note that the decompose and freeze method successfully handles the strong interaction. The single waves assume a common velocity and asymptotically converge to two steady profiles which sum up to the final profile (which is identically 1 in this case). So far, we have no theory which proves this behavior for the case of strong interaction.

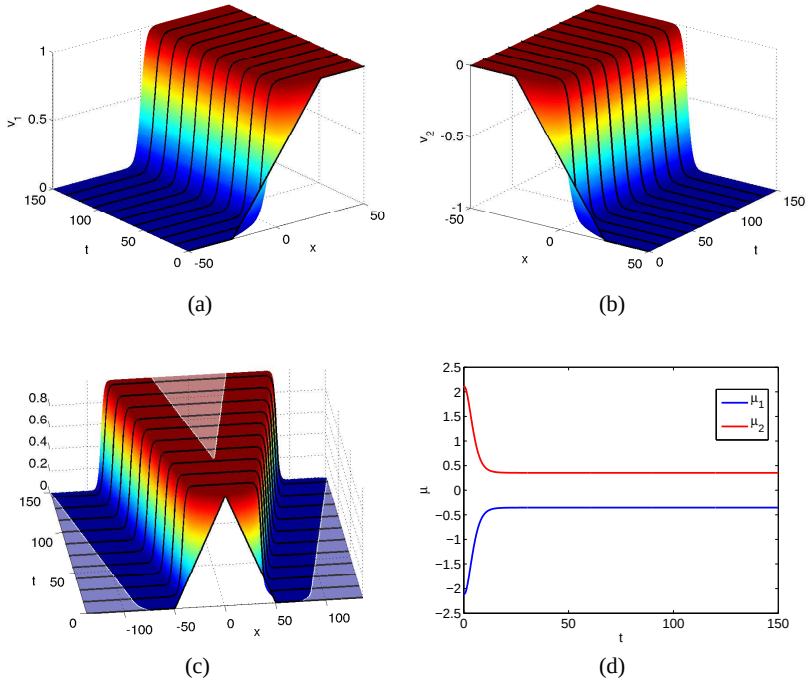

Fig. 35 The decompose and freeze method for a repelling double front in the Nagumo equation. The v_1 component (a) and the v_2 component (b), plot of the superposition $u(\cdot,t) = v_1(*,t) + v_2(*,t)$ with supports of single fronts indicated by dark shading (c), evolution of the individual speeds converging to $\bar{\mu}_1 = -\bar{\mu}_2 = 0.3536$ (d). Solution of (143) by Comsol Multiphysics with piecewise linear finite elements, Neumann boundary conditions, $\triangle x = 0.1$, $\triangle t = 0.1$, BDF of order 2.

Example 19 (Quintic Nagumo equation). As an example supporting multi-structures with more than two patterns, we consider the quintic Nagumo equation

$$u_t = u_{xx} - \prod_{i=1}^{5}(u - a_i), \quad x \in \mathbb{R},\ t \geq 0, \tag{144}$$

with parameters $0 = a_1 < a_2 < a_3 < a_4 < a_5 = 1$. Depending on the choices of a_2, a_3, a_4 one observes different patterns which can be captured by the decompose and freeze method. We present the results for a selection of parameter values. In all cases we solve (143) with Neumann boundary conditions, choose the bump function $\varphi(x) = \operatorname{sech}\left(\frac{x}{20}\right)$ and use spatial step-size $\Delta x = 0.4$.

(a) Parameters: $a_2 = 0.03125$, $a_3 = 0.4$, $a_4 = 0.73$, $\Delta t = 0.8$, initial data: $g_1(0) = g_2(0) = 0$, , $u_2^- = a_3$, $v_1^0(x) = \frac{u_2^-}{2}\left(\tanh\left(\frac{x}{5}\right) + 1\right)$, $v_2^0(x) = \frac{(1-u_2^-)}{2}\left(\tanh\left(\frac{x}{5}\right) + 1\right)$. The solutions are shown in Figure 37. We start with the superposition of two front-like functions located at the same position. Then two fronts develop, a fast one traveling traveling at speed $\bar{\mu}_1 = -0.159$ and a slow one with speed $\bar{\mu}_2 = -0.02131$. The

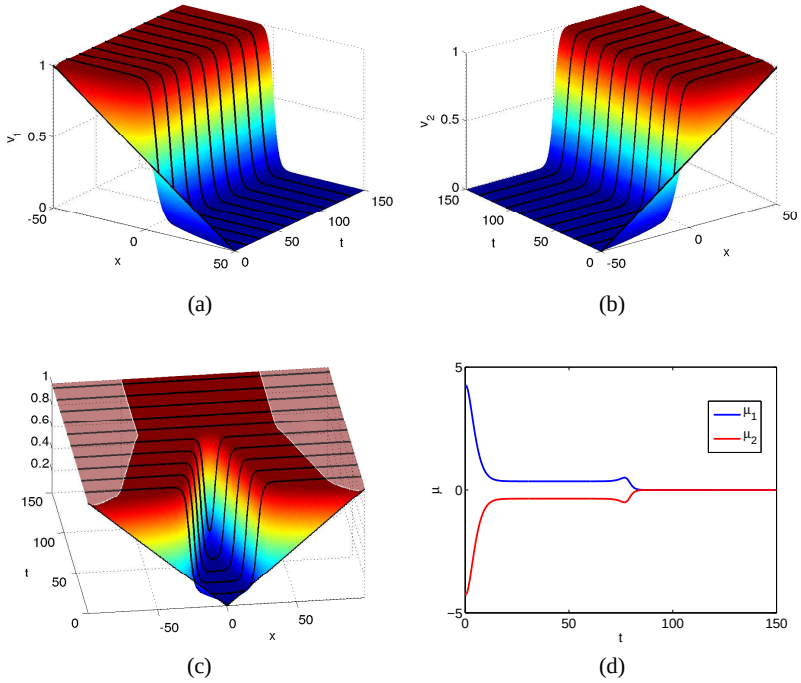

Fig. 36 Freezing two colliding fronts in the Nagumo equation. Plot of v_1 component (a), v_2 component (b), superposition $u(\cdot,t) = v_1(*,t) + v_2(*,t)$ with supports of single fronts indicated by dark shading (c), evolution of speeds μ_a,μ_2 of the components v_1 ,v_2, both converging ultimately to $\bar{\mu}_1 = \bar{\mu}_2 = 0$. Solution of (143) by Comsol Multiphysics with piecewise linear finite elements, Neumann boundary conditions, $\triangle x = 0.1$, $\triangle t = 0.1$, BDF of order 2.

single fronts v_1 in (a) and v_2 in (b) converge, Figure 37 shows their superposition according to (138) with the supports of v_1,v_2 indicated by dark shading. This is a case of weak interaction.

(b) Parameters: $a_2 = 0.125$, $a_3 = 0.4$, $a_4 = 0.58$, $\Delta t = 0.3$, initial data: $g_1(0) = -50, g_2(0) = 50, u_2^- = a_3, v_1^0(x) = \frac{u_2^-}{2}\left(\tanh\left(\frac{x}{5}\right)+1\right), v_2^0(x) = \frac{(1-u_2^-)}{2}\left(\tanh\left(\frac{x}{5}\right)+1\right)$. The results are shown in Figure 38. Starting with a staircase function, two fronts of different speed develop, with the faster one overtaking the slower one. Then strong interaction takes place and both fronts merge to a single front of speed $\bar{\mu}_1 = \bar{\mu}_2 = -0.08312$, cf. Figure 38 (d). The components v_1,v_2 stabilize at profiles with little kinks that add up to the merged travelling front. The decompose and freeze method is able to handle this case of strong interaction.

(c) Parameters: $a_2 = 0.0625$, $a_3 = 0.4$, $a_4 = 0.7$, $\Delta t = 0.8$, initial data: $g_1(0) = -50, g_2(0) = 0, g_3(0) = 50, u_2^- = a_3, u_3^- = a_5, v_1^0(x) = \frac{u_2^-}{2}\left(\tanh\left(\frac{x}{5}\right)+1\right), v_2^0(x) = \frac{(1-u_2^-)}{2}\left(\tanh\left(\frac{x}{5}\right)+1\right), v_3^0(x) = \frac{(u_2^- - u_3^-)}{2}\left(\tanh\left(\frac{x}{5}\right)+1\right)$. Results are shown in Figure 39. We start with a multi-front consisting of three stairs. Three fronts develop, one

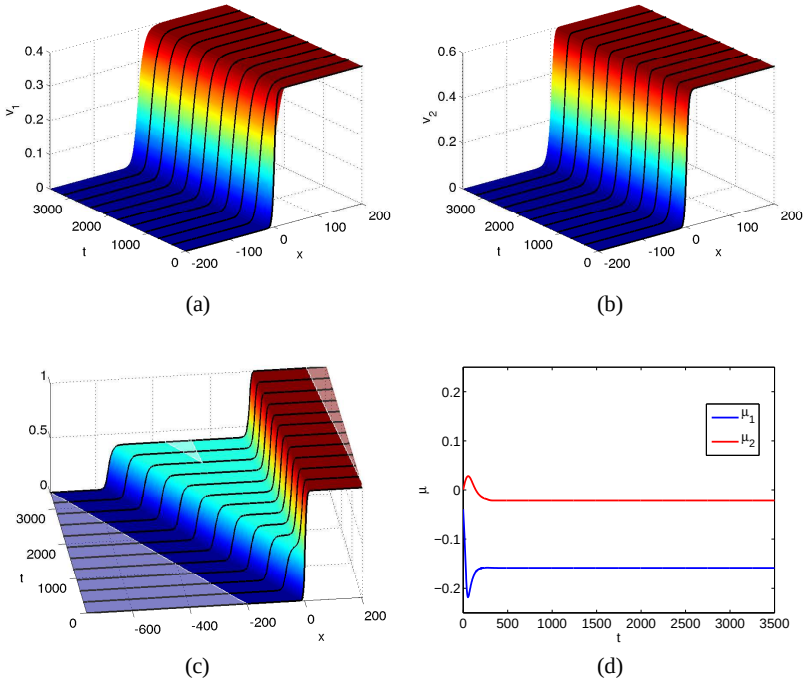

Fig. 37 Two fronts of different speed developing out of a single front in the quintic Nagumo equation (144): convergence of the decompose and freeze method for single fronts v_1 (a) and v_2 (b), plot of superposition (138) with supports of v_1,v_2 indicated by dark shading (c), time-dependence of single speeds (d).

traveling to the right with speed $\bar{\mu}_3 = 0.05088.$ and two traveling to the left with speeds $\bar{\mu}_1 = -0.1172$, $\bar{\mu}_2 = -0.05088$. This is a case of weak interaction since the initial locations of fronts are in the same order as the corresponding velocities. The system (143) is now solved with $N = 3$.

Example 20 (FitzHugh-Nagumo system). Our final example are repelling and colliding pulses in the FitzHugh-Nagumo system from Example 7. We take the parameter values

$$\varepsilon = 0.1, \quad \phi = 0.08, \quad a = 0.7, \quad b = 0.8,$$

for which we know traveling pulses to exist (see also [49]). The spatial domain is $J = [x_-, x_+] = [-100, 100]$ and we impose Neumann boundary conditions.

(a) In our simulation for two repelling pulses we use the following initial data

$$v_1^0(x) = u_2^- + \begin{pmatrix} \frac{2.5}{1+\left(\frac{x}{3}\right)^2} \cdot \mathrm{flc2hs}(-x,5) \\ 0 \end{pmatrix}, \quad v_2^0(x) = \begin{pmatrix} \frac{2.5}{1+\left(\frac{x}{3}\right)^2} \cdot \mathrm{flc2hs}(x,5) \\ 0 \end{pmatrix},$$

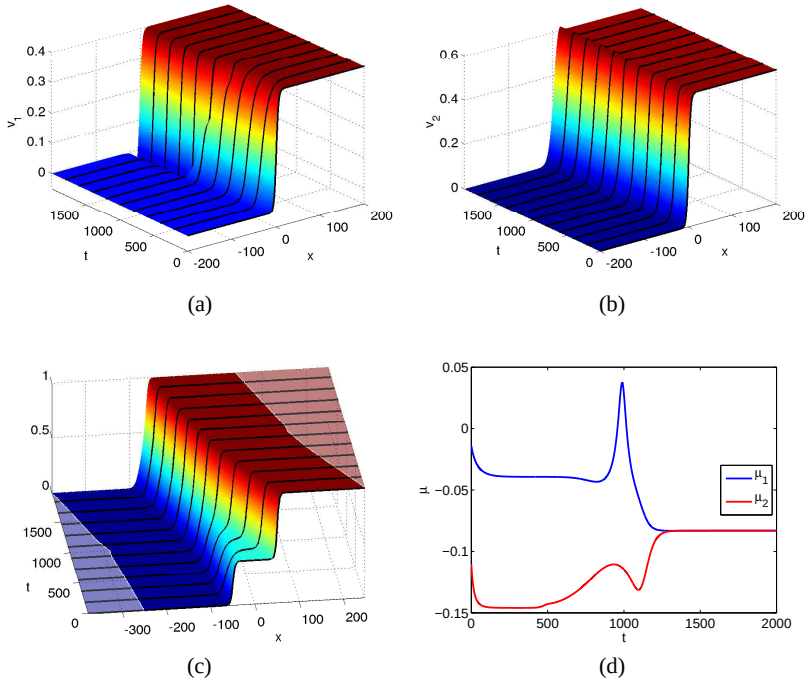

Fig. 38 Strong interaction in the quintic Nagumo equation (144): a fast wave overtaking a slow wave and merging into a single travelling front. Single fronts v_1 (a), v_2 (b), superposition (138) of both functions with their supports indicated by dark shading (c), time-dependence of speeds μ_1,μ_2 during strong interaction (d).

with initial positions $g_1^0 = g_2^0 = 0$, where u_2^- denotes the unique zero of f from Example 7 and flc2hs$(x, scale)$ is a smoothed Heaviside function provided by Comsol Multiphysics. Note that the superposition of v_1^0 and v_2^0 coincides with the initial value u_0 from Example 7, see also Figure 12. For the computation we choose the fixed phase condition in both frames with template functions $\hat{v}_j(x) = v_j^0(x)$ for $j = 1,2$ and the bump function $\varphi(x) = \operatorname{sech}(bx)$ with $b = 0.5$. We discretize with continuous piecewise linear finite elements in space with stepsize $\triangle x = 0.5$ and with the BDF method of order 2 in time with stepsize $\triangle t = 0.1$. The results for the case of two repelling pulses are shown in Figure 40. One clearly observes the evolution of two pulses traveling in opposite directions with velocities $\bar{\mu}_1 = -\bar{\mu}_2 = -0.7966$, both being nicely captured by the method.

(b) A situation with two colliding pulses occurs for the initial conditions

$$v_1^0(x) = u_2^- + \begin{pmatrix} w(x) \\ 0 \end{pmatrix}, \quad v_2^0(x) = \begin{pmatrix} w(-x) \\ 0 \end{pmatrix},$$

where w is a ramp function given by

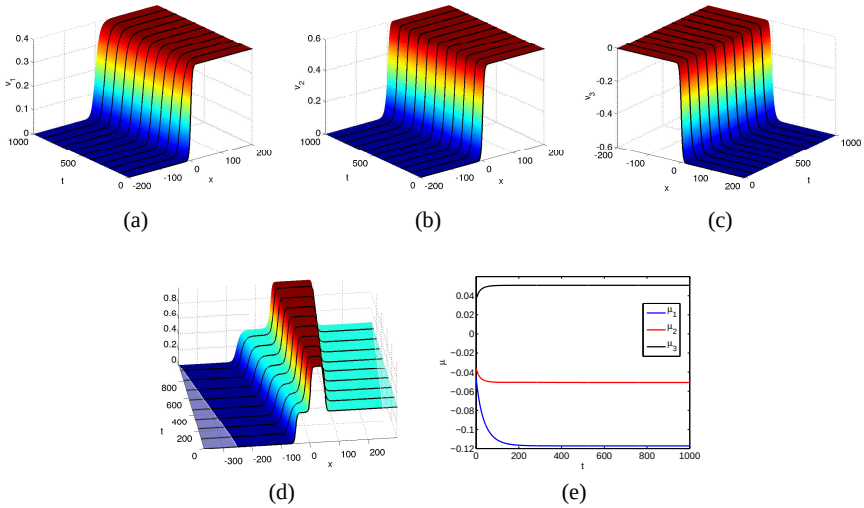

Fig. 39 Weak interaction of three traveling fronts in the quintic Nagumo equation (144). The initial function develops into the superposition of three single fronts (d), the functions v_1,v_2,v_3 converge to their limiting profiles (a)-(c), and the speeds μ_1,μ_2, μ_3 attain their limiting values (e).

$$w(x) = \begin{cases} 1 & , x \in [-100,-10], \\ \frac{1}{20}(10-x) & , x \in [-10,10], \\ 0 & , x \in [10,100]. \end{cases}$$

The initial positions are $g_1^0 = -100$ and $g_2^0 = 100$. Thus, for the decompose and freeze method with spatial domain $[-100,100]$, these are completely separated at $t = 0$ and only influence each other through interpolated data. In contrast to all previous experiments, we choose the orthogonal phase condition in both frames. The bump function is $\varphi(x) = \operatorname{sech}(bx)$ with $b = 0.01$. We discretize in space with continuous piecewise linear finite elements with stepsize $\triangle x = 0.5$ and with the BDF method of order 5 with stepsize $\triangle t = 0.1$. First the two pulses are generated from the opposite ramps, then they travel towards each other until their domains begin to overlap. Then the two pulses collide and finally cancel each other. A result of the simulation is shown in Figure 41. When both pulses are extinguished to their stationary values, the PDAE system (141) becomes ill-posed, since the derivatives $v_{j,\xi}$ vanish and the velocities can no longer be determined from the phase condition. As shown in Figure 41(d), the two velocities start to become singular after collision. This phenomenon happens already at collision for the fixed phase condition, which is the reason for taking the orthogonal phase conditions.

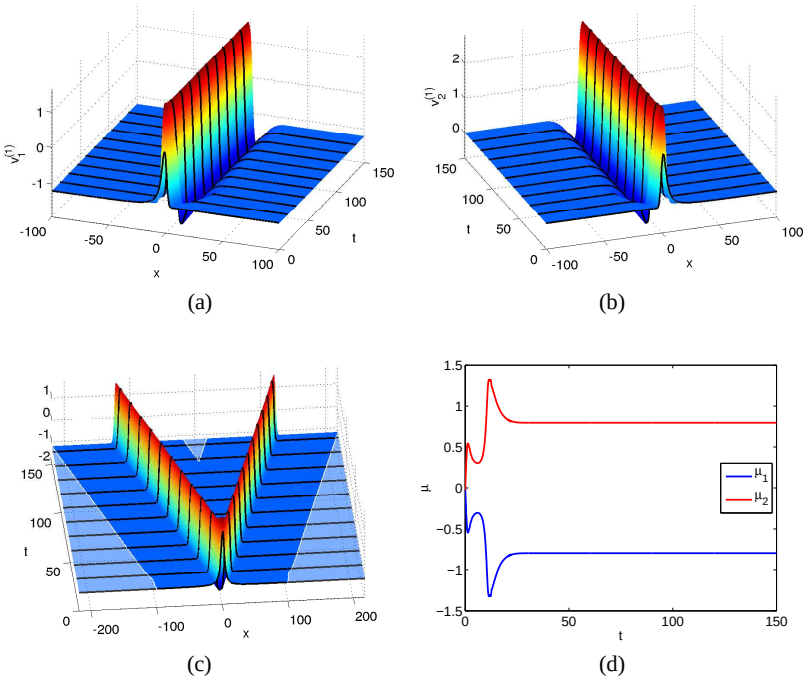

Fig. 40 Two repelling pulses in the FitzHugh-Nagumo system. (a)-(b): First components of the profiles v_1 and v_2, (c): first component of the superposition of v_1 and v_2, (d): time evolution of the velocities μ_1 and μ_2

5.3 Stability of the decomposition system

In this subsection we present the main stability result for the decomposition system (143). We sketch only the main ideas in the rather technical and involved proof which can be found in the PhD thesis of S. Selle [64]. The result is related to the work of J.D. Wright [63, 70], who constructs manifolds for the (PDE) that are invariant for certain time intervals during which they attract the multi-structures.

We impose the following conditions.

(A1) Let $f \in C^2(\mathbb{R}^m, \mathbb{R}^m)$ and let $A \in \mathbb{R}^{m,m}$ be positive definite.

(A2) The system $u_t = Au_{xx} + f(u)$ has N traveling wave solutions

$$u_j(x,t) = w_j(x - c_j t), \quad j = 1, \ldots, N,$$

such that $c_1 < c_2 < \cdots < c_N$ and the limits $w_j^{\pm} = \lim_{x \to \pm\infty} w_j(x)$ satisfy $w_j^+ = w_{j+1}^-, j = 1, \ldots, N-1$.

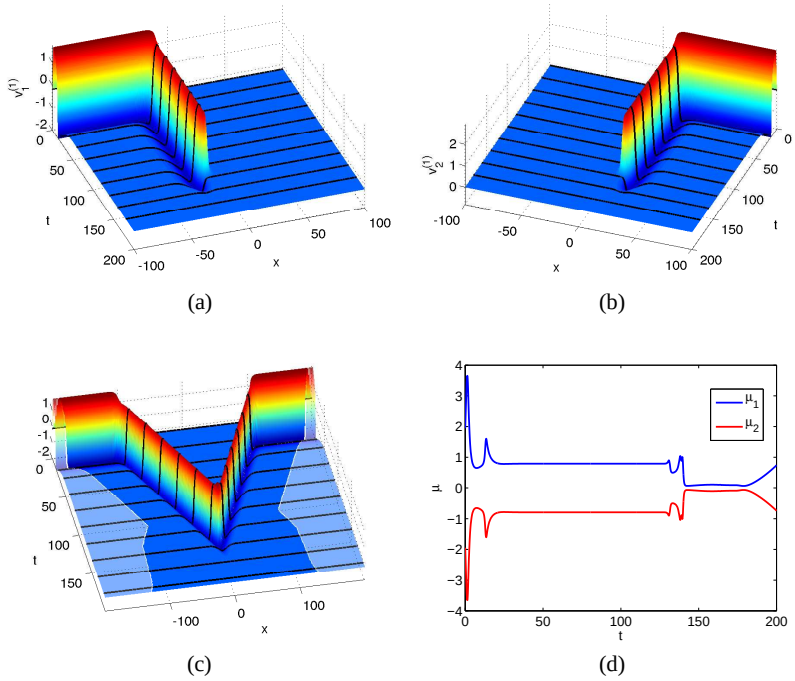

Fig. 41 Simulation of two colliding pulses in the FitzHugh-Nagumo system with the decompose and freeze method. (a)-(b): First components of the profiles v_1 and v_2, (c): first component of the superposition of v_1 and v_2, (d): time evolution of the velocities μ_1 and μ_2

(A3) For some $\beta > 0$, the constant coefficient operators $\Lambda_{j,\pm} := A\partial_{xx} + c_j\partial_x + C_{j,\pm}$ with $C_{j,\pm} = Df(w_j^{\pm})$ for $j = 1,\dots,N$ satisfiy the **Spectral Condition SC** from Sect. 1.5 for the given β, cf. (33).

(A4) The variable coefficient operators $\Lambda_j = A\partial_{xx} + c_j\partial_x + Df(w_j)$ $j = 1,\dots,N$, have the simple eigenvalue 0 and no further eigenvalues with $\operatorname{Re} s \geqslant -\beta$ and eigenfunctions in $L^2(\mathbb{R},\mathbb{R}^m)$.

(A5) There exist $C_1, C_2, C_3 > 0$ such that $\varphi \in C^\infty(\mathbb{R},\mathbb{R})$ satisfies for all $x \in \mathbb{R}$

$$C_1 e^{-\beta|x|} \leqslant \varphi(x) \leq C_2 e^{-\beta|x|},$$
$$\left|\varphi'(x)\right| \leqslant C_3 e^{-\beta|x|}.$$

(A6) The template functions $\hat{v}_j$, $j = 1,\dots,N$, satisfy $\hat{v}_j + u_j^- - w_j \in H^2(\mathbb{R},\mathbb{R}^m)$,

$$\left(\hat{v}_j + u_j^- - w_j, \hat{v}_{j,x}\right)_{L^2} = 0 \quad \text{and} \quad (w_{j,x}, \hat{v}_{j,x})_{L^2} \neq 0.$$

Note that the same constant β appears in all conditions (A3)-(A5). In essence, $\beta > 0$ should be chosen such that $-\beta$ is an upper bound for the spectrum of all Λ_j's except

zero. Then one can take a bump function with the asymptotic behavior of $e^{-\beta|x|}$, for example $\varphi(x) = \operatorname{sech}(\beta x), x \in \mathbb{R}$.

Under these assumptions one can prove what is called *joint asymptotic stability* in [64], i.e. stability of the system (143) for initial data that lead to weak interaction, see Theorem 11 below. The result holds in weighted L^2 and H^1 spaces given by

$$L^2_b(\mathbb{R},\mathbb{R}^m) = \{u : \cosh(b\cdot)u \in L^2(\mathbb{R},\mathbb{R}^m)\} \text{ with norm } \|u\|_{L^2_b} = \|\cosh(b\cdot)u\|_{L^2}$$

and

$$H^1_b(\mathbb{R},\mathbb{R}^m) = \{u : \cosh(b\cdot)u \in H^1(\mathbb{R},\mathbb{R}^m)\} \text{ with norm } \|u\|_{H^1_b} = \|\cosh(b\cdot)u\|_{H^1},$$

where $b > 0$ must be chosen positive and sufficiently small.

Theorem 11 (Stability Theorem, [64]). *Assume (A1)–(A6). Then there exists $b_0 > 0$ so that for every $b_0 \geq b > 0$ there exist $\delta > 0$, $g_{min} > 0$ such that for all initial data v_j^0, g_j^0, satisfying*

$$\left\| v_j^0 + u_j^- - w_j \right\|_{H^{1,b}} \leqslant \delta, \quad \left(\hat{v}_{j,x}, v_j^0 - \hat{v}_j\right)_{L^2} = 0,$$
$$g_1^0 < g_2^0 < \cdots < g_N^0,\ g_{min} \leqslant \left|g_{j+1}^0 - g_j^0\right|, \quad \text{for all } j = 1,\ldots,N,$$

the PDAE (143) *has a unique global solution $v(t) = (v_1(t),\ldots,v_N(t))$, $\mu(t) = (\mu_1(t),\ldots,\mu_N(t))$, $g(t) = (g_1(t),\ldots,g_N(t))$ for all $t \geq 0$.*

Moreover, there exist asymptotic phases $\tau_j^\infty \in \mathbb{R}$, $j = 1,\ldots,N$ such that the solution converges exponentially fast with some rate $0 < \varepsilon < \beta$,

$$\left\| v_j + u_j^- - w_j \right\|_{H^{1,b}} + \left|g_j(t) - c_j t - g_j^0 - \tau_j^\infty\right| + \left|\mu_j(t) - c_j\right| \leq Ce^{-\varepsilon t},\ \forall j = 1,\ldots,N.$$

Consider the original PDE (136) with initial condition $u_0(x) = \sum_{j=1}^N v_j^0(x - g_j^0)$, where v_j^0 and g_j^0 satisfy the assumptions from Theorem 11. Then the theorem implies exponential convergence of the solution u to a (linear) superposition of the individual traveling waves with individual asymptotic phases:

$$\left\| u(\cdot,t) - \sum_j w_j(\cdot - c_j t - g_j^0 - \tau_j^\infty) \right\|_{H^{1,b}} \leqslant Ce^{-\varepsilon t}.$$

In [70] results of this type are proved directly for the original system (136) by using analytic information about the single waves. On the contrary, Theorem 11 states a result about the 'blown-up' system (143) which is accessible to numerical computation.

Proof (A sketch of ideas, for details see [64, pp. 37–98]).

Step 1: First linearize the system (141) at the shifted exact waves $w_j - u_j^-$ (see (142)) and their speeds c_j for each $j = 1,\ldots,N$. This yields a system of the form

$$\begin{aligned} u_{j,t} &= \Lambda_j u_j + \lambda_j(t) w_{j,x} + E_j(t)u + T_j(t) + N_j(t,u,r,\lambda), \\ r_{j,t} &= \lambda_j(t), \\ 0 &= (\hat{v}_{j,x}, u_j)_{L^2}, \end{aligned}$$

for the unknowns $u_j = v_j - \left(w_j - u_j^-\right)$, $r_j(t) = g_j(t) - c_j t - g_j^0$, $\lambda_j = \mu_j - c_j$. When omitting the coupling terms E_j, T_j, and N_j, the system decouples with linear differential operators known from the analysis of single traveling waves in Sects. 1 and 2.

Step 2: All coupling terms E_j, T_j and N_j turn out to be nonlocal. The term $T_j(t)$ collects the nonlocal terms $f\left(\sum_{k=1}^N v_k(*)\right) - \sum_{k=1}^N f(v_k(*))$ from (140) obtained by inserting the exact traveling waves w_j shifted to the initial and well separated positions g_j^0, $j = 1,\dots,N$. Due to assumption (A2), the individual waves w_j, $j = 1,\dots,N$ are exponentially converging towards their limits. Therefore, the influence of one wave on the other decays exponentially in time. This statement still holds in the weighted space H_b^1, if the weight b is taken sufficiently small (which is the reason for the smallness assumption on b in the theorem). In a sense this property expresses the well-known phenomenon of *convective (in)stability*, see [61].

The operator $E_j(t)$ is the linearization of the nonlinear coupling terms above, when applied to the different patterns $u_1,\dots,u_N$, located at the positions $c_j t + g_j^0$ of the individual traveling waves. Here the use of the weighted spaces with $b > 0$ implies that the u_j are exponentially located. An interplay with the separation of the positions as time increases, then shows exponential decay of the operator E_j in the weighted space.

Combining these considerations yields an estimate in the weighted space L_b^2 of the form

$$\left\|T_j(t)\right\|_{L_b^2} + \left\|E_j(t)\right\|_{L_b^2 \to L_b^2} \le C_L \exp\left(-C_L' g_{min}\right) \exp\left(-C_L'' t\right) \quad \text{for all } t \ge 0,$$

with positive constants C_L, C_L', C_L''. Therefore, these terms decay exponentially in time and exponentially with respect to the initial separation of patterns.

Step 3: The terms N_j contain the nonlinear and nonlocal terms in all variables that are at least of second order. Using the weighted norm one can show an estimate

$$\begin{aligned} \|N_j(t,u,r,\lambda)\|_{L_b^2} \le{}& C_N \|u\|_{H_b^1} \left(\|u\|_{H_b^1} + |\lambda_j| + \exp\left(C_N' \|r\|\right) \|r\| \right) \\ &+ C_N \exp\left(C_N' \|r\|\right) \|r\| \left(1 + \|u\|_{H_b^1}\right) \exp\left(-\gamma_N t - \gamma_N g_{min}\right) \quad \text{for all } t \ge 0. \end{aligned}$$

Step 4: Consider the linear PDAE with T_j and N_j replaced by an inhomogeneity, i.e. the following coupled system ($j = 1,\dots,N$),

$$\begin{aligned} u_{j,t} &= \Lambda_j u_j + \lambda_j(t) w_{j,x} + E_j(t)u + k_j(t), \\ r_{j,t} &= \lambda_j(t), \\ 0 &= (\hat{v}_{j,x}, u_j)_{L^2}. \end{aligned} \tag{145}$$

This can be reduced to a PDAE of index 1 with the algebraic variables λ eliminated. For this inhomogeneous system one shows a variation of constants formula by first proving that the systems yield sectorial operators. The variation of constants formula is then used to prove an estimate of the form

$$\sup_{0\le s\le t} e^{\varepsilon s}\|u(s)\|_{H^1_b} \le C\Big(\|u^0\|_{H^1_b} + \sup_{0\le s\le t}\|k(s)\|_{L^2_b}\Big)$$

with a suitable $\varepsilon > 0$ for the solution $u = (u_1, \dots, u_N)$ of the coupled linear problem (145).

Step 5: Finally, the estimates from Steps 2–4 are combined and yield global existence as well as the asserted exponential decay. □

5.4 Generalization to an abstract framework

The idea to decompose and freeze multi-structures can be combined with the general idea of freezing solutions in equivariant evolution equations. For this we consider the setting from Sect. 1.7, i.e.

$$u_t = F(u), \quad u(0) = u_0, \tag{146}$$

where $F : Y \subset X \to X$ with X is a Banach space and Y a dense subspace. The evolution equation (146) is assumed to be equivariant under the action of a Lie group G so that

$$a : G \to GL(X), \quad F(a(\gamma)u) = a(\gamma)F(u)$$

holds. To generalize the idea of a time-dependent partition of unity from Sect. 5.2, we use the abstract concept of a module E (a vector space with abelian multiplication) that acts on the state space X

$$\bullet : E \times X \to X, \quad (\varphi, u) \to \varphi \bullet u.$$

As a standard example consider $E = C^1_{\text{unif}}(\mathbb{R}^d)$ and $X = H^1(\mathbb{R}^d, \mathbb{R}^m)$ with the action of E on X given by multiplication.

We assum that the Lie group G also acts on E, denoting the action by

$$\mathfrak{a} : G \to \mathrm{GL}(E), \quad \gamma \mapsto \mathfrak{a}(\gamma).$$

We require that both actions a and $\mathfrak{a}$ satisfy the identities:

$$\begin{aligned} \mathfrak{a}(\gamma)(\varphi\psi) &= (\mathfrak{a}(\gamma)\varphi) \bullet (\mathfrak{a}(\gamma)\psi), \\ a(\gamma)(\varphi \bullet u) &= (\mathfrak{a}(\gamma)\varphi) \bullet (a(\gamma)u) \end{aligned} \tag{147}$$

for all $\gamma \in G$, $\varphi, \psi \in E$ and $u \in X$.

Example 21 (Ginzburg-Landau equation in 1*D).* Reconsider Example 5, i.e.

$$u_t = \alpha u_{xx} + \delta u + \beta |u|^2 u + \gamma |u|^4 u, \quad x \in \mathbb{R},\, t \geq 0, \tag{148}$$

where $u(x,t) \in \mathbb{C}$. Recall that (148) is equivariant under the action $a : G \to \mathrm{GL}(X)$ of the Lie group $G = \mathbb{R} \times S^1 \ni (\tau, \theta)$ on X given by

$$[a(\tau,\theta)u](x) = e^{-i\theta} u(x-\tau), \quad \text{for all } (\tau,\theta) \in G,\, u \in X.$$

As above choose the Banach space $X = L^2(\mathbb{R},\mathbb{C})$ and the module $E = C^0_{\mathrm{unif}}(\mathbb{R},\mathbb{R})$, which acts on X by multiplication, i.e. $(\varphi \bullet u)(x) = \varphi(x)u(x)$ for all $x \in \mathbb{R}$ and all $\varphi \in E$, $u \in X$.

The group G acts on the module E via the action $\mathfrak{a} : G \to \mathrm{GL}(E)$ given by

$$[\mathfrak{a}(\tau,\theta)\varphi](x) = \varphi(x-\tau), \quad \text{for all } (\tau,\theta) \in G,\, \varphi \in E.$$

In this case, (147) follows from

$$\Big[a(\tau,\theta)\big(\varphi \bullet u\big)\Big](x) = \varphi(x-\tau) e^{-i\theta} u(x-\tau), \quad \forall x \in \mathbb{R},$$

for all $\varphi \in C^0_{\mathrm{unif}}(\mathbb{R})$, $u \in L^2(\mathbb{R},\mathbb{C})$, $\tau \in \mathbb{R}$, $\theta \in [0, 2\pi)$.

In the abstract framework, the idea of the decomposition (138) is generalized as follows

$$u(t) = \sum_{j=1}^{N} a(g_j(t)) v_j(t), \tag{149}$$

where $g_j : [0,\infty) \to G$ denotes the time dependent location in the group G of the j-th profile $v_j : [0,\infty) \to Y$.

Assume an element $\varphi \in E$ such that the inverse of $\sum_j \mathfrak{a}(g_j)\varphi \in E$ with respect to the multiplication in E exists for all $g_1, \ldots, g_N \in G$. We denote this inverse $\big(\sum_j \mathfrak{a}(g_j)\varphi\big)^{-1}$ by $\frac{1}{\sum_j \mathfrak{a}(g_j)\varphi}$. Then a calculation, similar to (140) and (72) yields

$$\begin{aligned}
&\sum_{j=1}^{N} a(g_j)\left[v_{j,t} + a(g_j)^{-1} d[a(g_j)v_j] g_{j,t}\right] = u_t = F(u) \\
&\quad = \sum_{j=1}^{N} \left[F(a(g_j)v_j) + \frac{\mathfrak{a}(g_j)\varphi}{\sum_{k=1}^{N} \mathfrak{a}(g_k)\varphi} \left(F\left(\sum_{k=1}^{N} a(g_k) v_k \right) - \sum_{k=1}^{N} F(a(g_k)v_k) \right) \right] \\
&\quad = \sum_{j=1}^{N} a(g_j) \left[F(v_j) + \frac{\varphi}{\sum_{k=1}^{N} \mathfrak{a}(g_j^{-1}g_k)\varphi} \left(F\left(\sum_{k=1}^{N} a(g_j^{-1}g_k) v_k \right) \right.\right. \\
&\qquad\qquad \left.\left. - \sum_{k=1}^{N} F(a(g_j^{-1}g_k)v_k) \right) \right].
\end{aligned} \tag{150}$$

As in the derivation of the decompose and freeze method for multi-pulses and multi-fronts in Sect. 5.2, we now require that for each $j = 1, \ldots, N$ the summand on the left hand side and on the right hand side of (150) coincides. This yields the fol-

lowing nonlinear coupled system for the unknowns $v_j \in Y$, $\mu_j \in \mathscr{A}$, and $g_j \in G$, $j = 1,\dots,N$:

$$v_{j,t} = F(v_j) - d[a(\mathbb{1})v_j]\mu_j + \frac{\varphi}{\sum_k \alpha(g_j^{-1}g_k)\varphi}\left(F\left(\sum_k a(g_j^{-1}g_k)v_k\right) - \sum_k F(a(g_j^{-1}g_k)v_k)\right), \quad (151)$$

$$\begin{aligned} v_j(0) &= v_j^0, \\ g_{j,t} &= dL_{g_j}(\mathbb{1})\mu_j, \quad g_j(0) = g_j^0, \\ 0 &= (v_j - \hat{v}_j, d[a(\mathbb{1})\hat{v}_j]\lambda)_H \ \forall \lambda \in T_{\mathbb{1}}G. \end{aligned}$$

For the second summand in the first line we used the identity $a(g_j)^{-1}d[a(g_j)v_j]g_{j,t} = d[a(\mathbb{1})v_j]\mu_j$, where $\mu_j = dL_{g_j}(g_j)^{-1}g_{j,t} \in T_{\mathbb{1}}G$.

As in Sect. 5.2 we obtain that a solution of (151) with initial data v_j^0, g_j^0, satisfying $u_0 = \sum_{j=1}^N a(g_j^0)v_j^0$, yields a solution to the original Cauchy problem (146) by setting

$$u(t) = \sum_{j=1}^N a(g_j(t))v_j(t) \quad \text{for all } t \geq 0. \quad (152)$$

Example 22 (Freezing pulse and front simultaneously in Ginzburg-Landau equation). As an example in $1D$ we consider the quintic-cubic Ginzburg-Landau equation in $1D$ from Example 21 again

$$u_t = \alpha u_{xx} + \left(\delta + \beta|u|^2 + \gamma|u|^4\right)u, \quad x \in \mathbb{R},\ t \geq 0$$

with $u(x,t) \in \mathbb{C}$. The parameter values are $\alpha = 1$, $\delta = -0.1$, $\beta = 3 + i$, and $\gamma = -2.75 + i$. In this case one finds a multi-structure, consisting of a standing rotating pulse v_1 and a rotating front v_2 that travels to the right. In Figure 42 we show the result obtained by the decompose and freeze method for this problem. One observes that the individual structures are well captured in their respective frames and the single speed correctly reproduced for the single waves, compare Example 5. Note that this is a case of weak interaction. However, for strong interactions, such as the collision of a rotating and a traveling pulse, the decompose and freeze method did not work properly.

5.5 Multisolitons: Interaction of spinning solitons

We finish with numerical results of the method where we try to capture simultaneously two and more solitons in the $2D$ quintic-cubic complex Ginzburg-Landau equation from Example 13.

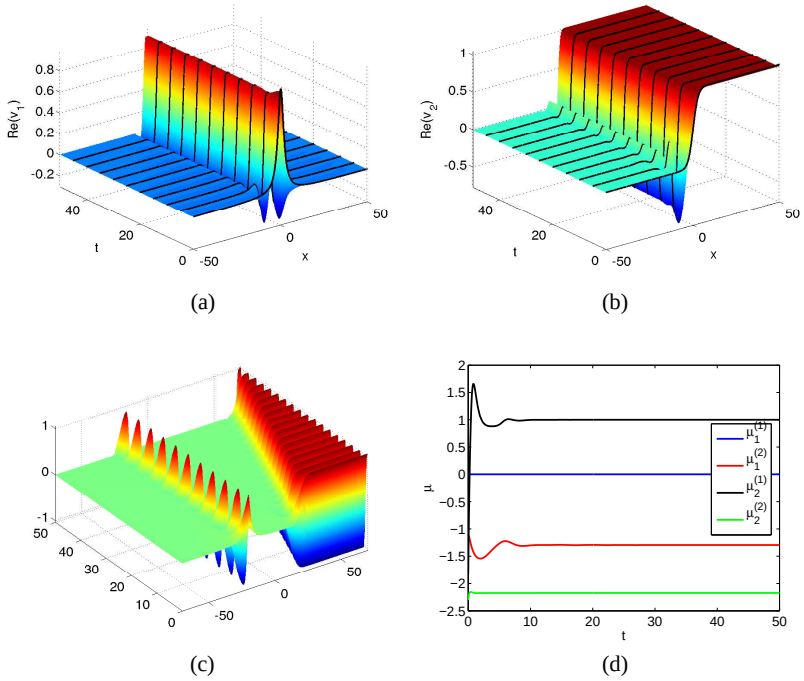

Fig. 42 Result of the decompose and freeze method for a multi-structure in the quintic-cubic Ginzburg-Landau equation, weak interaction of a standing and rotating pulse and a traveling front. Profile of the standing and rotating pulse v_1 (a), profile of the rotating and right traveling front v_2 (b) , simulation of the nonfrozen equation (c), time-dependence of the derivatives of the group variables (d).

Example 23 (Quintic-cubic Ginzburg-Landau equation in 2D).

$$u_t = \alpha\triangle u + \delta u + \beta|u|^2u + \gamma|u|^4u, \quad (x,y) \in \mathbb{R}^2,\ u(x,y,t) \in \mathbb{C}. \tag{153}$$

The parameter values are the same as in (115) for which single spinning solitons are known to exist. As initial data we take the sum of two such solitons, shifted a certain distance apart. If this distance is large enough, we have weak interaction and a multi-structure consisting of two (or more) spinning solitons stabilizes. The result of such a simulation is shown in Figure 43. The first row shows the superposition of the profiles obtained from the decompose and freeze method at different time instances. The next row contains the single profiles v_1 (d) and v_2 (e) and the trace $\{\tau_j(t) : t \geq 0\}$ of the two group orbits $g_j(t) = (\theta_j(t), \tau_j(t)), j = 1,2$ from the reconstruction equation in (151). Figure 43 (g)-(i) displays the time-dependence of all 6 velocities. The translational velocities μ_j^1, μ_j^2 converge to zero and the angular velocities to their limiting values. However, the convergence is oscillatory and very

slow (oscillations become invisible at $t \approx 1000$). Therefore, we show details in the interval $0 \le t \le 100$.

Figure 44 shows a case of strong interaction of two spinning solitons with pictures selected as in Figure 43. The solution converges to single soliton (c), which is represented by the decompose and freeze method as the superposition of two single but deformed solitons (d),(e). The two group orbits apparently trace a circle, and velocities slowly decay as in the case of weak interaction. **(b)** (Strong interaction of 2

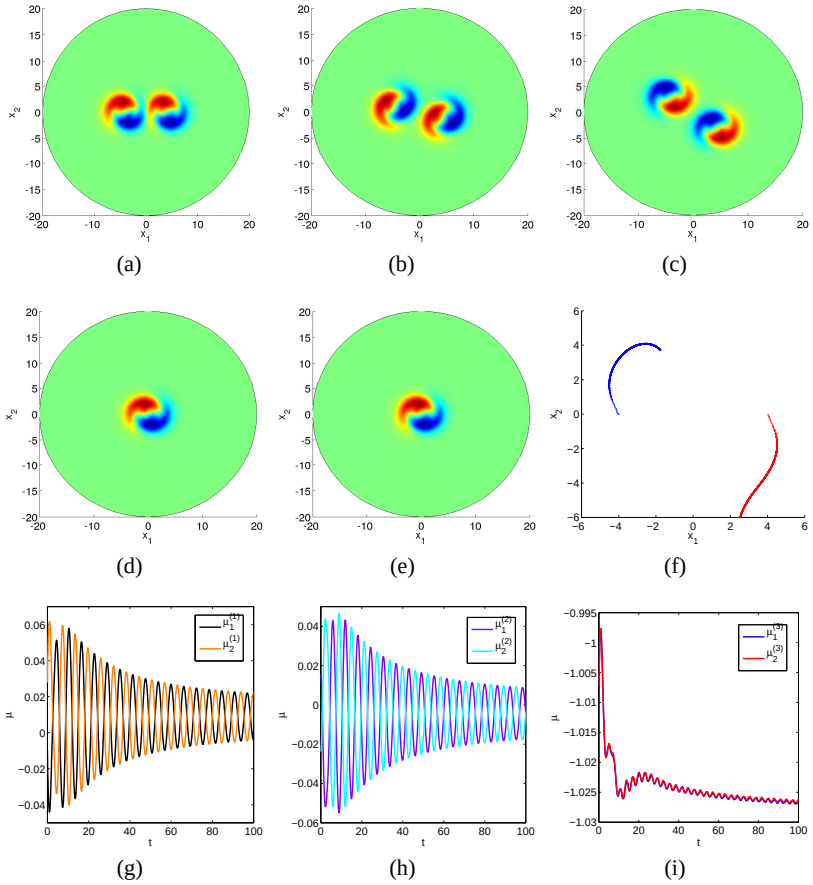

Fig. 43 Weak interaction of two spinning solitons. Initial location of the profiles at $\pm(4,0)$, real part of superposition at time $t = 0$, 30, 150 (a)-(c), real parts of profiles v_1 and v_2 at time $t = 150$ (d),(e), position of the centers of the profiles v_1, v_2 from $t = 0$ to $t = 500$ calculated by solving the reconstruction equation (f), time evolution of translational velocities $\mu_1^{1/2}(t)$ and $\mu_2^{1/2}(t)$ in x-direction (g) and in y-direction (h), evolution of angular velocities (i). The colorbar is scaled to $[-1.65, 1.65]$. Solution by Comsol Multiphysics with piecewise linear finite elements, Neumann boundary conditions, $\Delta x = 0.5$, $\Delta t = 0.1$, BDF of order 2.

spinning solitons) Finally, we consider the strong interaction of 3 spinning solitons,

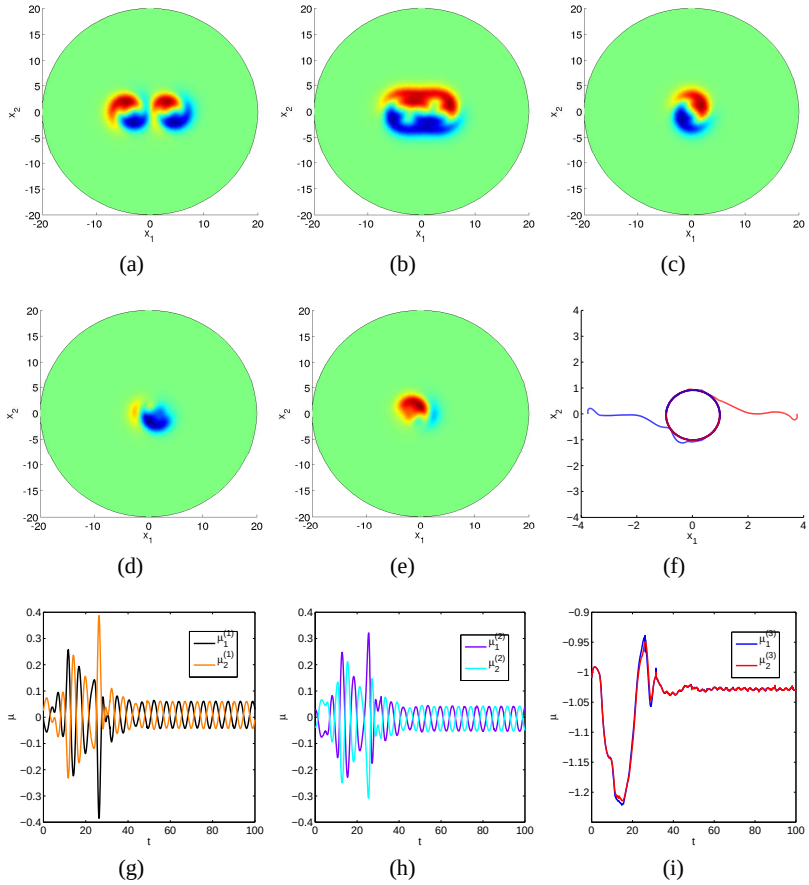

Fig. 44 Strong interaction of two spinning solitons. Initial location of profiles at $\pm(3.75, 0)$, real part of superposition at time $t = 0$, 7.2, 36 (a)-(c), real part of profiles v_1 and v_2 at time $t = 150$ (d),(e), position of centers for the profiles v_1, v_2 for $0 \le t \le 500$ (f), evolution of translational velocities $\mu_1^{1/2}(t)$ and $\mu_2^{1/2}(t)$ in x-direction (g) and y-direction (h), angular velocities (i), further data are as in Figure 43

see Figure 45. Initially, the solitons are put on the vertices of an equilateral triangle. The behavior is quite similar to the two-solitons case. Translational velocities oscillate rapidly for a long time before tending to zero, and the traces of the group orbits, after a sharp turn, seem to follow a common circle with different phases.

5.6 Summary

A summary of this section is the following:

- Excitable reaction diffusion systems in $1D$ show multi-structures composed of fronts and pulses.
- The freezing method is extended to a 'decompose and freeze' method to capture solutions consisting of multi-structures.
- Numerical solution of a system of nonlinear and nonlocal coupled systems of partial differential algebraic equations.
- Proof of stability for the decomposition method in case of weakly interacting fronts and pulses.
- The method generalizes to equivariant evolution equations.
- Numerical computations with freezing multi-structures in dimensions ≥ 2 are in initial state, no theory available.

References

1. Ahuja, S., Kevrekidis, I.G., Rowley, C.W.: Template-based stabilization of relative equilibria in systems with continuous symmetry. *J. Nonlinear Sci.* **17**, 109–143 (2007)
2. Alexander, J., Gardner, R., Jones, C.K.R.T.: A topological invariant arising in the stability analysis of travelling waves. *J. Reine Angew. Math.* **410**, 167–212 (1990)
3. Alt, H.W.: Lineare Funktionalanalysis (3rd ed.). Springer, (1999)
4. Arendt, W., Batty, C.J.K., Hieber, M., Neubrander, F.: Vector-valued Laplace transforms and Cauchy problems. *Monographs in Mathematics*, vol. 96. Birkhäuser Verlag, Basel (2001)
5. Arrieta, J.M.,López-Fernández, M.,Zuazua, E.: Approximating travelling waves by equilibria of nonlocal equations. *Asymptot. Anal.* **78**, 145–186 (2012)
6. Barkley, D.: A model for fast computer simulation of waves in excitable media. *Physica D* **49**, 61–70 (1991)
7. Bates, P.W., Jones, C.K.R.T.: Invariant manifolds for semilinear partial differential equations. In: Dynamics reported, Vol. 2, *Dynam. Report. Ser. Dynam. Systems Appl.*, vol. 2, pp. 1–38. Wiley, Chichester (1989)
8. Beyn, W.-J.: The numerical computation of connecting orbits in dynamical systems. *IMA J. Numer. Anal.* **10**(3), 379–405 (1990)
9. Beyn, W.-J., Lorenz, J.: Nonlinear stability of rotating patterns. *Dynamics of PDEs* **5**, 349–400 (2008)
10. Beyn, W.-J., Lorenz, J.: Stability of traveling waves: dichotomies and eigenvalue conditions on finite intervals. *Numer. Funct. Anal. Optim.* **20**, 201–244 (1999)
11. Beyn, W.-J., Rottmann-Matthes, J.: Resolvent estimates for boundary value problems on large intervals via the theory of discrete approximations. *Numer. Funct. Anal. Optim.* **28**(5-6), 603–629 (2007)
12. Beyn, W.-J., Selle, S., Thümmler, V.: Freezing multipulses and multifronts. *SIAM Journal on Applied Dynamical Systems* **7**, 577–608 (2008)
13. Beyn, W.-J., Thümmler, V.: Freezing solutions of equivariant evolution equations. *SIAM Journal on Applied Dynamical Systems* **3**(2), 85–116 (2004)

14. Beyn, W.-J., Thümmler, V.: Phase conditions, Symmetries, and PDE Continuation. In B. Krauskopf, H. Osinga, and J. Galan-Vioque, editors, *Numerical Continuation Methods for Dynamical Systems*, Series in Complexity, 301–330. Springer (2007)
15. Beyn, W.-J., Thümmler, V.: Dynamics of patterns in nonlinear equivariant PDEs. *GAMM Mitteilungen* **32**(1), 7–25 (2009)
16. Bridges, T.J., Derks, G., Gottwald, G.: Stability and instability of solitary waves of the fifth-order KdV equation: a numerical framework. *Physica D* **172**, 196–216 (2002)
17. Brin, L.Q.: Numerical testing of the stability of viscous shock waves. *Math. Comp.* **70**, 1071–1088 (2001)
18. Brin, L.Q., Zumbrun, K.: Analytically varying eigenvectors and the stability of viscous shock waves. *Math. Contemp.* **22**, 19–32 (2002)
19. Cattaneo, C.: Sulla conduzione del calore. Atti Semin. Mat. Fis. Univ., Modena **3**, 83–101 (1948)
20. Chossat, P., Lauterbach, R.: Methods in equivariant bifurcations and dynamical systems. *Advanced Series in Nonlinear Dynamics*, vol. 15, World Scientific Publishing Co. Inc. (2000)
21. Coppel, W.A.: Dichotomies in stability theory. *Lecture Notes in Mathematics*, vol. 629. Springer-Verlag, Berlin (1978)
22. Crasovan, L.-C., Malomed, B.A., Mihalache, D.: Spinning solitons in cubic-quintic nonlinear media. *Pramana Journal of Physics* **57**, 1041–1059 (2001)
23. Demmel, J.W., Dieci, L., Friedman, M.J.: Computing connecting orbits via an improved algorithm for continuing invariant subspaces. *SIAM J. Sci. Comput.* **22**(1), 81–94 (electronic) (2000)
24. Evans, J.W.: Nerve axon equations. I. Linear approximations. *Indiana Univ. Math. J.* **21**, 877–885 (1971/1972)
25. Evans, J.W.: Nerve axon equations. II. Stability at rest. *Indiana Univ. Math. J.* **22**, 75–90 (1972/1973)
26. Evans, J.W.: Nerve axon equations. III. Stability of the nerve impulse. *Indiana Univ. Math. J.* **22**, 577–593 (1972/1973)
27. Evans, J.W.: Nerve axon equations. IV. The stable and the unstable impulse. *Indiana Univ. Math. J.* **24**(12), 1169–1190 (1974/1975)
28. Engel, K.-J., Nagel, R.: One-Parameter Semigroups for Linear Evolution Equations. *Graduate Texts in Mathematics*, Springer (2000)
29. Fife, P.C., McLeod, J.B.: The approach of solutions of nonlinear diffusion equations to travelling front solutions. *Arch. Rat. Mech. Anal.* **65**, 335–361 (1977)
30. Friedman, M.J., Doedel, E.J.: Numerical computation and continuation of invariant manifolds connecting fixed points. *SIAM J. Numer. Anal.* **28**(3), 789–808 (1991)
31. Field, M.J.: Dynamics and symmetry, *ICP Advanced Texts in Mathematics.* vol. 3 Imperial College Press, London (2007)
32. FitzHugh, R.: Impulses and physiological states in theoretical models of nerve membrane. *Biophysical Journal* **1**, 445–466 (1961)
33. Froehlich, S., Cvitanović, P. : Reduction of continuous symmetries of chaotic flows by the method of slices *Commun. Nonlinear Sci. Numer. Simulat.* **17**, 2074-2084 (2012).
34. Foulkes, A. J., Biktashev, V. N. : Riding a spiral wave; numerical simulation of spiral waves in a comoving frame of reference. *Phys. Rev. E (3)* **81**, 046702 (2010)
35. Ghazaryan, A., Latushkin, Y., Schecter, S.: Stability of traveling waves for degenerate systems of reaction diffusion equations. *Indiana Univ. Math. J.* **60**(2), 443–472 (2011)
36. Gohberg, I.C., Krěin, M.G.: Introduction to the Theory of Linear Nonselfadjoint Operators. *Translations of Mathematical Monographs* vol. 18, American Mathematical Society (1969)
37. Golubitsky, M., Stewart, I.: The symmetry perspective. *Progress in Mathematics* vol. 20, Birkhäuser Verlag, Basel (2002)

38. Hastings, S.: On travelling wave solutions of the Hodgkin-Huxley equations. *Arch. Ration. Mech. Anal.* **60**, 229–257 (1976).
39. Henry, D.: Geometric theory of semilinear parabolic equations. *Lecture Notes in Mathematics* vol. 840, Springer (1981)
40. Hermann, S., Gottwald, G.A.: The large core limit of spiral waves in excitable media: a numerical approach. *SIAM J. Appl. Dyn. Syst.* **9**, 536–567 (2010)
41. Hodgkin, A.L., Huxley, A.F.: A quantitative description of membrane current and its application to conduction and excitation in nerve. *J. Physiol.* **117**, 500–544 (1952)
42. Humpherys, J., Sandstede, B., Zumbrun, K.: Efficient computation of analytic bases in Evans function analysis of large systems. *Numer. Math.* **103**, 631–642 (2006)
43. Humpherys, J., Zumbrun, K.: An efficient shooting algorithm for Evans function calculations in large systems. *Phys. D* **220**, 116–126 (2006)
44. Keener, J., Sneyd, J.: Mathematical physiology. I: Cellular physiology. 2nd ed. Springer, New York (2009)
45. Kim, Y.J., Tzavaras, A.E.: Diffusive N-waves and metastability in the Burgers equation. *SIAM J. Math. Anal.* **33**(3), 607–633 (electronic) (2001)
46. Kreiss, G., Kreiss, H.O., Petersson, N.A.: On the convergence of solutions of nonlinear hyperbolic-parabolic systems. *SIAM J. Numer. Anal.* **31**(6), 1577–1604 (1994)
47. Ledoux, V., Malham, S., Thümmler, V.: Grassmannian spectral shooting. *Math. Comp.* **79**, 1585–1619 (2010)
48. Malham, S., Niesen, J.: Evaluating the Evans function: order reduction in numerical methods. *Math. Comp.* **261**, 159–179 (2008)
49. Miura, R.M.: Accurate computation of the stable solitary waves for the FitzHugh-Nagumo equations. *Journal of Mathematical Biology* **13**, 247–269 (1982)
50. Palmer, K.J.: Exponential dichotomies and transversal homoclinic points. *J. Differential Equations* **55**(2), 225–256 (1984)
51. Pazy, A.: Semigroups of linear operators and applications to partial differential equations (2. corr.print) *Applied Mathematical Sciences* 44, Springer (1983)
52. Pego, R.L., Weinstein, M.I.: Eigenvalues, and instabilities of solitary waves, *Philos. Trans. Roy. Soc. London Ser. A* **340**, 47–94 (1992)
53. Rottmann-Matthes, J.: Computation and Stability of Patterns in Hyperbolic-Parabolic Systems. *PhD thesis*, Shaker Verlag, Aachen (2010)
54. Rottmann-Matthes, J.: Linear Stability of Traveling Waves in First-Order Hyperbolic PDEs. *J. Dynam. Differential Equations* **23**(2), 365–393 (2011)
55. Rottmann-Matthes, J.: Stability and Freezing of Nonlinear Waves in First Order Hyperbolic PDEs. *J. Dynam. Differential Equations* **24**(2), 341–367 (2012)
56. Rottmann-Matthes, J.: Stability of parabolic-hyperbolic traveling waves. Dyn. Partial Differ. Equ. **9**(1), 29–62 (2012)
57. Rottmann-Matthes, J.: Stability and freezing of waves in non-linear hyperbolic-parabolic systems. *IMA J. Appl. Math.* **77**(3), 420–429 (2012)
58. Rowley, C.W., Kevrekidis, I.G., Marsden, J.E., Lust, K.: Reduction and reconstruction for self-similar dynamical systems. *Nonlinearity* **16**(4), 1257–1275 (2003)
59. Saad, K.M., El-shrae, A.M.: Numerical methods for computing the Evans function. *ANZIAM J. Electron. Suppl.* **52** (E), E76–E99 (2010)
60. Sandstede, B.: Stability of traveling waves. In B. Fiedler, editor, *Handbook of Dynamical Systems* vol. 2, 983–1055, North Holland (2002)
61. Sandstede, B. and Scheel, A.: Absolute and convective instabilities of waves on unbounded and large bounded domains. *Physica D* **145**(3-4), 233–277 (2000)
62. Sandstede, B., Scheel, A., Wulff, C.: Dynamics of spiral waves on unbounded domains using center manifold reductions, *J. Differential Equations* **141**, 122-149 (1997)
63. Scheel, A. and Wright, J.D.: Colliding dissipative pulses – the shooting manifold. *J. Differ. Equations* **245**(1), 59–79 (2008)
64. Selle, S.: Decomposition and stability of multifronts and multipulses. *PhD thesis*, Univ. Bielefeld, Bielefeld (2009)

65. Stewart, G.W., Sun, J.G.: Matrix perturbation theory. Computer Science and Scientific Computing. Academic Press Inc., Boston, MA (1990)
66. Thümmler, V.: Numerical Analysis of the method of freezing traveling waves. *PhD thesis*, Bielefeld University (2005)
67. Thümmler, V.: The effect of freezing and discretization to the asymptotic stability of relative equilibria. *J. Dynam. Differential Equations* **20**, 425–477 (2008)
68. Thümmler, V.: Numerical approximation of relative equilibria for equivariant PDEs. *SIAM J. Numer. Anal.* **46**, 2978–3005 (2008)
69. Volpert, A., Volpert, V.A., Volpert, V.A.: *Traveling wave solutions of parabolic systems*. *Translations of Mathematical Monographs* vol. 140, AMS (1994)
70. Wright, J.D.: Separating dissipative pulses: the exit manifold. *J. Dyn. Differ. Equations* **21**(2), 315–328 (2009)

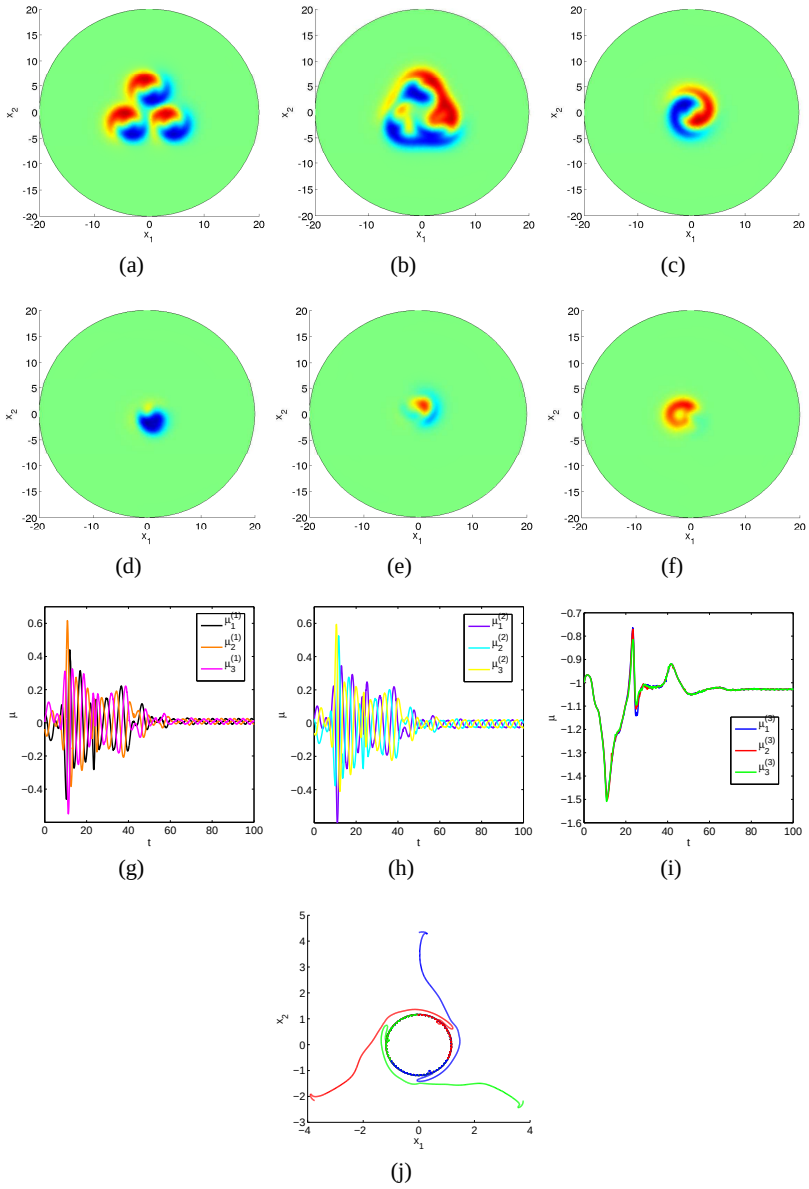

Fig. 45 Strong interaction of three spinning solitons. Centers are put initially on an equilateral triangle with radius of circumcircle 3.75, real part of superposition at times $t = 0$, 7.2, 36 (a)-(c), real parts of profiles v_1, v_2 and v_3 at time $t = 150$ (d)-(f), evolution of translational velocities $\mu_1^{1/2}(t)$, $\mu_2^{1/2}(t)$ and $\mu_3^{1/2}(t)$ in x-direction (g), y-direction (h) and evolution of angular velocities (i), reconstruction of the group orbits for the profiles v_1, v_2 and v_3 for $0 \leq t \leq 500$ (j). The colorbar is scaled to $[-1.8, 1.8]$ while further data are as in Figure 43.